New Photo-Luminescent Inorganic Materials: High-Tec Application in Chemical Sensing and Labeling

DISSERTATION ZUR ERLANGUNG DES DOKTORGRADES DER NATURWISSENSCHAFTEN (DR. RER. NAT.) DER FAKULTÄT CHEMIE UND PHARMAZIE DER UNIVERSITÄT REGENSBURG

vorgelegt von

El-Sayed Mahmoud Mohamed Saleh

aus Suez; Ägypten

im Juni 2011

New Photo-Luminescent Inorganic Materials: High-Tec Application in Chemical Sensing and Labeling

Doctoral Thesis

by

El-Sayed Mahmoud Mohamed Saleh

Submitted to

Faculty of Chemistry & Pharmacy

University of Regensburg

in June 2011

Diese Doktorarbeit entstand in der Zeit von Juli 2007 bis Juli 2011 am Institut für Analytische Chemie, Chemo- und Biosensorik an der Universität Regensburg.

Die Arbeit wurde angeleitet von Prof. Dr. Otto S. Wolfbeis.

Promotionsgesuch eingereicht am:	June 2011
Kolloquiumstermin:	12. July 2011
Prüfungsausschuss:	
Vorsitzender:	Prof. Dr. Frank-M. Matysik
Erstgutachter:	Prof. Dr. Otto S. Wolfbeis
Zweitgutachter:	Prof. Dr. Joachim Wegener
Drittprüfer:	Prof. Dr. Achim Göpferich

Acknowledgements

Most importantly, I have to thank Prof. Dr. Otto S. Wolfbeis for his continuous guidance, valuable discussion, significant advises throughout this work and the excellent working conditions at his chair.

Also, I gratefully acknowledge the support and consultancy provided by Dr. Axel Dürkop during this work and during my stay in Germany. As well, I appreciate very much all help and support produced by Dr. Thomas Hirsch and Dr. Hans-Heiner Gorris.

Additionally , I wish to express my appreciation and gratitude to Dr. Josef Schröder and Heiko Ingo Siegmund of the Central Electron Microscopy Lab of the University Hospital, Regensburg and Dr. Reinhard Rachel of the Institute of Molecular and Cellular Anatomy for the acquisition of the TEM images. I also want to thank Dr. Rainer Müller of the Institute of Physical Chemistry for his help with the IR and TGA measurements. I am further grateful to Martin Meier (Institute of Inorganic Chemistry) who is thanked for his help with the tempering of the upconverting nanoparticles.

I am also indebted to the secretaries Edeltraud Schmid, Sabine Rudloff and Magdalena Bauer for organizational support, and to our technicians Gisela Emmert, Gisela Hierlmeir, Angelika Stoiber, Barbara Goricnik and Joachim Rewitzer for much practical work.

I want to thank my good friends Robert Meier, Dr. Heike Mader and Katrin Uhlmann for all the advices and backup in hard times, and for making the university a better place.

I would like to thank all members of the institute for the good atmosphere and lots of help concerning so many things throughout this work, particularly, Daniela Achatz, Thomas Lang, Dominik Grögel, Lorenz Fischer and Sven Kochmann for many fruitful discussions and support regarding nanoparticles and biolabeling. Dr. Peter Kele, Dr. Martin Link, Xu-Dong Wang, Dr. Xiaohua Li and Dr. Mark-Steven Steiner are thanked for lots of help and discussion.

Finally special thanks to my wife, Reham Ali for her help, emotional support and by making a conscious effort to incorporate more humor to our life.

Dedicated to my family

إلي قرتي عيني سلمى وجنى

Table of Contents

1 Introduction

1.1 Nanoparticles

Nanoparticles (NPs) have taken scientists around the world by storm. They promise to revolutionize the world with a radical break through numerous areas such as materials and manufacturing, electronics, medicine and healthcare, environment and energy, chemistry and pharmacy, biology and agriculture, computation and information technology. [1] NPs are small clusters of atoms about 1 to 100 nanometers in size.[2] In general, when the dimension of a material is reduced from a large size, the properties remain the same at first, and then little changes occur, until finally, when the size drops to below 100 nm, dramatic changes in properties can take place. Suitable control of the properties of nm-scale structures has become a vast area of research with respect to new devices and technologies.[1]

NPs can be formed from most elements of the periodic table,[3] and they can be classified as metallic, semiconductor, ionic, rare gas or molecular according to their constituents. NPs are further characterized as homogeneous if they contain only a single type of atom,[4] or heterogeneous if they comprise more than one constituent.[5] They may be neutral or charged (anions or cations).[6] Also, NPs offer a lot of attractive possibilities in biotechnology. First, they have controllable sizes ranging from a few nanometers up to tens of nanometers, which places them at dimensions that are smaller than, or comparable to, those of a cell (10–100 μm), a virus (20–450 nm), a protein (5–50 nm) or a gene (2 nm wide and 10–100 nm long)[7] giving them the ability to be coated with biological molecules to make them interact with or bind to a biological entity providing a controllable means of delivering it into biological systems.[8]

1.1.1 Metallic Nanoparticles

Metallic nanoparticles display fascinating properties that are quite different from those of individual atoms or bulk materials. Their properties are affected by their electronic energy levels, which contrast with the continuum of energy states found in bulk materials. The existence of a surface has a major influence. Atoms at the surface are in a different environment from those in bulk and this will modify the overall electronic, chemical and

magnetic properties of the cluster. Even for clusters of 2000 atoms, about 20% of the atoms lie on the surface.

Understanding the novel behaviour of these materials provides a challenge to the experimental and theoretical techniques of fundamental science, but it is also a reward due to their huge potential in future applications. They include, for example, catalysis,[9] chemical and biological sensors,[10,11] systems for nanoelectronics and nanostructured magnetism (e.g. data storage devices). [12] In medicine, there is interest in their potential as agents for drug delivery. [13] Understanding the properties of NPs is dependent on their behaviour as free particles, but in most situations they are deposited on a substrate or embedded in a matrix of another material and it is necessary to study the influence of their environment. In many applications, the attachment of chemical or biological molecules to the NPs is of major interest.[14]

1.1.2 Magnetic Nanoparticles

In bulk materials, magnetism occurs in a limited range of the periodic table. Iron, cobalt and nickel exhibit ferromagnetism due to the unfilled 3d electron bands. The rare earths, with unfilled 4f shells, exhibit complex magnetic behaviour. At the atomic level, on the other hand, the majority of elements exhibit a non-zero magnetic moment in the ground state.

An enhanced magnetic moment is observed for Fe, Co and Ni nanoparticles up to several hundred atoms in size. It was anticipated that some metals that are non-magnetic in bulk would exhibit a magnetic moment when in the form of small clusters but, apart from rhodium, for which a moment has been observed in clusters of fewer than 100 atoms, the outcome has been negative. The focus remains therefore on metals that are magnetic in bulk.

Magnetic nanoparticles (MNPs) obey Coulomb's law and can be affected by an external magnetic field. This, combined with the intrinsic penetrability of magnetic fields into human tissue,[15] enables many applications involving the transport and/or immobilization of MNPs, or of magnetically tagged biological entities. [16] They can be used to deliver such things as an anticancer drug to a targeted region of the body, such as a tumor.[17] Furthermore, they can be synthesized to resonantly respond to a time-varying magnetic field, transferring energy from the exciting field to the nanoparticle. As a result of their special physical properties, there are many potential applications of MNPs.[18]

1.1.3 Carbon Nanotubes

Carbon materials as adsorbents offer many advantages because of their low mass density. Hydrogen storage in nano-scaled carbon materials has attracted much attention in recent years owing to the development of carbon nanotubes and nanofibers, and the reported unusual high storage capacities.[19,20] Moreover, carbon nanotubes (CNTs) are an attractive material for the development of biosensors due to its capability to provide strong electrocatalytic activity[21] and minimize surface fouling of the sensors.[22] These result in successful developments of biosensors based on CNT materials.

1.1.4 Quantum Dots

Quantum dots (QDs) are spherical, luminescent inorganic nanocrystals made of semiconductor materials,[23] of the order of 2–10 nm arranged in a spherical crystalline core and capped with a shell consisting of a second metal alloy composition. They are composed of periodic groups of II/VI (e.g., CdSe) or III/V (e.g., InP).[24] Their optical properties are size-dependent.[25] Owing to their optical and electronic properties, particularly their ability to fluorescence at discrete wavelengths directly proportional to their sizes and material compositions, QDs have been widely applied to many fields of science including medicine, biology and electronic.[26,27]

The use of QDs is one of the fastest growing and most exciting interfaces of nanotechnology in biology.[28] While the unique optical properties of QDs make them appealing as in vivo and in vitro fluorophores in a variety of biological investigations,[29] QDs have a number of advantages over organic dyes,[30] including resistance to photobleaching; narrow, nearly symmetrical emission peaks; a broad absorbance band;[31] the ability to excite at a single wavelength an entire family of QDs having different emission characteristics, thus providing multiplexed assay capability;[32] the capacity to design QDs with emission characteristics ranging from the low visible wavelengths to well within the IR region; and the potential for relatively high quantum yield of fluorescence. Therefore, QDs are widely used in applications involving imaging, labelling and sensing.[33] Their toxicity has limited their use so far, however.

1.1.5 Polystyrene Nanoparticles

A common class of fluorescent materials is based on polystyrene latex beads in combination with organic dyes.[34] Generally, the dye incorporates the NPs by covalent attachment of the dye molecules to the polymer chain or physical entrapment in a cross-linked particle,[35] thus preventing probes from leaching, quenching and photobleaching. Meanwhile, as the number of procedures regarding synthesis of the polystyrene nanoparticles (PSNPs) containing differently sized fluorescent particles is rapidly increasing. This is also true for bioanalytical applications of particulate labels and particle-based platforms.[36,37] Additionally, they are widely used in biological application such as nanosensors, [38] drug delivery,[39] and flow cytometry.[40]

1.1.6 Gold Nanoparticles

Gold nanoparticles (GNPs) possess unique optical, electronic, and molecular-recognition properties[41] that make them useful for numerous applications.[42] The rich surface chemistry of GNPs allows surface modification reactions with wide varieties of chemical and biochemical species to impart specificity to their biological applications including imaging and therapy of cancer.[43] The major advantages using GNPs in biomedical application are that they are stable and excellent biocompatible to both in vitro and in vivo environments.[44] Further, the optical properties of GNPs provide vast range of opportunities for constructing optical biosensors.[45] The basic principle involved in the design of a biosensor based on GNPs is that the GNPs are functionalized or capped with a thiolated biomolecule which upon identifying the complementary biomolecule causes change in the optical absorption of GNPs.[46] GNPs also are widely used in lateral flow assays, for example in pregnancy tests.

1.1.7 Silica Nanoparticles

Silica nanoparticles (SiNPs) represent an interesting class of materials because they are available in well defined size and size distribution, are rather affordable, and have fairly good biocompatibility and a surface reactive enough to allow for various kinds of functionalization.[47] While SiNPs, in contrast to quantum dots, are not fluorescent by themselves, they can be rendered fluorescent by methods such as incorporation of dyes into

the interior of the material, or by methods that are comparable to processes that can be used to modify glass surfaces.

One of the most promising applications of silica nanobeads is their use as fluorescent labels in bioassays. In fact, fluorescent NPs have been used for various purposes[48] including nanotechnology for gene delivery,[49,50] drug delivery[51,52] and scanning probe microscopy-based imaging and sensing techniques.[53] Besides, silica-based NPs have been extensively used in bioanalytical applications, such as immuno and gene assays,[54,55] where they are conjugated, for example, to biomolecules for analyte recognition and subsequent signal generation.

1.1.8 Upconverting Nanoparticles

Inorganic rare earth (RE) (lanthanide) nanomaterials recently have been shown to be most viable luminescent biolabels, as the rigid crystal host lattice protects the emitting RE dopants from adverse environmental effects.[56] Moreover, lanthanide ions are known to exhibit not only downconversion (i.e. conventional Stokes type) luminescence but also efficient upconversion (anti-Stokes) luminescence.[57] The term upconversion (UC) relates to an effect by which low-energy near-infrared (NIR) radiation is converted to higher energy (visible) light by (sequential) multi-photon NIR absorption and subsequent emission of shorter wave luminescence. The phenomenon[58] has been known since 1960s but primarily been exploited for the development of optical devices[59] such as infrared quantum counters, temperature sensors and solid-state lasers. Thus, the use of the UC effect has been limited to bulk glass or crystalline materials for more than 30 years. Up from the late 1990s, however, when nanoparticle (NP) research experienced fast momentum, the potential of UC materials for bioanalytical assays and luminescent imaging was recognized.

UCLNPS inherit from the respective bulk material the advantage of being photoexcitable in the NIR (most often at around 980 nm) where the auto-absorption of any biological matter is quite weak, thereby reducing to virtually zero any background absorption and luminescence (which would occur, along with Raman scatter, at wavelengths of above 980 nm anyway). Also, the absorption of water is fairly weak at this wavelength. Secondly, the large anti-Stokes shift allows easy separation of the discrete emission peaks from the excitation source. Thirdly, the emission bands are rather narrow and this enables easy separation of bands. On the other hand, one needs to keep in mind that many UCLNPs most often emit not only two if not more major bands (all fairly narrow), but also side bands of weaker intensity which may

overlap the band of a second dopant lanthanide ion. UCLNPs are chemically stable, do not bleach and unlike many quantum dots (QDs) do not blink. The peak emission wavelengths of the UCLNPs are not size dependent (as in the case of QDs), and multicolor emission can easily be accomplished by varying host crystal and RE dopant. Applications of UCLNPs (which are virtually invisible in low concentrations) include authentication and security in general, anti-counterfeit, brand protection, flow cytometry, photodynamic therapy, and point-of-care diagnostics. In bioanalytical terms, they have been demonstrated to be useful in immunoassays and gene assays,[60] as luminescent labels,[56] in chemical sensing,[61] and in imaging of cells.[59] In order to be useful in affinity assays (such as in highthroughput screening) and bioassays, the surface of UCLNPs has to be functionalized in order to enable covalent immobilization of appropriate biomolecules.

Such surface chemistries are expected to be versatile so as to enable immobilization of proteins, receptors, enzymes, or nucleic acid oligomers, to mention a few. Moreover, UCLNPs whose surface is not appropriately modified may be suspended fairly well in certain organic solvents but not so in water. This is crucial, however, with respect to many bioapplications. Upconversion materials inorganic crystals in general do not display UC luminescence at room temperature. The UC phenomenon typically occurs in singly or multiply doped host systems. Hence, research concentrates on materials that consist of a crystalline host and RE dopants added to the host lattice in low concentrations. The composition is particularly crucial in the case of nanoscale materials with distinct optical properties. At least two types of RE ions are needed as dopants to put into effect a material emitting efficient luminescence. Quite a variety of UC materials are known but fluorides and oxides are most frequently used as host crystals at present. The most common UCLNPs consist of either $NaYF_4$ or Y_2O_3 as a host material. Sulfides are widely used in UC micro particles but are hardly used in case of NPs. Most lanthanide ions are capable of emitting UC luminescence. Their (weak) absorption bands peak at around 980 nm. Low-cost diode lasers perfectly match this wavelength. However, excited states and intermediate states have to be in energetic proximity so as to enable photon absorption and energy transfer, and thus to warrant efficient emission. Such a ladder-like configuration of the energy levels is particularly featured by the Er^{3+} and Tm^{3+} ions. These ions are frequently used as emitting dopants. The ions of holmium,[62] dysprosium,[63] terbium,[64] praseodymium[63] and cerium[62] also have been used in UCLNPs. Numerous and highly different emission colors can be obtained by the variation of the kind and concentration of dopants.[65]

1.2 Fluorescence Quenching

Fluorescence quenching is defined as any process decreasing the fluorescence intensity of substance. A variety of processes can result in fluorescence quenching,[66] including a fluorescence resonance energy transfer (FRET) between two adjacent molecules,[67,68] or the energy transfer attributed to a collisional quenching.[66] Both types require an interaction between the fluorophore and quencher. Fluorescence quenching has been widely studied both as a fundamental phenomenon, and as a source of information about biochemical systems.[66] Further, it is widely used for determination of the quencher concentration such as heavy metal ions or halides.[69,70,71] Additionally, the most common method for oxygen sensing is based on the quenching of fluorescence from an appropriate chemical species.[72,73]

1.2.1 Fluorescence Resonance Energy Transfer

Fluorescence or Förster resonance energy transfer (FRET) [67,74] is a type of energy transfer between two adjacent molecules. During this process non-radiative energy transfer occurs from donor to acceptor, a donor (fluorophore) is excited by absorption of a photon, but instead of emitting a fluorescent photon, the excitation is transferred to the acceptor molecule which raises the energy state of the electron to higher vibrational levels of the excited singlet state. As a result, the energy level of the donor fluorophore returns to the ground state, without emitting its own fluorescence. This mechanism is extremely dependent on the dipole orientations and the distance between the two molecules. FRET can typically be observed over distances in the 10 to 100 Å range.[74] Additionally, the fluorescence emission spectrum of the donor molecule must overlap the absorption spectrum of the acceptor molecule.[66] The acceptor molecule can be a fluorescent[75] or non-fluorescent[76] molecule. If the acceptor molecule is a fluorophore or luminescent nanoparticle,[77] the transferred energy can be emitted as fluorescence, characteristic for that fluorophore. If the acceptor molecule is non-fluorescent, the absorbed energy is released in the form of heat, and no fluorescent light is emitted from the complex (“dark quenching”).

1.2.2 Collisional Quenching

Dynamic or collisional quenching occurs when a fluorophore that is raised to its excited state,[78] is deactivated upon contact with another molecule in the same solution. Thereby, the fluorophores return to the ground state without emission of fluorescence light. They undergo radiationless deactivation. The extent of quenching depends on the nature of the fluorophore, its structure, and the manner of its interaction with the other molecule. Examples of molecules that can act as collisional quenchers are oxygen,[79,80] halogens,[81,82,83] heavy metal ions,[84,85] and amines.[86] Dynamic quenching of fluorescence is expressed by the Stern-Volmer equation:

$$\frac{\tau_o}{\tau} = \frac{I_o}{I} = 1 + k_{sv}[Q]$$

Where τ_o, I_o and τ, I are the luminescence lifetimes and intensities in the absence and the presence of the quencher, respectively; k_{sv} is the bimolecular quenching constant and [Q] the quencher concentration. The Stern-Volmer equation is a linear equation, and hence it allows for very easy experimental determination of the quenching rate constant k_{sv}. If the emission intensity (or lifetime) in the absence of quencher and then in the presence of incremental amounts of quencher is measured, and the resulting ratio of emission intensities (I_o/I) is plotted as a function of quencher concentration, the resulting graph will have an intercept of 1 and a slope called the Stern-Volmer constant, K_{SV}.

1.2.3 Static Quenching

Besides collisional quenching, there is also static quenching which occurs when a ground state complex is formed between the fluorophore and the quencher. If this complex absorbs light, it immediately returns to the ground state without emission of a photon.[66] The quencher is somehow associated with the fluorophore in solution prior to light absorption. Therefore, the reduction in emission intensity will be affected by the extent to which the quencher associates to the luminophore and the number of quenchers present. In comparison between dynamic and static quenching, the collisional quenching only affects the excited states of the fluorophores, hence there is no change in the absorption spectra expected. In contrast the ground-state complex formation in case of static quenching will frequently result in perturbation of the absorption spectrum of the fluorophore.[78]

1.3 Aim of the Work

The aim of this work was to investigate the potential of various kinds of luminescent nanoparticles with respect to chemical sensing and biosensing. In the first part, I will describe a complete set of colored SiNPs that were obtained by covalent attachment of fluorophores to the amino-modified surface of SiNPs, with excitation maxima ranging from 337 to 659 nm and emission maxima ranging from 436 nm to the near infrared (710 nm). These fluorescent SiNPs were to be used in novel kinds of FRET-based affinity assays at the interface between nanoparticle and sample solution.

Different types of nanoparticles (SiNPs, PSNPs, and UCLNPs) carrying longwave absorbing and emitting fluorescent labels were to be prepared by conjugating reactive dyes to the surface of amino-modified particles. This type of dyes have a reactive chloro group capable of reacting with amino groups and thereby undergoing a change in color, typically from green to blue. Furthermore, the dual emission property of labeled UCNP depending on whether their luminescence is photoexcited with visible light or near-infrared light was to be demonstrated.

The UCLNPs were to be synthesized by coprecipitation and solvothermal methods with different types of dopant particles Er^{3+}, Tm^{3+} and Ho^{3+}. Quenching of these luminescence UCLNPs by heavy metal ions and halides was to be demonstrated in aqueous solution. UCLNPs were prepared by the coprecipitation method and were to be modified by coating of NPs with a thin layer of silica to improve dispersibility, followed by producing epoxy groups on surface in order to covalently immobilize biomolecules on their surface such as avidin. The resulting modified nanoparticles were to be used for application in affinity assays as detection of biotin-avidin affinity binding based on gold nanoparticles.

1.4 References

1 Bhushan B (2007) **Springer Handbook of Nanotechnology**, second ed., Springer-Verlag, Heidelberg.

2 Müller A, Cheetham AK (2007) **Nanomaterials Chemistry**, Wiley-VCH, Weinheim.

3 Carlson ED (2009) **Encyclopedia of Nanotechnology**, Nova Science Publ. Inc., NY.

4 Boisselier E, Astruc D (2009) **Gold nanoparticles in nanomedicine: preparations, imaging, diagnostics, therapies and toxicity**, Chem. Soc. Rev. 38, 1759–1782.

5 Gorris H-H, Ali R, Saleh SM, Wolfbeis OS (2011) **Ratiometric Encoding with Two Types of Photon-Upconverting Nanoparticles**, Adv. Mater. 23:1652-1655.

[6] Kalsin AM, Kowalczyk B, Smoukov SK, Klajn R, Grzybowski BA (2006) **Ionic-like behavior of oppositely charged nanoparticles**, J. Am. Chem. Soc. 128:15046-15047.

[7] Mukhopadhyay SC, Gupta GS, Huang Y-MR (2009) **Recent Advances in Sensing Technology,** first ed., Springer-Verlag, Heidelberg.

[8] Katz E, Willner I (2004) **Integrated nanoparticle-biomolecule hybrid systems: Synthesis, properties, and applications**, Angew. Chem. Int. Ed. 43:6042-6108.

[9] Crooks RM, Zhao MQ, Sun L, Chechik V,Yeung LK (2001) **Dendrimer-encapsulated metal nanoparticles: Synthesis, characterization, and applications to catalysis**, Acc. Chem. Res. 3: 181-190.

[10] McFarland AD,Van Duyne RP (2003) **Single silver nanoparticles as real-time optical sensors with zeptomole sensitivity**, Nano Lett. 8: 1057-1062.

[11] De M, Ghosh PS,Rotello VM(2008) **Applications of Nanoparticles in Biology**, Adv. Mater. 22: 4225-4241.

[12] Matsui I (2005) **Nanoparticles for electronic device applications: A brief review**, J. Chem. Eng. Jpn. 8: 535-546.

[13] Zhang L, Gu FX, Chan JM, Wang AZ, Langer RS,Farokhzad OC (2008) **Nanoparticles in medicine: Therapeutic applications and developments**, Clin. Pharmacol. Ther. 5: 761-769.

[14] Chowdhury MH, Ray K, Gray SK, Pond J,Lakowicz JR (2009) **Aluminum Nanoparticles as Substrates for Metal-Enhanced Fluorescence in the Ultraviolet for the Label-Free Detection of Biomolecules**, Anal. Chem. 4: 1397-1403.

[15] Jordan A, Scholz R, Maier-Hauff K, Johannsen M, Wust P, Nadobny J, Schirra H, Schmidt H, Deger S, Loening S, Lanksch W, Felix R (2001) **Presentation of a new magnetic field therapy system for the treatment of human solid tumors with magnetic fluid hyperthermia**, J. Magn. Magn. Mater. 225:118-126.

[16] Pardoe H, Chua-Anusorn W, St Pierre TG, Dobson J (2001) **Structural and magnetic properties of nanoscale iron oxide particles synthesized in the presence of dextran or polyvinyl alcohol**, J. Magn. Magn. Mater. 225:41-46.

[17] Chertok B, Moffat BA, David AE, Yu FQ, Bergemann C, Ross BD,Yang VC (2008) **Iron oxide nanoparticles as a drug delivery vehicle for MRI monitored magnetic targeting of brain tumors**, Biomat. 4: 487-496.

[18] Giri S, Trewyn BG, Stellmaker MP, Lin VSY (2005) **Stimuli-responsive controlled-release delivery system based on mesoporous silica nanorods capped with magnetic nanoparticles**, Angew. Chem. Int. Ed. 44:5038-5044.

[19] Lee SM, Lee YH (2000) **Hydrogen storage in single-walled carbon nanotubes**, Appl. Phys. Lett. 76:2877-2879.

[20] Ma YC, Xia YY, Zhao MW, Ying MJ (2002) **Hydrogen storage capacity in single-walled carbon nanotubes**, Phys. Rev. B 65: 155430-155436.

[21] Lee K, Zhang JJ, Wang HJ, Wilkinson DP (2006) **Progress in the synthesis of carbon nanotube- and nanofiber-supported Pt electrocatalysts for PEM fuel cell catalysis**, J. App. Electrochem. 36:507-522.

[22] Li J, Lu YJ, Ye Q, Cinke M, Han J, Meyyappan M (2003) **Carbon nanotube sensors for gas and organic vapor detection**, Nano Lett. 3:929-933.

[23] Alivisatos AP (1996) **Perspectives on the physical chemistry of semiconductor nanocrystals**, J. Phys. Chem., 100:13226–13239.

[24] Alivisatos AP, Gu W, Larabell C (2005) **Quantum Dots As Cellular Probes**, Annu. Rev. Biomed. Eng. 7:55-76.

[25] Weller H (1998) **Quantum size colloids: from size-dependent properties of discrete particles to self-organized superstructures**, Curr. Opin. Colloid Interface Sci. 3:194-199.

[26] Schmid, G. **Nanoparticles**, Wiley, New York, 2010.

[27] Gao XH, Cui YY, Levenson RM, Chung LWK, Nie SM (2004) **In vivo cancer targeting and imaging with semiconductor quantum dots**, Nat. Biotechnol. 22:969-976.

[28] Parak WJ, Pellegrino T, Plank C (2005) **Labeling of cells with quantum dots**, Nanotech. 16:R9-R25.

[29] Klostranec JM,Chan WCW(2006) **Quantum dots in biological and biomedical research: Recent progress and present challenges**, Adv. Mater. 15: 1953-1964.

[30] Resch-Genger U, Grabolle M, Cavaliere-Jaricot S, Nitschke R, Nann T(2008) **Quantum dots versus organic dyes as fluorescent labels**, Nat. Meth. 5:763-775.

[31] Yu, W.W., Qu, L., Guo, W. & Peng, X. (2003) **Experimental determination of the extinction coefficient of CdTe, CdSe and CdS nanocrystals**, Chem. Mater. 15, 2854–2860.

[32] Hermanson GT (2008) **Bioconjugate techniques**, 2nd edn. Elsevier, Amsterdam.

[33] Medintz IL, Uyeda HT, Goldman ER, Mattoussi H (2005) **Quantum dot bioconjugates for imaging, labelling and sensing**, Nat. Mat. 4:435-446.

[34] Burns A, Ow H, Wiesner U (2006) **Fluorescent core-shell silica nanoparticles: towards "Lab on a Particle" architectures for nanobiotechnology**, Chem. Soc. Rev. 35:1028-1042.

[35] Wang F, Tan WB, Zhang Y, Fan XP, Wang MQ (2006) **Luminescent nanomaterials for biological labelling**, Nanotech. 17:R1-R13.

[36] Borisov SM, Mayr T, Klimant I (2008) **Poly(styrene-blockvinylpyrrolidone) beads as a versatile material for simple fabrication of optical nanosensors**, Anal. Chem. 80:573–582.

[37] Seydack M (2005) **Nanoparticle labels in immunosensing using optical detection methods**, Biosens. Bioelectron. 20:2454–2469.

[38] Wolfbeis OS (2005) **Materials for fluorescence-based optical chemical sensors**, J. Mat. Chem. 15:2657-2669.

[39] Zhu H, McShane MJ (2005) **Loading of hydrophobic materials into polymer particles: implications for fluorescent nanosensors and drug delivery**, J. Am. Chem. Soc. 127:13448–13449.

[40] Bhalgat MK, Haugland RP, Pollack JS, Swan S, Haugland RP (1998) **Green- and red-fluorescent nanospheres for the detection of cell surface receptors by flow cytometry**, J. Immun. Meth. 219:57-68.

[41] Daniel MC, Astruc D (2004) **Gold nanoparticles: Assembly, supramolecular chemistry, quantum-size-related properties, and applications toward biology, catalysis, and nanotechnology**, Chem. Rev. 104:293-346

[42] Eustis S,El-Sayed MA (2006) **Why gold nanoparticles are more precious than pretty gold: Noble metal surface plasmon resonance and its enhancement of the radiative and nonradiative properties of nanocrystals of different shapes**, Chem. Soc. Rev. 3: 209-217.

[43] Astruc D, Daniel MC, Ruiz J (2004) **Dendrimers and gold nanoparticles as exo-receptors sensing biologically important anions**, Chem. Comm.2637-2649.

[44] Khlebtsov N, Dykman L (2011) **Biodistribution and toxicity of engineered gold nanoparticles: a review of in vitro and in vivo studies**, Chem. Soc. Rev. 40:1647-1671.

[45] Kneipp J, Kneipp H, Wittig B, Kneipp K (2010) **Novel optical nanosensors for probing and imaging live cells**, Nanomedicine 6:214-26

[46] Boisselier E, Astruc D (2009) **Gold nanoparticles in nanomedicine: preparations, imaging, diagnostics, therapies and toxicity**, Chem. Soc. Rev. 38:1759-1782.

[47] Mader H, Li X, Saleh S, Link M, Kele P, Wolfbeis OS (2008) **Fluorescent Silica Nanoparticles**, Ann. N.Y. Acad. Sci. 1130:218–223.

[48] Tan WH, Wang KM, He XX, Zhao XJ, Drake T, Wang L, Bagwe RP (2004) **Bionanotechnology based on silica nanoparticles**, Med. Res. Rev. 24:621-638.

[49] Soppimath KS, Aminabhavi TM, Kulkarni AR, Rudzinski WE (2001) **Biodegradable polymeric nanoparticles as drug delivery devices**, J. Cont. Release 70:1-20.

[50] Kneuer C, Sameti M, Bakowsky U, Schiestel T, Schirra H, Schmidt H, Lehr CM (2000) **A nonviral DNA delivery system based on surface modified silica-nanoparticles can efficiently transfect cells in vitro**, Bioconjug. Chem. 11:926-32.

[51] Benns JM, Kim SW (2000) **Tailoring new gene delivery designs for specific targets**, J. Drug. Target. 8:1-12.

[52] Sershen SR, Westcott SL, Halas NJ, West JL (2000) **Temperature-sensitive polymer-nanoshell composites for photothermally modulated drug delivery**, J. Biom. Mater. Res. 51:293-298.

[53] Senarath-Yapa MD, Phimphivong S, Coym JW, Wirth MJ, Aspinwall CA, Saavedra SS (2007) **Preparation and characterization of poly(lipid)-coated, fluorophore-doped silica nanoparticles for biolabeling and cellular imaging**, Langmuir 23:12624-12633.

[54] Kubitschko S, Spinke J, Bruckner T, Pohl S, Oranth N (1997) **Sensitivity enhancement of optical immunosensors with nanoparticles**, Anal. Biochem. 253:112-122.

[55] Schaertl S, Meyer-Almes FJ, Lopez-Calle E, Siemers A, Kramer J (2000) **A novel and robust homogeneous fluorescence-based assay using nanoparticles for pharmaceutical screening and diagnostics**, J. Biomol. Screen. 5:227-237.

[56] Shen J, Sun L-D, Yan X-H (2008) **Luminescent rare earth nanomaterials for bioprobe applications**, Dalton Trans. 5687-5697.

[57] Escribano P, Julián-López B, Planelles-Aragó J, Cordoncillo E, Viana B, Sanchez C (2008) **Photonic and nanobiophotonic properties of luminescent lanthanide-doped hybrid organic–inorganic materials**, J. Mater. Chem. 18:23-40.

[58] Auzel F (2004) **Upconversion and anti-Stokes processes with f and d ions in solids**, Chem. Rev. 104:139-173.

[59] Wang F, Liu X (2009) **Recent advances in the chemistry of lanthanidedoped upconversion nanocrystals**, Chem. Soc. Rev. 38:976-989.

[60] Soukka T, Rantanen T, Kuningas K (2008) **Photon upconversion in homogeneous fluorescence-based bioanalytical assays**, Ann. N. Y. Acad. Sci. 1130:188-200.

[61] Achatz D, Ali R, Wolfbeis OS (2010) **Fluorescent sensing, biosensing, and screening using upconverting nanoparticles**, Topics Curr. Chem. 300:29-50.

[62] Chen G, Liu H, Somesfalean G, Liang H, Zhang Z (2009) **Upconversion emission tuning from green to red in Yb^{3+}/Ho^{3+} codoped $NaYF_4$ nanocrystals by tridoping with Ce^{3+} ions**, Nanotechnology 20.

[63] Yu X, Li M, Xie M, Chen L, Li Y, Wang Q (2010**) Dopant-controlled synthesis of water-soluble hexagonal $NaYF_4$ nanorods with efficient upconversion fluorescence for multicolor bioimaging**, Nano Res. 3:51-60.

[64] Liang HJ, Chen GY, Li L, Liu Y, Qin F, Zhang Z (2009) **Upconversion luminescence in Yb^{3+}/Tb^{3+} codoped monodisperse $NaYF_4$ nanocrystals**, Optics Commun. 282:3028-3031.

[65] Wang M, Mi C, Zhang Y, Liu J, Li F, Mao C, Xu S (2009) **NIR responsive silica-coated $NaYbF_4$:Er/Tm/Ho upconversion fluorescent nanoparticles with tunable emission colors and their applications in immunolabeling and fluorescent imaging**, J. Phys. Chem. C 113:19021-19027.

[66] Lakowicz JR (2006) **Principles of Luminescence Spectroscopy**, 3rd ed., Plenum Press, New York.

[67] Förster T (1948) **Intermolecular Energy Migration and Fluorescence,** Ann. Phys. 2*:*55-75.

[68] Clegg RM (1996) **Fluorescence resonance energy transfer Fluorescence Imaging Spectroscopy and Microscopy** Wiley, New York 137:179–252.

[69] Wolfbeis OS , Boehmer M, Duerkop A, Enderlein J, Gruber M, Klimant I, Krause Ch, Kuerner J, Liebsch G, Lin Zh, Oswald B, Wu M (2002) **Advanced Luminescent Labels, Probes and Beads, and Their Application to Luminescence Bioassay and Imaging**, in Fluorescence Spectroscopy, Springer Berlin-Heidelberg, pp. 3-42.

[70] Liebsch G, Klimant I, Krause C, Wolfbeis OS (2001) **Fluorescent imaging of pH with optical sensors using time domain dual lifetime referencing**, Anal. Chem. 73:4354-4363.

[71] Liebsch G, Klimant I, Frank B, Holst G, Wolfbeis OS (2000) **Luminescence lifetime imaging of oxygen, pH, and carbon dioxide distribution using optical sensors**, Appl. Spectrosc. 54:548-559.

[72] Klimant I, Wolfbeis OS (1995) **Oxygen-Sensitive Luminescent Materials Based on Silicone-Soluble Ruthenium Diimine Complexes,** Anal. Chem. 67:3160-3166.

[73] McEvoy AK, McDonagh CM, MacCraith BD (1996) **Dissolved oxygen sensor based on fluorescence quenching of oxygen-sensitive ruthenium complexes immobilized in sol-gel-derived porous silica coatings,** Analyst 121:785-788.

[74] Stryer L (1978) **Fluorescence energy transfer as a spectroscopic ruler**, Annu. Rev. Biochem. 47:819-846.

[75] Wang L, Tan WH (2006) **Multicolor FRET silica nanoparticles by single wavelength excitation**, Nano Lett. 6:84-88.

[76] Dubertret B, Calame M, Libchaber AJ (2001) **Single-mismatch detection using gold-quenched fluorescent oligonucleotides,** Nat. Biotech. 19:680-681.

[77] Wang L, Zhao WJ, Tan WH (2008) **Bioconjugated Silica Nanoparticles: Development and Applications**, Nano Res. 1:99-115.

[78] Valeur B (2002) **Molecular Fluorescence. Principles and Applications,** Wiley-VCH, Weinheim.

[79] Kawaoka K, Khan AU, Kearns DR (1967) **Role of Singlet Excited States of Molecular Oxygen in Quenching of Organic Triplet States**, J. Chem. Phys. 46:18421853.

[80] Kearns DR, Stone AJ (1971) **Excited-State Intermolecular Interactions Involving Paramagnetic Molecules - Effect of Spin-Spin and Spin-Orbit Interactions on Quenching of Triplets**, J. Chem. Phys. 55:3383-3389.

[81] Eftink MR, Selva TJ, Wasylewski Z (1987) **Studies of the Efficiency and Mechanism of Fluorescence Quenching Reactions Using Acrylamide and Succinimide as Quenchers**, Photochem. Photobiol. 46:23-30.

[82] Zhang JW, Roek DP, Chateauneuf JE, Brennecke JF (1997) **A steady-state and time-resolved fluorescence study of quenching reactions of anthracene and 1,2-benzanthracene by carbon tetrabromide and bromoethane in supercritical carbon dioxide**, J. Am. Chem. Soc. 119:9980-9991.

[83] Lessard G, Durocher G (1978) **Singlet and Triplet Quenching of Indole by Heavy-Atom Containing Molecules in a Low-Temperature Glassy Matrix - Evidence for Complexation in Triplet-State**, J. Phys. Chem. 82:2812-2819.

[84] Chen J, Zheng A, Gao Y, He C, Wu G, Chen Y, Kai X, Zhu C (2008) **Functionalized CdS quantum dots-based luminescence probe for detection of heavy and transition metal ions in aqueous solution**, Spectrochim. Acta. Part A 69:1044-1052.

[85] Wang J, Liang J, Sheng Z, Han H (2009) **A novel strategy for selective detection of Ag^+ based on the red-shift of emission wavelength of quantum dots**, Microchim. Acta 167:281-287.

[86] Landes CF, Braun M, El-Sayed MA (2001) **On the nanoparticle to molecular size transition: Fluorescence quenching studies,** J. Phys. Chem. B 105:10554-10558.

2. Physical Background

2.1. Silica Nanoparticles

2.1.1 Surface Modification and Bioconjugation

Numerous methods have been developed for surface modification of silica NPs (SiNPs) in order to enable their coupling to biomolecular targets.[1] For example, DNA oligonucleotides,[2,3] proteins,[4] and antibodies[5] have been linked to SiNPs which, in turn, enabled sensitive fluorometric bioassays. Different types of functional groups can easily be introduced onto the SiNPs for conjugation with biomolecules. In addition, the silica surface renders such NPs chemically inert and physically stable.[6] These properties make SiNPs excellent labeling reagents for bioanalysis and bioimaging techniques.[7,8,9,10]

Different procedures were used for functionalization of SiNPs through the silanol groups. The surface hydroxyl group can react with various silane reagents such as carboxyethylsilanetriol sodium salt for introduction of carboxy groups,[11] 3-aminopropyltriethoxysilane for amino groups,[12] 3-(glycidyloxypropyl)trimethoxysilane for epoxy groups,[13] O-(propargyloxy)-N-(triethoxysilylpropyl)urethane for alkyne groups,[14] (3-azidopropyl)triethoxysilane for azido groups[14,15] or 3-mercaptopropyl trimethoxysilane for thiol groups. [16] On the other hand, silica surface modification is not limited to chemically-mediated procedures. Passive adsorption of biomolecules such as attachment of avidin to the negatively charged SiNPs surface through electrostatic interactions is common. The versatility of surface modifications of SiNPs offers a great advantage for application in bioanalysis.

Amino group functionalization is a commonly used protocol for the immobilization of enzymes and antibodies. The NPs are silanized with N1-[3-(trimethoxysilyl)-propyl] diethylenetriamine in acetic acid. After silanization, glutaraldehyde is added as a crosslinker before subsequent binding with amino-containing groups such as enzymes and antibodies. Alternatively, carboxy-modified NPs can be produced by using succinic anhydride in dimethylformamide. The carboxy-modified particles can be further reacted with carbodiimide hydrochloride before subsequent enzyme immobilization.[18]

Another procedure for SiNPs functionalization is activation by Br-CN. Surface silanol groups of SiNPs are first converted into their anions by addition of sodium carbonate, and a solution of cyanogen bromide in acetonitrile would then be added to suspension to yield-OCN groups

on the surface of the SiNPs. The particles would then be available for bioconjugation to the biomolecules containing free amino groups. After the appropriate surface modification, the SiNPs can then be directly used in bioanalytical applications.

As a result of producing active sites for conjugation with biomolecules, the functional groups change the SiNPs stability in solution. Further, modification with amine-containing organosilane compounds neutralizes the negative charge on SiNPs surface at neutral pH which leads to decrease in the colloidal stability and increase in the aggregation probability of SiNPs in aqueous solution. To overcome this problem, stabilizing agents, such as organosilane compounds that contain polyethylene glycol (PEG), a neutral polymer, are introduced during surface functionalization to prevent the aggregation of SiNPs. The PEGylated surface is highly hydrophilic and enhances the aqueous dispersibility of the silica nanoparticles.[17,18]

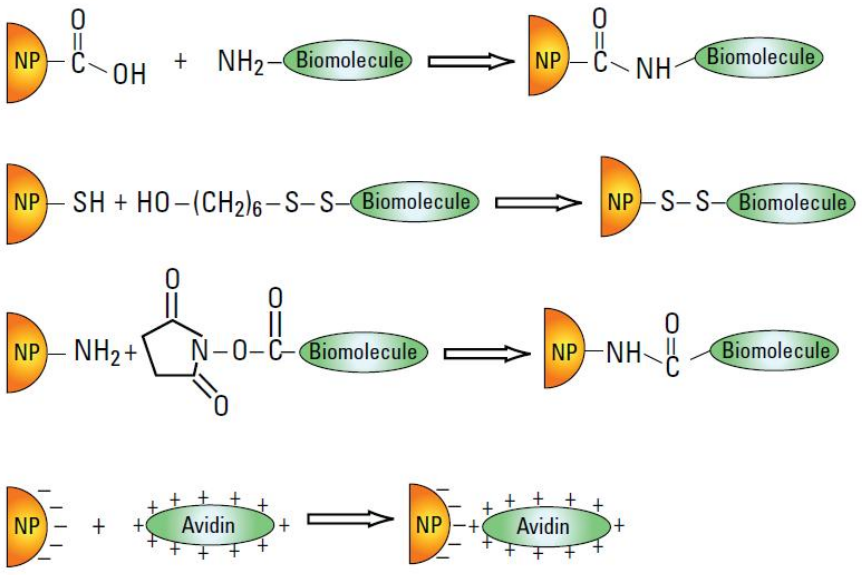

Figure 2.1 Bioconjugation schemes for attaching biomolecules to surface-modified silica nanoparticles.

After the SiNPs have been modified with different functional groups, biomolecules such as DNA oligonucleotides, antibodies, peptides can be immobilized by standard covalent bioconjugation schemes (Figure 2).[19] For example, carboxy-modified nanoparticles provide the opportunity to covalent coupling of proteins and other amine-containing biomolecules by the aid of water-soluble carbodiimide reagents.[20] Disulfide-modified oligonucleotides can be immobilized onto thiol-functionalized nanoparticles by disulfide-coupling chemistry.[17] Amine-modified nanoparticles can be coupled to a wide variety of haptens and drugs via

succinimidyl esters or isothiocyanates.[21] The bioconjugation or labeling strategy depends on the biomolecular function available. After the bioconjugation step, the nanoparticles can be separated from unbound biomolecules by centrifugation, dialysis, filtration, magnetism, or other laboratory techniques.[19]

2.2 Upconversion

2.2.1 Luminescence Mechanism of Upconversion Process

Upconversion is a nonlinear optical process that is characterized by the successive absorption of two or more pump photons with intermediate long-lived energy states followed by the emission of the output radiation at a shorter wavelength than the excited wavelength. The upconversion luminescence is classified into three main processes: excited state absorption (ESA), energy transfer upconversion (ETU), and photon avalanche (PA). These processes refer to sequential absorption of two or more photons and are completely different from the multiple photon absorption process which occurs simultaneously.[22,23,24]

In the ESA process, excitation occurs by successive absorption of two photons in a single ion. The energy diagram of the ESA process is shown in figure 2.2a. The first pump photon promotes the electron to transfer from the ground state (G) to the higher excited metastable state E1 in a process known as ground state absorption (GSA). Subsequently, the second pump photon promotes the electron to the higher metastable state E2, and this results in upconversion emission corresponding to the E2 $\longrightarrow$ G optical transition. This process is independent of the rare earth ion concentration of upconverting material [22,23,24]

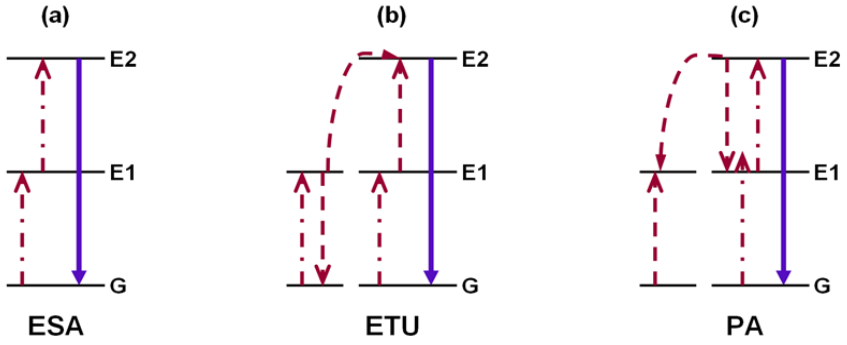

Figure 2.2 Schematic representation of the upconversion processes for rare earth doped crystals. (a) Excited state absorption; (b) energy transfer upconversion; (c) photon avalanche. The dashed/dotted lines refer to photon excitation, dashed lines to non-radiative energy transfer, and full arrows to emissive processes, respectively.

The process of ETU is based on the same principle as ESA. ETU refers to sequential absorption of two photons populating the metastable energy E2, but the excitation is realized through resonant energy transfer between two neighboring ions. The first ion acts as sensitizer (donor) and the second as activator (acceptor). Further, the two adjacent ions can absorb a photon at the same energy and populate the metastable level E1, this step followed by a non-radiative energy transfer process promotes one of the ions to emitting upper state E2 while others relax to the ground state G (see figure 2.2b). EUT is dependent on the dopant rare earth ion concentration that determines the average distance between neighboring doped ions.[23,25]

The PA conversion is the most frequent upconversion luminescence process. The mechanism is based on producing a strong emission from E2 metastable state without any resonant of ground state absorption GSA. The process starts with population of E1 by non-resonant weak GSA followed by a resonant ESA to populate the higher metastable state E2 (figure 2.2c). Then, cross-relaxation energy transfer (or ion pair relaxation) occurs between the excited ion and a neighboring ground state ion, resulting in both ions to occupation intermediate level E1. The two ions can be promoted to level E2 by resonant ESA again, thus producing strong UC emission as an avalanche process.[23,25]

In all of three UC processes, the luminescence efficiency is considerably different from one process to another. ESA is the lowest efficient UC process. Efficient UC is possible in PA with metastable, intermediate levels that can act as a storage reservoir for pump energy. The PA process suffers from pump power dependence and slow response to excitation (up to

several seconds) due to numerous looping cycles of ESA and cross-relaxation processes. On the other hand, ETU is instant independent of pump power, and occurs after excitation without delay.[23]

2.2.2 Photochemical Characterization of Upconverting Materials

All luminescent light emitters are based on the known principle of the Stokes law which states that excitation photons are at a higher energy than emitted ones or, the output photon energy is weaker than input photon energy. However, in the upconversion processes the emission is found to exceed excitation energies by 10-1000 times kT.[24] If two or more lanthanide f-block ions and transition-metal d-ions are embedded in solids, the resulting crystals deviate from the Stokes principle, producing upconversion emissions under moderate to strong excitation density.[24]

In general, inorganic crystals do not display UC luminescence at room temperature but in case of singly or multiply doped hosts the UC phenomenon occurs. Therefore, research is directed to materials that consist of a crystalline host and rare earth dopants added to the host lattice in low concentrations. The exact composition is extremely significant for studying the optical properties of micro and nano upconversion materials. Two different rare earth ions are used as dopants as localized luminescent centers in order to effect a material emitting ETU-luminescence. In principle, efficient UC can be predicted from most lanthanide-doped crystalline host materials and is realized by using a small number of well selected dopant-host concentrations.[23,24]

The trivalent lanthanides commonly have long-lifetime excited states typically between 10 ns to 100 μs, which can operate as metastable state excited from a ground state to be excited again or transfer its energy to another ion. This property is very important for efficient UC. With the exception of La^{3+}, Ce^{3+}, Yb^{3+} and Lu^{3+}, lanthanide ions have more than one excited 4f energy level and exhibit UC luminescence of small band width.[24]

In the case of the sensitized crystalline host with RE dopants, luminescence occurs from the dopant ion radiation upon its excitation to a higher energetic state obtained from the non-radiative transfer of the energy from another dopant ion. The ion that emits the radiation is called an activator, while the donator of the energy is the sensitizer. To demonstrate the efficient ETU process and to enhance UC luminescence efficiency between the sensitizer and activator, a sensitizer with a sufficient absorption cross-section in the NIR region is usually

co-doped along with the activator. The most common sensitizer used in synthesis of UC crystals is Yb^{+3} which exhibits an extremely simple energy level scheme with only one excited 4f level of $^2F_{5/2}$ (see figure 2.3).[24]

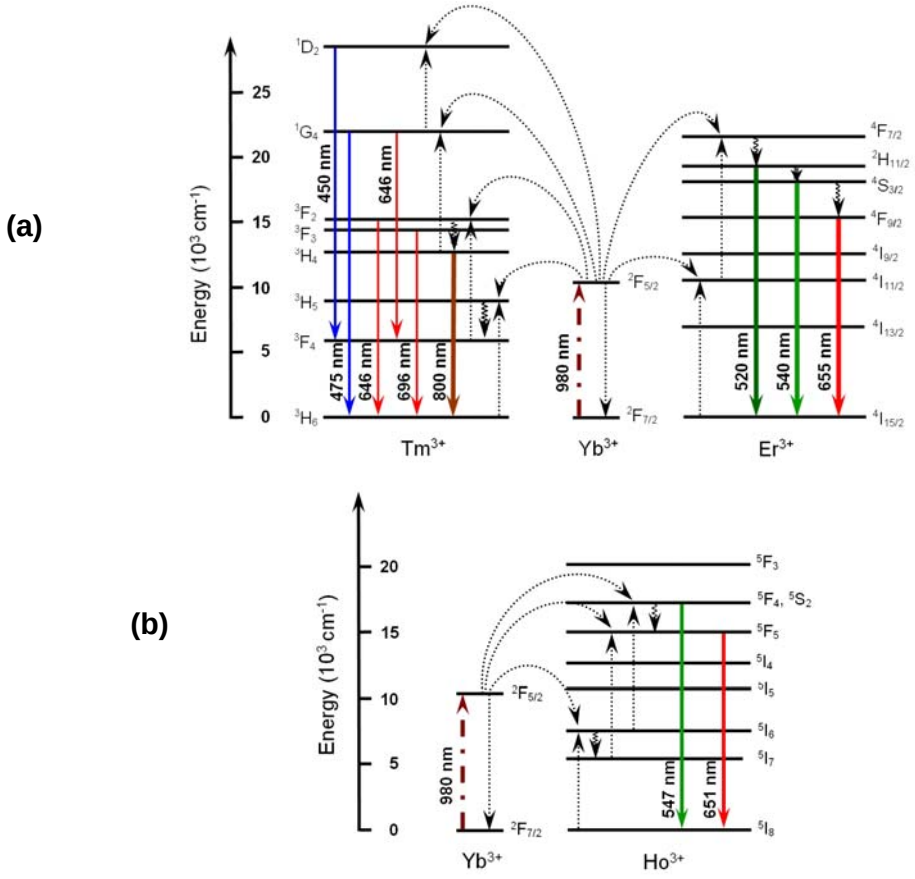

Figure 2.3. Energy transfer and upconversion emission mechanisms in a $NaYF_4$ nanocrystal doped with Yb^{3+}, Er^{3+}, and Tm^{3+} doped under 980-nm excitation. The dashed-dotted, dotted, curly, and full arrows refer to photon excitation, energy transfer, multi-photon relaxation, and upconversion emission. The $^{2S+1}L_J$ notation applied to label the f energy states represent the spin (S), orbital (L) and angular (J) momentum quantum numbers according to the Russel-Saunders notation.[24,26]

The absorption band of Yb^{3+} that is located around 980 nm due to the $^2F_{7/2}$ - $^2F_{5/2}$ transition has a larger absorption cross section than other lanthanide ions. Furthermore, the $^2F_{7/2}$- $^2F_{5/2}$ transition of Yb^{3+} is well resonant with many f-f transitions of typical upconverting lanthanide ions (Er^{3+}, Tm^{3+}, and Ho^{3+}) which increases the probability of energy transfer from Yb^{3+} to other ions. These unique optical properties of Yb^{3+} enable in use as a UC sensitizer. The concentration of the sensitizer is kept high (~ 20 mol%) in doubly or triply doped

nanocrystals, while the activator is relatively low (< 2 mol%) in order to minimizing cross relaxation energy loss.[24]

The blue luminescent UC nanoparticles doped Tm ions show intense blue emissions at 451 and 478 nm corresponding to $^1D_2 \longrightarrow {}^3F_4$ and $^1G_4 \longrightarrow {}^3H_6$ transitions of Tm^{3+} ions, respectively. The weak red emissions at 650 and 695 nm are usually assigned to the $^3F_3$/ $^3F2 \longrightarrow {}^3H_6$ or $^1G_4 \longrightarrow {}^3F_4$. Additionally, the intense near infrared emissions at 800 nm corresponding to $^3H_4 \longrightarrow {}^3H_6$ transitions of Tm^{3+} ions.[26,27] The green luminescent nanoparticles doped with Er exhibit characteristic sharp emission peaks, which are located at 520 nm, 540 nm, and 655 nm and these peaks can be attributed to $^2H_{9/2} \longrightarrow {}^4I_{15/2}$, $^2H_{11/2}$, $^4S_{3/2} \longrightarrow 4I_{15/2}$, and $4F_{9/2} \longrightarrow 4I_{15/2}$ transitions of Er^{3+} which is involving two photons processes.[26,27] Ho^{3+} doped NPs have two main emission peaks located at 547 and 651 nm and can be refered to the $^5F_4/^5S_2 \longrightarrow {}^5I_8$ and $^5F_5 \longrightarrow {}^5I_8$ transitions of Ho^{+3} with two photons processes.[26] Other rare ions such as Ce^{+3} and Gd^{+3} were used as activators [28,29] but the most efficient UC processes were detected by using Er^{3+}, Tm^{3+}, or Ho^{3+} as emitters.

The variation of the crystal structure in the host material exhibit a significant effect on the optical properties of the nano-sized crystals. In case of using sodium yttrium fluoride $NaYF_4$, the optical properties can be attributed to the different crystal fields around the trivalent lanthanide ions in matrices of various symmetries. The hexagonal crystals structure β-$NaYF_4$ increases by an order of magnitude of UC emission compared to that of cubic crystals α-$NaYF_4$. This can be interpreted as the uneven components in hexagonal crystals increase the electronic coupling of 4f energy levels and higher electronic configuration and subsequently increase f-f transition probability of the dopant ions. However, in the high symmetric cubic host materials f-f transition is forbidden.[23]

2.2.3 Synthesis of Upconverting Nanoparticles

A variety of methods have been developed to prepare UCLNPs of different sizes. The co-precipitation method is simple and convenient, and permits UCLNPs to be prepared in tunable size and narrow size distribution. In a typical procedure, solutions of lanthanide nitrates (or chlorides) are injected into a solution of the host material (such as sodium fluoride) to form NPs of the type $NaYF_4$ or YF_3 that subsequently spontaneously precipitate.[30] Phosphoric acid (rather than sodium fluoride) also has been used to yield NPs of the type $LnPO_4$, where Ln can stand for almost any trivalent lanthanide ion. Particle growth can be tuned and stabilized using capping ligands (such as ammonium di-n-octadecyldithiophosphate)[31] or chelating

agents (such as EDTA).[30] Heat treatment (also termed 'annealing' or 'calcination') is required in case of $NaYF_4$-based NPs in order to obtain UCLNPs with high upconversion efficiency because co-precipitation preferably yields (cubic) α-$NaYF_4$ which is not an efficient upconverter. Calcination at high temperatures results in sharpening of the crystal structure or even in an at least partial phase transfer to (hexagonal) β-$NaYF_4$, which shows higher UC efficiency.[30] Fortunately, the co-precipitation method does not demand costly apparatus, complex procedures, or harsh reaction conditions and is not time consuming either, but the spectral properties of the resulting material in our experience seem to strongly depend on the time course and the temperature profile applied. The surface of the resulting UCLNPs is rather hydrophilic, possibly due to coordination of the RE ion by EDTA.

Thermal decomposition is another technique for synthesis and yields highly monodisperse UCLNPs.[32,33] In this method, RE trifluoroacetates are thermolyzed in the presence of oleic acid and octadecene. The latter acts as a high boiling solvent (b.p. 315°C), whereas oleic acid serves as a stabilizing agent to suppress particle agglomeration. In case of $NaYF_4$, thermal decomposition directly yields (hexagonal) β-$NaYF_4$, with no need for annealing. Drawbacks of this method are its expensive and air-sensitive metal precursors, and its toxic by-products. The oleic acid used coordinates to the surface of the particles, thus rendering it hydrophobic.[34] It is almost impossible to remove this layer from the surface. UCLNPs synthesized via thermal decomposition can be well dispersed in organic solvents but hardly so in aqueous solutions.

The hydro(solvo)thermal method uses a pressurized solvent and reaction temperatures above the critical point to improve the solubility of solids and to accelerate reactions between solid states.[35,36] This approach allows for the preparation of highly crystalline material at much lower temperatures and without the need for an annealing process. However, specialized reaction vessels, known as autoclaves, which resist the high pressures during the reaction, are required. Crystal size and morphology is tunable via mediation with polyols or micelles.[37,38] Recently, ionic liquids have been used to prepare β-$NaYF_4$ under relatively mild conditions.[39]

The sol–gel process provides UCLNPs for applications such as thin film coating or glass materials. The method is based on the hydrolysis and polycondensation of metal alkoxide or metal acetate precursors.[40] Usually, this is to be followed by a heat treatment process. UCLNPs prepared by the sol–gel technique commonly are not suitable for biological application and cannot be dispersed in aqueous solutions due to their tendency toward aggregation. Other less common methods include combustion[41,42] and flame synthesis.[43] In

summary, the proper choice of the method for synthesis allows for the development of UCLNPs whose properties match the need for the applications envisioned.

The wavelength of the emission and its peak are hardly dependent on the size and chemical composition of the UCLNPs. However, luminescence intensity can vary to a wide extent. Generally speaking, smaller UCLNPs give weaker luminescence. Small NPs (5–10 nm) are preferred, on the other hand, in most bioassays and in biophysics. Not all synthetic methods presented here enable the preparation of very small and, at the same time, bright UCLNPs, and improvements in terms of controlling size and size distribution are still sought. An overview on representative types of NPs is given in Table 1.

Host lattice	Dopant ion	λ_{exc} [nm]	Emission peaks [nm]	Diameter [nm]	Method of Preparation	Ref.
$NaYF_4$	Yb, Er	980	518, 537, 652	33 - 166	Coprecipitation	30 44
	Yb, Tm	980	449, 474, 644, 693, 800	33		45
	Yb, Er	980	521, 539, 651	21	Solvothermal	46
	Yb, Er, Tm	980	449, 474, 525, 545, 644, 693, 800	20		47
	Yb,Ho, Tm	980	450, 475, 545, 650, 695	Rods; diameter 110 nm; length ~1 µm	Hydrothermal	48
	Yb, Er	970	541, 647	100		49
	Tb,Ce	970	380, 413, 436, 488, 542, 584, 620	70		50
	Yb, Er Yb, Tm	980	510 -530, 530 – 570, 635 – 675; 440 – 500, 630 – 670, 750 – 850	25 – 70	Ionothermal	39
	Yb, Ho	980	542, 645, 658	5-20	Thermal decomposition	51
	Yb, Er	975	538, 667	20 – 30		52
	Yb, Er	980	540, 668	10		53
$NaYbF_4$	Ho Tm Er	980	540, 650 476, 800 520, 540, 655	20	Solvothermal	54
CaF_2	Yb, Er	980	410, 524, 541, 654	< 10	Solvothermal	55
GdOF	Yb, Er	980	521, 545, 659	~ 4	Thermal decomposition	56
$BaTiO_3$	Yb, Er Yb, Tm	980	523, 542, 662 461, 478	~ 20	Sol-gel processing	57
La_2O_3	Yb, Er	976	240, 335, 350, 380, 409, 460, 475, 495, 523, 548, 672	~ 50	Combustion	58
Lu_2O_3	Yb, Er, Tm	980	477/490, 540/565, 662	~ 40	Solvothermal	59
Y_2O_3	Yb, Er	980	550, 660	200	Precipitation	60

2.2.4 Surface Modification and Bioconjugation

If used in biosciences, UCLNPs typically are applied in aqueous solution. Hence, they have to be dispersible in water. If used *in-vivo*, the lack of (cell) toxicity is an additional important issue. Both plain (unmodified) UCLNPs and surface modified UCLNPs have been applied as will be shown in the following. The introduction of functional groups to the surface of the particle is essential for covalent attachment of biomolecules that usually provide biorecognition capability, examples being proteins, antibodies, or polynucleotides. Physical adsorption of biomolecules to the surface of the UCLNPs is possible. However covalent linkage is preferred because the number and orientation of the immobilized reporter molecules can be well controlled and because desorption is prevented. There is substantial literature available on the chemical modification of the surface of UCLNPs which sometimes is event entangling and probably reflects the fact that there is no universal method available that may be applied to any of the many conceivable applications of bioconjugated UCLNPs.

Covalent surface modification of nanoparticles (NPs) is mostly based on the introduction of carboxy, thiol, or amino groups.[61] Carboxy-modified NPs allow for the coupling to biomolecules such as proteins or oligomers containing amino groups via established carbodiimide chemistry. Disulfide-modified oligonucleotides may be linked to thiol-functionalized NPs by disulfide-coupling chemistry. NPs carrying amino groups can be attached to a large variety of amino-reactive entities via succinimidyl esters or iso(thio)cyanates.[62] Two major strategies have been pursued to render the UCLNPs water-dispersible and biofunctional. In the first, reagents other than silanes are used, while in the second strategy silanes are being employed that eventually also form a thin layer of silica on the surface of the UCNP. These methods shall be discussed in the following.

2.2.4.1 Modifications without using Silane Reagents

Carboxy-functionalized UCLNPs can be prepared[63] by first synthesizing the particles via thermal decomposition or rare earth trifluoroacetates in oleylamine. The oleylamine located at the surface can then be replaced by a bifunctional poly(ethylene glycol) dicarboxy acid that generates the hydrophilicity needed for applications in aqueous systems and also provides carboxy functionalities. A general representation of the resulting UCLNPs (carrying a long-chain substituent on their surface) is shown in figure 2.4a. Boyer et al.[64] have reported on a similar method for preparation of UCLNPs possessing hydrophilic functionalities (and thus

being water-dispersible) by introducing a poly(ethylene glycol)-phosphate ligand. In another approach[65] towards rendering UCLNPs hydrophilic via ligand exchange, UCLNPs were prepared by the solvothermal route which leaves oleic acid on the particle surface. The acid was then replaced by the very hydrophilic citrate groups via ligand exchange. Kim et al.[66] replaced the oleic acid ligand by tert-butyl N-(2-mercaptoethyl)carbamate. This ligand possesses an acid-labile moiety that can be cleaved by UV light. As a result, the ligands are shortened and becoming more hydrophilic, so that the dispersibility of the particles improves significantly.

The microemulsion-based hydrothermal technique also enables[67] the preparation of UCLNPs coated with the bifunctional ligand 6-aminohexanoic acid. The resulting amino-modified nanoparticles were further conjugated to the carboxy group of folic acid using N-hydroxysuccinimide based conjugation chemistry. The resulting particles were then applied to both *in-vitro* and *in-vivo* targeting of HeLa cells overexpressing the folate receptor.

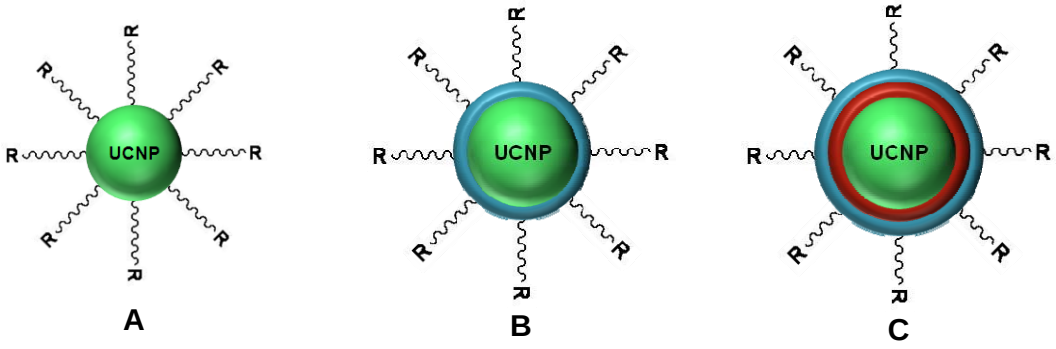

Figure 2.4 Common types of surface-modified UCNP. In A the UCNP is chemically modified with a ligand R, that can be poly(ethylene glycol)-X or alkyl-X, where X can be NH_2, COOH, N_3 or CHO. In B, the UCLNPs are also coated with a polymer. In C, the UCLNPs are modified with 2 different kinds of polymer with a layer by layer (LbL) technique.

Ligand oxidation provides another method[68] for obtaining particle functionalization. Hydrophilic carboxy groups were introduced to oleic acid-stabilized NPs of the $NaYF_4$ type by oxidation of the carbon-carbon double bonds in the oleic acid chain with the Lemieux-von Rudloff reagent. The carboxy groups were then conjugated to streptavidin via a carbodiimide route (see figure 2.5) Attachment of biotinylated oligonucleotides led to a FRET-based nanoprobe for DNA. A rhodamine was used to label the reporter DNA. The absorbance of this

dye (peaking at around 550 nm) overlaps the green emission of the UCLNPs. Hybridization of the target DNA with the labeled reporter DNA and the particle-labeled capture DNA brings the particle into close proximity to the rhodamine label so that energy transfer can occur from particle to probe. Alternatively,69 ozone may be used to oxidize the oleic acid ligand so to give azelaic aldehyde which then can be conjugated to a fluorescent probe or to 2-aminoethanethiol to enable crosslinking with gold NPs.[70]

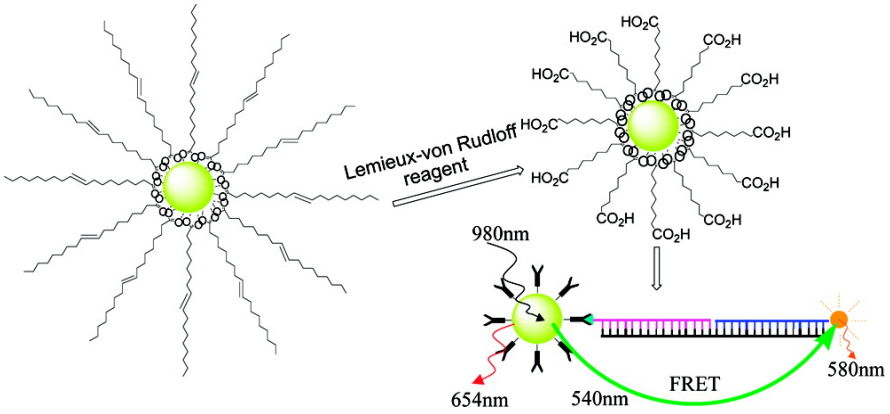

Figure 2.5 Carboxy-functionalized UCLNPs obtained by oxidation of the oleic acid capped precursor nanoparticle, and scheme of the DNA nanoprobe (from JACS with permission).

A further method for modifying the surface of UCLNPs consists of first covering them with a thin layer of a polymer as schematically shown in figure 2.4b. Direct coating of UCLNPs with a layer of polyethyleneimine (PEI) via a modified hydrothermal synthesis was reported by Chatterjee and coworkers.[35,71] PEI contains free amino groups and therefore allows for further functionalization of the particle surface with proteins or other biomolecules.

Oleylamine-stabilized $NaYF_4$ nanocrystals have also been modified by ligand attraction of an additional layer of an amphiphilic block copolymer[72] onto the particle surface so to render the NPs water-dispersible and bioconjugatable. Surface coating of UCLNPs may as well be accomplished with layers of poly(acrylic acid) (PAA) [73] or a protective block poly(ethylene glycol) co-polymer[74] in a one-pot solvothermal process.

Hilderbrand et al.[75] have obtained hydrophilic and functional UCLNPs of the Y_2O_3 type by first coating the particles with a layer of PAA (via electrostatic attraction). An amino-modified PEG was then covalently linked to the carboxy groups of the PAA via standard amide coupling chemistry. A green cyanine dye with NIR emission peaking at 797 nm) was loaded on the surface of the UCLNPs (see figure 2.6). The resulting water-dispersible, dually luminescent particles (~100 nm i. d.) were found to display low cytotoxicity. The probes showed strong upconversion emission at 660 nm when excited at 980 nm, whilst excitation at 780 nm produced the fluorescence of the cyanine fluorophore peaking at around 790 to 800 nm.

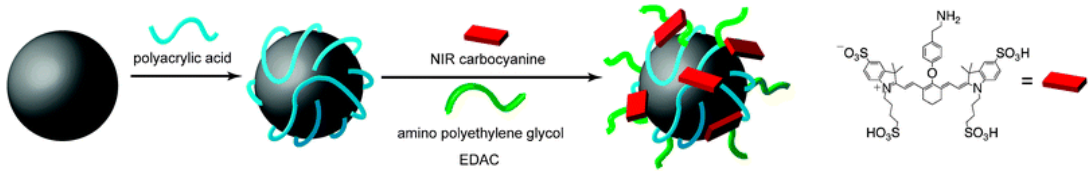

Figure 2.6 Surface modification of Y_2O_3 nanoparticles with polymers and NIR-emitting fluorophores. The resulting particles display the characteristic emission of UCLNPs and the organic dye at 660 and 797 nm, depending on whether excited at 980 or 750 respectively.

A third method for modifying the surface of UCLNPs is based on the layer-by-layer (LbL) technique as shown in figure 2.4c. Usually, an assembly of oppositely charged polyions[44,76] is deposited on their surface. The LbL method is of the electrostatic type rather than of the covalent type. Positively charged poly(allylamine) hydrochloride and negatively charged polystyrenesulfonate were sequentially adsorbed onto the UCLNPs, thus forming a stable amino-functionalized shell. The particles were then modified with biotin or oligonucleotides. The LbL method provides versatile, highly stable, and biocompatible NPs with controllable shell thickness and charge. Drawbacks include the washing steps that are required, and the limitation of this process to hydrophilic UCLNPs. A similar method was used by Zhang et al.[77] to prepare UCLNPs of the $NaYF_4$ type that were additionally coated with gold nanolayer to enable the plasmonic modulation of the upconversion emission of the NPs. This is schematically shown in figure 2.7.

The LbL methods seem to be quite attractive in requiring affordable reagents, being fairly reproducible (up to 10 single layers), and in enabling the surface to be characterized by established methods of spectroscopy, imaging, and electroanalysis.

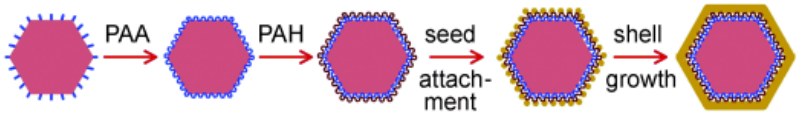

Figure 2.7 Illustration of surface functionalization by the LbL method by sequential deposition of (anionic) poly(acrylic acid) (PAA) and (cationic) poly(allylamine hydrochloride) (PAH), followed by attachment of seed gold NPs and the growth of a gold nanoshell on the surface of the UCLNPs.

2.2.4.2 Modifications using Silane Reagents

Surface silanization is a powerful technique for covalent modification of various kinds of surfaces including silica, metal oxides (including tin, iron, and the like), and even graphite.[78] Silanization with reagents of the type shown in figure 2.8a can be performed in either of the following ways: (a) Direct reaction with the particles to form a silane-modified surface ("end-capping") to give particles of the type shown in figure 2.8b; or (b), coating the surface with tetraethoxysilane (TEOS) to first create a layer of silica and thereby yielding particles of the type UCNP@SiO_2, and then coating this layer with a silanizing reagent (Fig. 2.8C). The surface of the UCLNPs may however also be coated with a mixture of a tetraalkoxysilane and a reagent of the type shown in figure 2.8A; this will result in simultaneous coating of the UCLNPs with silica and its functionalization, and also requires one separation step only.[88] The resulting UCLNPs are non-toxic,[79] monodisperse and can be well dispersed in aqueous solution. The silica layer in particles of the type shown in 2.8C also protect the UCNP from undesired external effects such as quenching, penetration by small species, or leaching.

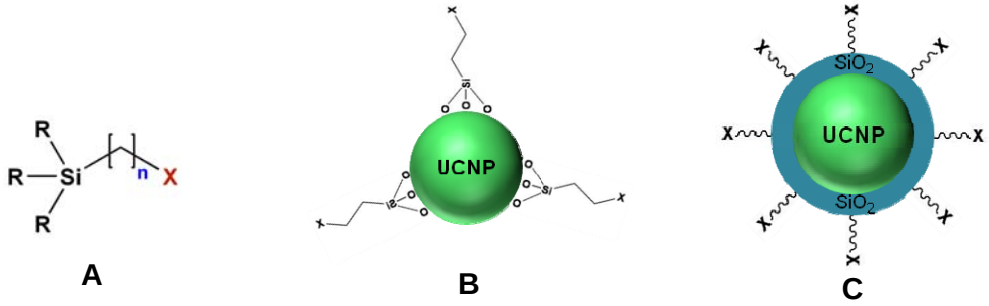

Figure 2.8 A: typical structure of a reagent for silane functionalization of oxidic surfaces, where X represents a functional group such as amino or epoxy, and R a hydrolysable group such as alkoxy. B: direct functionalization of UCLNPs (mainly of the Y_2O_3 type) using a modified silane. C: coating of the UCLNPs with a layer of SiO_2 and subsequent functionalization using a modified silane. This can be performed either in a one-step or a two-step procedure.

In order to obtain particles of the type shown in figure 2.8b, UCLNPs were coated with a thin layer of silica (SiO_2) by controlled hydrolysis and polycondensation of precursors such as TEOS or other tetraalkoxysilanes of the type $(RO)_4Si$, where R is an alkyl substituent. Aminosilanes (e. g. aminopropyl triethoxysilane) have been used most often in direct modifications of the surface of UCLNPs. Amino-modified UCLNPs can be further biofunctionalized by covalent attachment of biomolecules such as biotin,[78] folic acid,[80] peptides,[81] proteins,[82] antibodies,[83,84] and DNA.[76,85] Hu et al.[80] have used particles modified with folic acid for the detection of tumor cells. A microemulsion method was applied to obtain silica-coated and amino-modified UCLNPs. These were further coupled to activated folic acid (FA). Fluorescein isothiocyanate (FITC) was incorporated into the silica shell as secondary fluorophore. Cytotoxicity tests revealed a good biocompatibility of the resulting particles (figure 2.9).

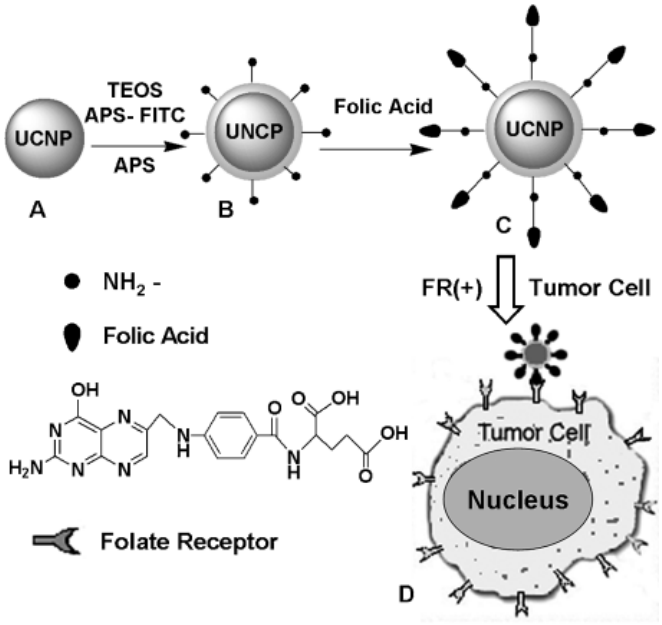

Figure 2.9 Schematic illustration of the synthesis of UCNP@SiO_2(FITC)-FA nanocomposites: (A) Oleic acid-capped $NaYF_4$:Yb,Er nanocrystals; (B) Amino-functionalized UCNP@SiO_2(FITC)-NH_2 core-shell nanocomposites; (C) UCNP@SiO_2(FITC)-FA nanocomposites; (D) Folate-mediated targeting with FR-positive [FR(+)] tumor cells. TEOS: tetraethylorthosilicate; APS: (3-aminopropyl)triethoxysilane

In order to immobilize antibodies, Wang et al.[83] first prepared silica-coated UCLNPs of the type $NaYF_4$:Yb,Er by the Stöber method, then amino-modified the surface with aminopropyl triethoxysilane, and subsequently conjugated rabbit antigoat IgG to the surface using glutaraldehyde. A sandwich-type luminescence resonance energy transfer (LRET) system was established (see figure 2.10) in which the IgG-modified UCLNPs acted as energy donors, and rabbit antigoat IgG-modified gold NPs acted as energy acceptors because the (red) gold nanoparticles absorb maximally at around 540 nm where the green emission of the UCLNPs (following excitation at 980 nm) has its peak. The addition of free goat antihuman IgG resulted in the occurrence of LRET, which enables the determination of the concentration of the goat antihuman IgG in the LRET system.

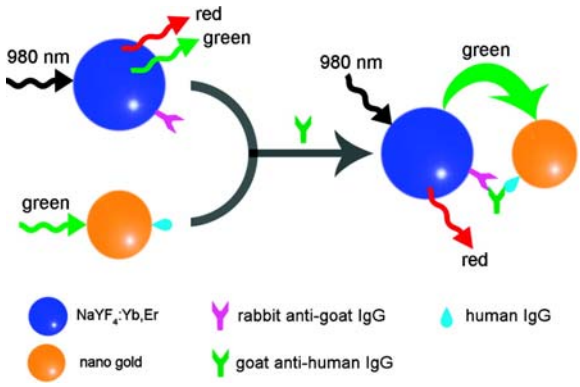

Figure 2.10 Schematic illustration of the LRET process between $NaYF_4$:Yb, Er UCLNPs (the donor) and gold nanoparticles (the acceptor).

Carboxyethyl triethoxysilane in combination with TEOS enable[86] the coating of the surface of such particles and to introduce anionic carboxy groups. The surface charge of these modified particles is about - 30 mV. Neural polymers such as poly(vinyl pyrrolidone)[87] have been used to stabilize the silica shell and control its thickness. The silica coating technique can be applied to both hydrophilic and hydrophobic UCLNPs and enables the entrapment of secondary reporters such as magnetic NPs of the Fe_3O_4 type[88] or organic dyes.[89] The microemulsion technique was also applied[89] to coat β-$NaYF_4$ with TEOS and aminopropyl triethoxysilane, simultaneously also incorporating fluorescein or rhodamine derivatives, or even quantum dots (QDs) into the silica shell. The emission of the UCLNPs excites the organic dye or QD, thereby producing multicolor emission. This may pave the way for the use of UCLNPs in multiplexing or encoding.

Silica coated UCLNPs also show potential for use in photodynamic therapy. Mesoporous silica coated UCLNPs were prepared[90] by the microemulsion method by first coating the UCLNPs of type $NaYF_4$ with TEOS (figure 2.11). Subsequently, the mesoporous layer was formed by treating the silica layer with a mixture of TEOS and octadecyl trimethoxysilane (C18TMS). The coated particles were calcinated at 500 °C to remove excess C18TMS to obtain a mesoporous layer. The photosensitizer zinc phthalocyanine was then incorporated into this layer. The upconversion emission of the UCLNPs activates the photosensitizer to release active singlet oxygen which possibly kills cancer cells.

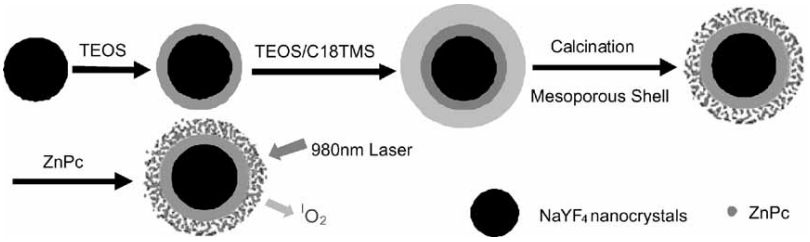

Figure 2.11 Schematic image showing how to load zinc phthalocyanine (ZnPc) into a mesoporous silica shell on $NaYF_4@SiO_2$ nanoparticles and to use them for PDT.

The functional groups used for the conjugations discussed before (mainly amino, carboxy, thiol) are abundant in proteinic biomolecules and thus may give rise to unspecific binding. In addition, the introduction of amino groups (cationic at pH 6 - 8) or carboxy groups (anionic at pH 6 - 8) will alter the overall charge of the particles. This can lead to a decrease in the colloidal stability of the NPs and thus cause particle aggregation which is a major problem in all biotechnologies based on the use of nanoparticles. Therefore, other functional groups suitable for bioconjugation have been looked for. Among these, azido and alkyne are an attractive alternative[91,92] because they undergo a mutual 1,3-dipolar cycloaddition that often is referred to as a click reaction. This so-called click chemistry (one type of several) is an attractive alternative because the functional groups involved (azido and alkyne) are hardly present in biomolecules including proteins and oligomers. It is therefore said to be "bioorthogonal". Mader et al.[93] used TEOS along with azido- or alkyne modified silanes respectively to coat and functionalize the UCLNPs in a one-pot Stöber process (figure 2.12). The clickable UCLNPs thus obtained were further conjugated to appropriately "click" modified biotin and maleimide to obtain versatile labels for avidin or thiol-group containing biomolecules. Furthermore, the particles were conjugated to clickable fluorophores to obtain dual-wavelength labels potentially suitable for encoding purposes.

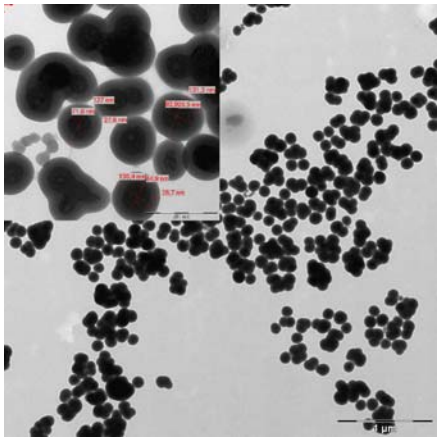

Figure 2.12 TEM image of silica-coated and azido-modified $NaYF_4$ UCLNPs.

2.2.5 Bioimaging

The ability of UCLNPs to convert low-energy radiation to higher energy (visible) fluorescence makes them very appealing for biological imaging applications due to their insensitivity for autoluminescence derived from the luminescence of biological samples (e.g. proteins, nucleic acids etc.). Moreover, the use of low energy, near-infrared (NIR) excitation reduces photodamage and permits deeper penetration into tissue,[94] as was demonstrated[95] nicely (in comparison to quantum dots) by Zhang and co-workers (Figure 2.13). All these factors contribute to an increased signal-to-noise ratio, which results in improved detection limits compared to classical organic or inorganic (e.g. quantum dots, QDs). Moreover, UCLNPs are easily internalized by many cells.

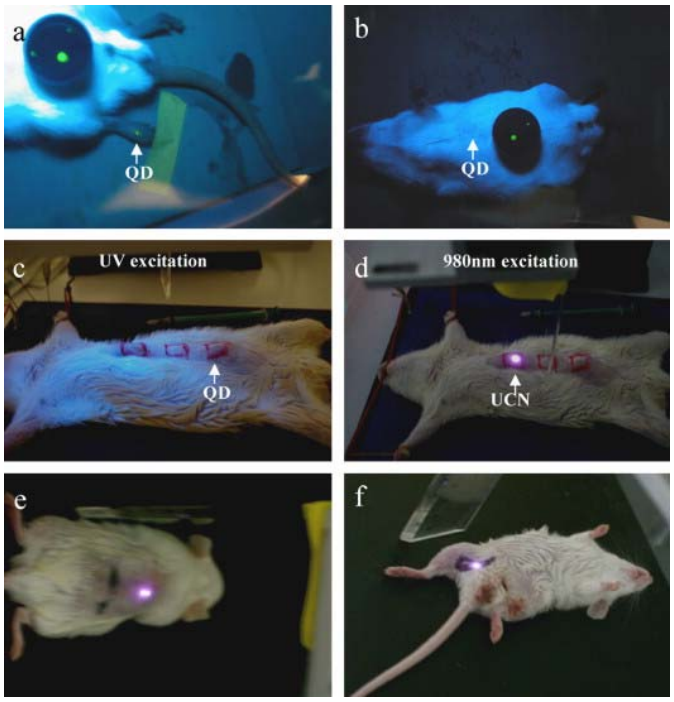

Figure 2.13 *In vivo* imaging of rat: quantum dots (QDs) injected into translucent skin of foot (a) show fluorescence, but not through thicker skin of back (b) or abdomen (c); PEI/$NaYF_4$:Yb,Er nanoparticles injected below abdominal skin (d), thigh muscles (e), or below skin of back (f) show luminescence. QDs deposited on a black disk in (a, b) are used as the control.

2.2.5.1 In vivo Applications

In a recent paper, Hildebrand et al.[75] have reported on the use of multi-channel luminescent UCLNPs for *in-vivo* imaging of blood vessels. The red-emitting (660 nm) particles of the type Y_2O_3:Er,Yb were first coated with amino-terminal poly(ethylene glycol). [75] The resulting multi-channel imaging probes were then injected into mice in order to investigate their practical utility in vascular imaging under excitation of clinically relevant low power density laser excitation. Co-localization of the cyanine and upconversion fluorescence indicated that the polymer coating remained intact *in vivo* (figure 2.14). Besides the acquisition of static images, the emission originating from upconversion was bright enough to enable real-time imaging providing a promising platform for *in vivo* diagnostic imaging.

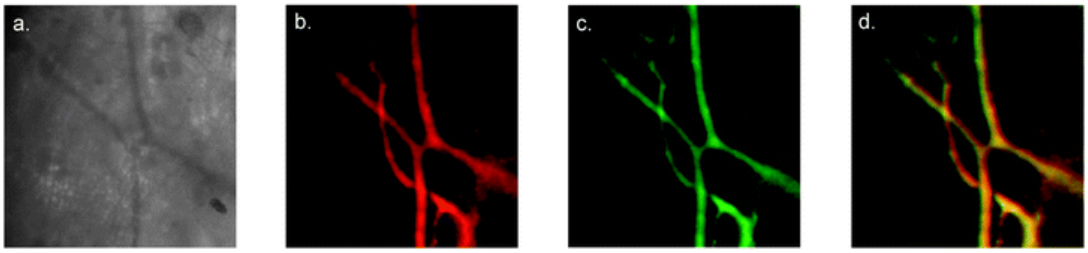

Figure 2.14 Optical imaging of blood vessels in the mouse ear following tail vein injection of the nanoparticles (10 mg); (a) blood vessels imaged with a blue light filter, (b) upconversion image with excitation at 980 nm and a laser power density of 550 mW cm^{-2}, (c) fluorescence image of the carbocyanine dye with excitation at 737 nm, (d) merged image of the upconversion and fluorescence signals. Both the upconversion and carbocyanine fluorescence images were taken with an exposure time of 10 s. (from *Chem. Commun.* with permission)

Wu *et al.*[96] investigated UCLNPs of the *β*-$NaYF_4$:Er,Yb type with respect to their suitability in terms of luminescence imaging. Their findings further supported the excellence of UCLNPs in imaging applications. They claimed that the improved s/n ratio is further increased by the absence of photobleaching and non-blinking behavior of their ~30 nm NP system. The particles were rendered water soluble by wrapping them with an amphiphilic polymer. The well-dispersed aqueous UCLNPs were subsequently incubated with murine fibroblasts and inoculated by endocytosis. The highly efficient upconversion process enabled the use of these nanoparticles as single molecule imaging probes both *in vivo* and *in vitro* studies.

UCLNPs with tunable emission colors have been demonstrated in brilliant work[84,97] to be well suited for purposes of immunolabeling and virtually zero-background imaging of cancer cells. The visible color of the upconversion luminescence was tuned by using different dopant ratios of Er, Tm and Ho salts. A silica shell on the nanoparticulate system provided excellent water dispersibility. Co-doping of the Er^{3+}, Tm^{3+} and Er^{3+} ions in a single $NaYbF_4$ matrix resulted in multicolor emission including orange, yellow, green, cyan and pink depending on the dopant concentration. Following further amino-functionalization of the silica shell with aminopropyltriethoxysilane, the NPs were linked to rabbit anti-CEA8 antibody and then used as fluorescent labels for the imaging of live HeLa cells (figure 2.15).

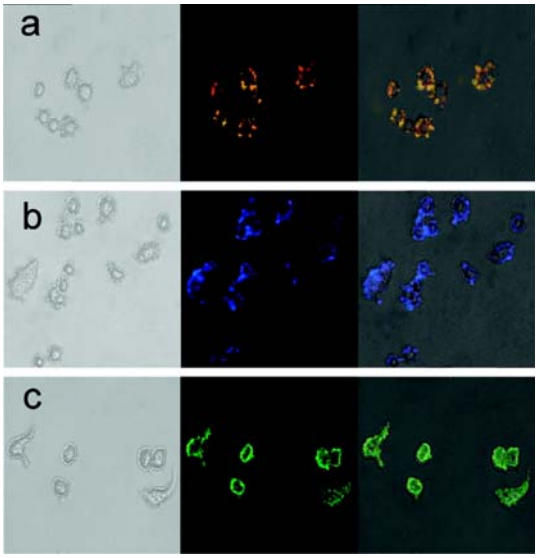

Figure 2.15 Fluorescence imaging of HeLa cells after being incubated with various UCLNPs conjugated to rabbit anti-CEA8 antibody and irradiated with 980 nm laser light. (a) $NaYbF_4$:Er; (b) $NaYbF_4$:Tm; (c) $NaYbF_4$:Ho. The left rows are bright field images, the middle rows are fluorescent images (dark field), and right rows are overlays of the left and central rows.

Earlier studies[79,98] had proven the biocompatibility of silica coated nanoparticles. Following this lead, Li and colleagues[80] also presented the preparation of silica-coated and folic acid-decorated UCLNPs that were used to image cells overexpressing folate receptors (FR) on their surface. The FR positive cell-lines were then quantitatively analyzed by flow cytometry.

UCLNPs, in combination with paramagnetism, were used to demonstrate the versatility of upconverting luminescence imaging together with magnetic resonance imaging (MRI) *in vivo*.[99] $NaGdF_4$ NPs, co-doped with Tm^{3+}/Er^{3+}/Yb^{3+}, were coated with azelaic acid to result in hydrophobic, upconverting and MRI-active nanoparticles. The gadolinium enhances the contrast of MR images, whereas the upconversion luminescence can be used for luminescent imaging. Besides being MRI active, this set up showed both NIR-to-NIR and NIR-to-visible luminescence. Both being non-invasive techniques, the combination of paramagnetism and UC luminescence enables deep tissue in-vivo imaging and 3D tomography. These dual-modal imaging probes were found to show excellent signal-to-noise ratio, good water solubility, low cellular toxicity and no obvious toxicity to the living body. Furthermore this probe did not accumulate in the body. Though not yet investigated, the authors claim that the carboxy-

functionalized surface can easily be modified further e.g. with sequences to specifically target tissues.

In another dual-mode set-up the upconverting luminescence was combined with ferromagnetism. Silica encapsulated magnetite nanoparticles were prepared with lanthanides ions doped into the outer silica shell and shown[100] to be ideal nanocomposites to targeted drug delivery purposes with the ability for NIR luminescence imaging.

Finally, the work of Zhang *et al.*[101] is probably suitable to demonstrate all the advantages of nanoparticulate systems that use the upconversion phenomenon. They used 50 nm diameter silica coated, non-aggregated UCLNPs to image transplanted cells of a living mouse. The authors also demonstrated the excellent photostability of the nanoparticulate system in comparison to common fluorescent organic dyes such as DAPI and Alexa Fluor 532. The fluorescence intensity of the latter two decreased to a minimal value within 15 min of irradiation, while the intensity of luminescence deriving from the UCLNPs remained unchanged. In order to image transplanted skeletal myoblast cells, they were loaded with silica coated upconverting particles. A suspension of these cells was then transplanted into a cryodamaged muscle of the hind limb of a mouse. Dynamic imaging of the labeled cells was possible in this otherwise strongly autofluorescent medium with negligible background and at least 1.3 mm deep in the tissue even 7 days after delivery (figure 2-16).

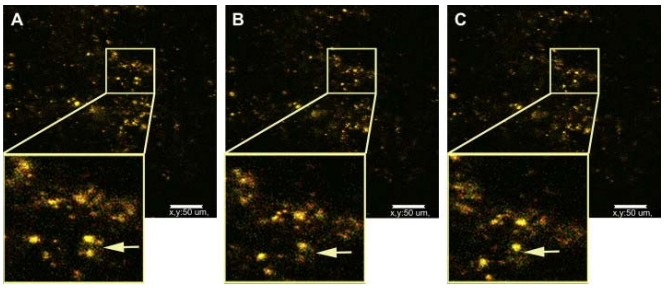

Figure 2.16 Dynamic real time tracking of cell migration *in vivo*. Time-lapse confocal imaging at a single *z*-plane on the hind limb muscle of a day 3 mouse captured subtle movement of nanoparticle-loaded cells over a 4 h time course. Snapshots from the movie displayed here at (A) 0 h, (B) 2 h and (C) 4 h. Insets show an enlarged area (marked by the box) to better demonstrate the more obvious (arrows) change in the cells' position as they migrate to new location (scale bar: 50 μm).

Despite the drawbacks of using UCLNPs as signaling units (e.g. the lack of generalized protocols for the synthesis and surface modification strategies) the overall gain the researchers can get by using UCLNPs and the typical advantages of UCLNPS as outlined in the introduction suggest that these methods hold promise for providing new and more sensitive techniques for (deep) tissue imaging and early diagnosis.

2.3 References

[1] Mader H, Li X, Saleh S, Link M, Kele P, Wolfbeis OS (2008) **Fluorescent silica nanoparticles**, Ann. N.Y. Acad. Sci. 1130:218–223.

[2] Csogor Z, Nacken M, Sameti M, Lehr CM, Schmidt H (2003) **Modified silica particles for gene delivery**, Materials Science & Engineering C-Biomimetic and Supramolecular Systems 23:93-97.

[3] Rao KS, Rani SU, Charyulu DK, Kumar KN, Lee BK, Lee HY, Kawai T (2006) **A novel route for immobilization of oligonucleotides onto modified silica nanoparticles**, Anal. Chim. Acta. 576:177-83.

[4] Kim SH, Jeyakumar M, Katzenellenbogen JA (2007) **Dual-mode fluorophore-doped nickel nitrilotriacetic acid-modified silica nanoparticles combine histidine-tagged protein purification with site-specific fluorophore labeling**, J. Am. Chem. Soc. 129:13254-64.

[5] Liu S, Zhang HL, Liu TC, Liu B, Cao YC, Huang ZL, Zhao YD, Luo QM (2007) **Optimization of the methods for introduction of amine groups onto the silica nanoparticle surface**, J. Biomed. Mater. Res. Part A 80A:752-757.

[6] Smith JE, Wang L, Tan WT (2006) **Bioconjugated silica-coated nanoparticles for bioseparation and bioanalysis**, Trac-Trends in Anal. Chem. 25:848-855.

[7] Bagwe RP, Yang CY, Hilliard LR, Tan WH (2004) **Optimization of dye-doped silica nanoparticles prepared using a reverse microemulsion method**, Langmuir 20:8336-8342.

[8] Yao G, Wang L, Wu YR, Smith J, Xu JS, Zhao WJ, Lee EJ, Tan WH (2006) **FloDots: luminescent nanoparticles**, Anal. Bioanal. Chem. 385:518-524.

[9] Bagwe RP, Hilliard LR, Tan WH (2006) **Surface modification of silica nanoparticles to reduce aggregation and nonspecific binding**, Langmuir 22:4357-4362.

[10] Zhao XJ, Bagwe RP, Tan WH (2004) **Development of organic-dye-doped silica nanoparticles in a reverse microemulsion**, Adv. Mater. 16:173-176.

[11] Wang L, Yang C, Tan W (2005) **Dual-Luminophore-Doped Silica Nanoparticles for Multiplexed Signaling**, Nano. Lett. 5:37-43.

[12] Saleh SM, Muller R, Mader HS, Duerkop A, Wolfbeis OS (2010) **Novel multicolor fluorescently labeled silica nanoparticles for interface fluorescence resonance energy transfer to and from labeled avidin**, Anal. Bioanal. Chem. 398:1615-1623.

[13] Ochi M, Takahashi R, Terauchi A (2001) **Phase structure and mechanical and adhesion properties of epoxy/silica hybrids**, Polymer 42:5151–5158.

[14] Mader HS, Link M, Achatz DE, Uhlmann K, Li XH, Wolfbeis OS (2010) **Surface-Modified Upconverting Microparticles and Nanoparticles for Use in Click Chemistries**, Chem. Eur. J. 16:5416-5424.

[15] Achatz DE, Heiligtag FJ, Li XH, Link M, Wolfbeis OS (2010) **Colloidal silica nanoparticles for use in click chemistry-based conjugations and fluorescent affinity assays**, Sens. Actuators B 150:211-219.

[16] Badley RD, Ford WT, McEnroe FJ, Assink RA (1990) **Surface modification of colloidal silica**, Langmuir 6:792–801.

[17] Hilliard LR, Zhao X, Tan W (2002) **Immobilization of oligonucleotides onto silica nanoparticles for DNA hybridization studies**, Anal. Chim. Acta 470:51–56.

[18] Roy I, Ohulchanskyy TY, Bharali DJ, Pudavar HE, Mistretta RA, Kaur N, Prasad PN (2005) **Optical tracking of organically modified silica nanoparticles as DNA carriers: A nonviral, nanomedicine approach for gene delivery,** Proc. Natl. Acad. Sci. U.S.A. 102:279–284.

[19] Wang L, Wang KM, Santra S, Zhao XJ, Hilliard LR, Smith JE, Wu JR, Tan WH (2006) **Watching silica nanoparticles glow in the biological world**, Anal. Chem. 78:646-654.

[20] Gerion D, Pinaud F, Williams SC, Parak WJ, Zanchet D, Weiss S, Alivisatos PA (2001) **Synthesis and Properties of Biocompatible Water-Soluble Silica-Coated CdSe/ZnS Semiconductor Quantum Dots**, J. Phys. Chem. B 105:8861–8871.

[21] Chan WCW (2007) **Bio-applications of nanoparticles***,* second ed.*,* Springer-Verlag, Heidelberg.

[22] Achatz DE, Ali R, Wolfbeis OS (2011) **Luminescent Chemical Sensing, Biosensing, and Screening Using Upconverting Nanoparticles,** Topics Curr. Chem. 300: 29-50.

[23] Wang F, Liu X (2009) **Recent Advances in the Chemistry of Lanthanide-Doped Upconversion Nanocrystals**, Chem. Soc. Rev. 38: 976-989.

[24] Auzel F (2004) **Upconversion and Anti-Stokes Processes with f and d Ions in Solids**, Chem. Rev. 104: 139-173.

[25] Joubert M-F (1999) **Photon Avalanche Upconversion in Rare Earth Laser Materials**, Opt. Mater. 11: 181-203.

[26] Yang LW, Han HL, Zhang YY, Zhong JX (2009) **White Emission by Frequency Up-Conversion in Yb^{3+}-Ho^{3+}-Tm^{3+} Triply Doped Hexagonal $NaYF_4$ Nanorods**, J. Phys. Chem. C 113: 18995-18999.

[27] Wang J, Liu X (2008) **Upconversion Multicolor Fine-Tuning: Visible to Near-Infrared Emission from Lanthanide-Doped $NaYF_4$ Nanoparticles**, J. Am. Chem. Soc. 130: 5642-5643.

[28] Chen G, Liu H, Somesfalean G, Liang H, Zhang Z (2009) **Upconversion Emission Tuning from Green to Red in Yb^{3+}/Ho^{3+}-codoped $NaYF_4$ Nanocrystals by Tridoping with Ce^{3+} Ions**, Nanotechnol. 20: 385704-1 - 385704-6.

[29] Mahalingam V, Naccache R, Vetrone F, Capobianco JA (2009) **Sensitized Ce^{3+} and Gd^{3+} Ultraviolet Emissions by Tm^{3+} in Colloidal $LiYF_4$ Nanocrystals**, Chem. Eur. J. 15: 9660-9663

[30] Yi G, Lu H, Zhao S, Ge Y, Yang W, Chen D, Guo L-H (2004) **Synthesis, characterization, and biological application of size-controlled nanocrystalline $NaYF_4$:Yb,Er infrared-to-visible up-conversion phosphors**, Nano Lett. 4:2191-9196.

[31] Yi G-S. Chow G-M (2005) **Colloidal LaF_3:Yb,Er, LaF_3:Yb,Ho and LaF_3:Yb,Tm nanocrystals with multicolor upconversion fluorescence**, J. Mat. Chem. 15:4460-4464.

[32] Shan J, Ju Y (2009) **A single-step synthesis and the kinetic mechanism for monodisperse and hexagonal-phase $NaYF_4$:Yb,Er upconversion nanophosphors**, Nanotechnol. 20:275603.

[33] Qian H-S, Zhang Y (2008) **Synthesis of hexagonal-phase core-shell $NaYF_4$ nanocrystals with tunable upconversion fluorescence**, Langmuir 24:12123-12125.

[34] Boyer J-C, Vetrone F, Cuccia LA, Capobianco JA (2006) **Synthesis of colloidal upconverting $nayf_4$ nanocrystals doped with Er^{3+}, Yb^{3+} and Tm^{3+}, Yb^{3+} via thermal decomposition of lanthanide trifluoroacetate precursors**, J. Am. Chem. Soc. 128:7444-7445.

[35] Wang F, Chatterjee DK, Li Z, Zhang Y, Fan X, Wang M (2006) **Synthesis of polyethylenimine/$NaYF_4$ nanoparticles with upconversion fluorescence**, Nanotechnol. 17:5786-5791.

[36] Liu C, Chen D (2007) **Controlled synthesis of hexagon shaped lanthanide-doped LaF_3 nanoplates with multicolor upconversion fluorescence**, J. Mater. Chem. 17:3875-3880.

[37] Zhang F, Wang Y, Yu T, Zhang F, Shi Y, Xie S, Li Y, Xu L, Tu B, Zhao D (2007) **Uniform nanostructured arrays of sodium rare-earth fluorides for highly efficient multicolor upconversion luminescence**, Angew. Chem. Int. Ed. 46:7976-7979, Angew. Chem. 119:8122-8125.

[38] Zhang F, Li J, Shan J, Xu L, Zhao D (2009) **Shape, size, and phase-controlled rare-earth fluoride nanocrystals with optical up-conversion properties**, Chem. Eur. J. 15:11010-11019.

[39] Liu X, Zhao J, Sun Y, Song K, Yu Y, Du C, Xianggui K, Zhang H (2009) **Ionothermal synthesis of hexagonal phase $NaYF_4$: Yb^{3+}, Er^{3+}/Tm^{3+} upconversion nanophosphors**, Chem. Commun. 6628-6630.

[40] Patra A, Friend CS, Kapoor R, Prasad PN (2003) **Fluorescence upconversion properties of Er^{3+}-doped TiO_2 and $BaTiO_3$ nanocrystallites**, Chem. Mater. 15:3650-3655.

[41] Lim SF, Riehn R, Tun C-K, Ryu WS, Zhuo R, Dalland J, Austin RH (2009) **Upconverting nanophosphors for bioimaging**, Nanotechnol. 20:405701.

[42] Pires AM, Serra OA, Davolos MR (2005) **Morphological and luminescent studies on nanosized Er, Yb-Yttrium oxide up-converter prepared from different precursors**, J. Lumin. 113:174-182.

[43] Qin X, Yokomori T, Ju Y (2007) **Flame synthesis and characterization of rare-earth (Er^{3+}, Ho^{3+}, and Tm^{3+}) doped upconversion nanophosphors**, Appl. Phys. Lett. 90:073104.

[44] Wang L, Yan R, Huo Z, Wang L, Zeng J, Bao J, Wang X, Peng Q, Li Y (2005) **Fluorescence resonant energy transfer biosensor based on upconversion-luminescent nanoparticles**, Angew Chem. Int. Ed. 44:6054-6057, Angew. Chem. 117:6208-6211.

[45] Wei Y, Lu F, Zhang X, Chen D (2007) **Synthesis and characterization of efficient near-infrared upconversion Yb and Tm codoped $NaYF_4$ nanocrystal reporter** J. Alloy Compd. 427:333-340.

[46] Li ZQ, Zhang Y (2008) **An efficient and user-friendly method for the synthesis of hexagonal-phase $NaYF_4$:Yb, Er/Tm nanocrystals with controllable shape and upconversion fluorescence**, Nanotechnol 9, 345606.

[47] Wang F, Liu XG (2008) **Upconversion multicolor fine-tuning: visible to near-infrared emission from lanthanide-doped $NaYF_4$ nanoparticles**, J. Am. Chem. Soc. 130:5642- 5643.

[48] Yang LW, Han HL, Zhang YY, Zhong JX (2009) **White emission by frequency up-conversion in Yb^{3+}-Ho^{3+}-Tm^{3+} triply doped hexagonal $NaYF_4$ nanorods,** J. Phys. Chem. C 113:18995–18999.

[49] Chen G, Liu H, Somesfalean G, Liang H, Zhang Z(2009) **Upconversion emission tuning from green to red in Yb^{3+}/Ho^{3+}-codoped $NaYF_4$ nanocrystals by tridoping with Ce^{3+} ions,** Nanotechnol 20:385704.

[50] Liang HJ, Chen GY, Li L, Liu Y, Qin F, Zhang Z (2009) **Upconversion luminescence in Yb3+/Tb3+ -codoped monodisperse $NaYF_4$ nanocrystals** Optics. Commun. 282:3028-3031.

[51] Shan J, Qin X, Yao N, Ju Y (2007) **Synthesis of monodisperse hexagonal $NaYF_4$:Yb, Ln (Ln = Er, Ho and Tm) upconversion nanocrystals in TOPO**, Nanotechnol 18:445607.

[52] Kumar R, Nyk M, Ohulchanskyy TY, Flask CA, Prasad PN (2009) **Combined optical and mr bioimaging using rare earth ion doped $NaYF_4$ nanocrystals**, Adv. Funct. Mater. 19:853-859.

[53] Wang H-Q, Nann T (2009) **Monodisperse upconverting nanocrystals by microwave-assisted synthesis**, ACS Nano 3:3804-3808.

[54] Ehlert O, Thomann R, Darbandi M, Nann T (2008) **A four-color colloidal multiplexing nanoparticle system**, ACS Nano 2:120-124.

[55] Wang G, Peng Q, Li Y (2009) **Upconversion luminescence of monodisperse CaF_2:Yb^{3+}/Er^{3+} nanocrystals**, J. Am. Chem. Soc. 131:14200-14201.

[56] Du Y-P, Zhang Y-W, Sun L-D, Yan C-H (2008) **Luminescent monodisperse nanocrystals of lanthanide oxyfluorides synthesized from trifluoroacetate precursors in high-boiling solvents**, J. Phys. Chem. C 112:405-415.

[57] Liu Y, Pisarski WA, Zeng S, Xu C, Yang Q (2009) **Tri-color upconversion luminescence of rare earth doped $BaTiO_3$ nanocrystals and lowered color separation**, Opt. Express 17:9089-9098.

[58] Singh SK, Singh AK, Kumar D, Prakash O, Rai SB (2010) **Efficient UV–visible up-conversion emission in Er^{3+}/Yb^{3+} co-doped La_2O_3 nano-crystalline phosphor**, Appl. Phys. B. 98:173-179.

[59] Yang J, Zhang C, Peng C, Li C, Wang L, Chai R, Lin J (2009) **Controllable red, green, blue (RGB) and bright white upconversion luminescence of Lu_2O_3:Yb^{3+}/Er^{3+}/Tm^{3+} nanocrystals through single laser excitation at 980 nm**, Chem. Eur. J 15:4649-4655.

[60] Kamimura M, Miyamoto K, Saito Y, Soga K, Nagasaki Y (2008) **Design of poly(ethylene glycol)/streptavidin coimmobilized upconversion nanophosphors and their application to fluorescence biolabeling**, Langmuir 24:8864-8870.

[61] Wang L, Zhao W, Tan W (2008) **Bioconjugated silica nanoparticles: development and applications**, Nano Res. 1:99-115

[62] Knopp D, Tang D, Niessner R (2009) **Review: bioanalytical applications of biomolecule-functionalized nanometer-sized doped silica particles**, Anal. Chim. Acta 7:14-30.

[63] Yi GS, Chow GM: **Synthesis of hexagonal-phase $NaYF_4$: Yb, Er and $NaYF_4$: Yb, Tm nanocrystals with efficient up-conversion fluorescence**, Adv. Funct. Mater. 2006, 16: 2324-2329.

[64] Boyer JC, Manseau MP, Murray JI, van Veggel FCJM (2010) **Surface modification of upconverting $NaYF_4$ nanoparticles with PEG-phosphate ligands for NIR (800 nm) biolabeling within the biological window**, Langmuir 26:1157-1164.

[65] Cao T, Yang T, Gao Y, Yang Y, Hu H, Li F (2010) **Water-soluble $NaYF_4$: Yb/Er upconversion nanophosphors: synthesis, characteristics and application in bioimaging.** Inorg. Chem. Comm. 13:392-394.

[66] Kim WJ, Nyk M, Prasad PN (2009) **Color-coded multilayer photopatterened microstructures using lanthanide (III) ion co-doped $NaYF_4$ nanoparticles with upconversion luminescence for possible applications in security**, Nanotechnol. 20:185301-185307.

[67] Xiong L-Q, Chen Z-G, Yu M-X, Li F-Y, Liu C, Huang C-H (2009) **Synthesis, characterization, and in vivo targeted imaging of amine-functionalized rare-earth up-converting nanophosphors**, Biomaterials 30:5592-5600.

[68] Chen Z, Chen H, Hu H, Yu M, Li F, Zhang Q, Zhou Z, Yi T, Huang C (2008) **Versatile synthesis strategy for carboxylic acid-functionalized upconverting nanophosphors as biological labels**, J. Am. Chem. Soc. 130:3023-3029.

[69] Zhou H-P, Xu C-H, Sun W. Yan C-H (2009) **Clean and flexible modification strategy for carboxyl/aldehyde-functionalized upconversion nanoparticles and their optical applications**, Adv. Funct. Mater. 19:3892-3900.

[70] Zhou H-P, Xu C-H, Sun W, Yan C-H(2009) **Clean and flexible modification strategy for carboxyl/aldehyde-functionalized upconversion nanoparticles and their optical applications,** Adv. Funct. Mater. 19:3892-3900.

[71] Chatterjee DK, Rufaihah AJ, Zhang Y (2008) **Upconversion fluorescence imaging of cells and small animals using lanthanide doped nanocrystals**, Biomaterials 29:937-943.

[72] Yi GS, Chow GM (2007) **Water-soluble $NaYF_4$:Yb,Er (Tm)/$NaYF_4$/polymer core/shell/shell nanoparticles with significant enhancement of upconversion fluorescence**, Chem. Mater. 19:341-343.

[73] Wang L, Zhang Y, Zhu Y (2010) **One-pot synthesis and strong near-infrared upconversion luminescence of poly(acrylic acid)-functionalized YF_3: Yb^{3+}/Er^{3+}**, Nano Res. 3:317-325.

[74] Ungun B, Prud'himme RK, Budijono SJ, Shan J, Lim SF, Ju Y, Austin R (2009) **Nanofabricated upconversion nanoparticles for photodynamic therapy**, Opt. Express 17:80-86.

[75] Hilderbrand SA, Shao F, Salthouse C, Mahmood U, Weissleder R (2009) **Upconversion luminescent nanomaterials: application to in vivo bioimaging**, Chem. Comm. 4188-4190.

[76] Wang L, Li Y (2006) **Green upconversion nanocrystals for DNA detection**, Chem. Comm. 2557-2559.

[77] Zhang H, Li Y, Ivanov IA, Qu Y, Huang Y, Duan X (2010) **Plasmonic modulation of the upconversion fluorescence in $NaYF_4$:Yb/Tm hexaplate nanocrystals using gold nanoparticles or nanoshells**, Angew. Chem. Int. Ed. 49:2865-2868.

[78] Sivakumar S, Diamente PR, van Veggel FCJM (2006) **Silica-coated Ln^{3+}-doped LaF_3 nanoparticles as robust down- and upconverting biolabels**, Chem. Eur. J. 12:5878-5884.

[79] Jalil RA, Zhang Y (2008) **Biocompatibility of silica coated $NaYF_4$ upconversion fluorescent nanocrystals**, Biomaterials 29:4122-4128.

[80] Hu H, Xiong L, Zhou J, Li F, Cao T, Huang C (2009) **Multimodal-luminescence core-shell nanocomposites for targeted imaging of tumor cells**, Chem. Eur. J. 15:3577-3584.

[81] Zako T, Nagata H, Terada N, Utsumi A, Sakono M, Yohda M, Ueda H, Soga K, Maeda M (2009) **Cyclic RGD peptide-labeled upconversion nanophosphors for tumor cell-targeted imaging**, Biochem. Biophys. Res. Comm. 381:54-58.

[82] Kong D, Quan Z, Yang J, Yang P, Li C, Lin J (2009) **Avidin conjugation to up-conversion phosphor $NaYF_4:Yb^{3+},Er^{3+}$ by the oxidation of the oligosaccharide chains**, J. Nanopart. Res. 11:821-829.

[83] Wang M, Hou W, Mi C-C, Wang W-X, Xu Z-R, Teng H-H, Mao C-B, Xu S-K (2009) **Immunoassay of goat antihuman immunoglobulin G antibody based on luminescence resonance energy transfer between near-infrared responsive $NaYF_4$: Yb, Er upconversion fluorescent nanoparticles and gold nanoparticles**, Anal. Chem. 81:8783-8789.

[84] Wang M, Mi C-C, Wang W-X, Liu C-H, Wu Y-F, Xu Z-R, Mao C-B, Xu S-K (2009) **Immunolabeling and NIR-excited fluorescent imaging of HeLa cells by using $NaYF_4$:Yb,Er upconversion nanoparticles**, ACS Nano 3:1580-1586.

[85] Jiang S, Zhang Y (2010) **Upconversion nanoparticles-based FRET system for study of siRNA in live cells**, Langmuir 26:6689-6694.

[86] Guo H, Li Z, Qian H, Hu Y, Muhammad IN (2010) **Seed-mediated synthesis of $NaYF_4$:Yb, Er/$NaGdF_4$ nanocrystals with improved upconversion fluorescence and MR relaxivity**, Nanotechnol. 21:125602 (6pp).

[87] Li Z, Zhang Y (2006) **Monodisperse silica-coated polyvinylpyrrolidone/$NaYF_4$ nanocrystals with multicolor upconversion fluorescence emission**, Angew. Chem. Int. Ed. 45:7732-7735, Angew. Chem. 118:7896-7899.

[88] Liu Z, Yi G, Zhang H, Ding J, Zhang Y, Xue J (2008) **Monodisperse silica nanoparticles encapsulating upconversion fluorescent and superparamagnetic nanocrystals**, Chem. Comm. 694-696.

[89] Li Z, Zhang Y, Jiang S (2008) **Multicolor core/shell-structured upconversion fluorescent nanoparticles**, Adv. Mater. 20:4765-4769.

[90] Qian HS, Guo HC, Ho PC-L, Mahendran R, Zhang Y(2009) **Mesoporous-silica-coated Up-conversion fluorescent nanoparticles for photodynamic therapy**, Small 5:2285-2290.

[91] Mader H, Li X, Saleh S, Link M, Kele P, Wolfbeis OS (2008) **Fluorescent silica nanoparticles**, Ann. N. Y. Acad. Sci. 1130:213-223.

[92] Achatz DE, Mező G, Kele P, Wolfbeis OS (2009) **Probing the activity of matrix metallopreteinase II with a sequentially click-labeled silica nanoparticle FRET probe**, ChemBioChem 10:2316-2320.

[93] Mader HS, Link M, Achatz DE, Uhlmann K, Li X, Wolfbeis OS (2010) **Surface-modified upconverting microparticles and nanoparticles for use in click chemistries,** Chem. Eur. J. 16:5419-5426.

[94] Xu CT, Svensson N, Axelsson J, Svenmarker P, Somesfalean G, Chen G, Liang H, Liu H, Zhang Z, Andersson-Engels S (2008) **Autofluorescence insensitive imaging using upconverting nanocrystals in scattering media**, Appl. Phys. Lett. 93:171103.

[95] Chatterjee DK, Jalil RA, Zhang Y (2008) **Upconversion fluorescence imaging of cells and small animals using lanthanide doped nanocrystals**, Biomaterials 29:937-943.

[96] Wu S, Han G, Milliron DJ, Aloni S, Altoe V, Talapin DV, Cohen BE, Schuck PJ (2009) **Non-blinking and photostable upconverted luminescence from single lanthanide-doped nanocrystals**, Proc. Natl. Acad. Sci. USA 106:10917–10921.

[97] Wang M, Mi C, Zhang Y, Liu J, Li F, Mao C, Xu S (2009) **NIR responsive silica-coated $NaYbF_4$:Er/Tm/Ho upconversion fluorescent nanoparticles with tunable emission colors and their applications in immunolabeling and fluorescent imaging**, J. Phys. Chem. C 113:19021–19027.

[98] Shan J, Chen J, Meng J, Collins J, Soboyejo W, Friedberg JS, Ju Y (2008) **Biofunctionalization, cytotoxicity and cell uptake of lanthanide doped hydrophobically ligated NaYF4 upconversion nanophosphors**, J. Appl. Phys. 104:094308-1-7.

[99] Zhou J, Sun Y, Du X, Xiong L, Hu H, Li F (2010) **Dual-modality in vivo imaging using rare-earth nanocrystals with near-infrared to near infrared (NIR-to-NIR) upconversion luminescence and magnetic resonance properties**, Biomaterials 31:3287–3295.

[100] Gai S, Yang P, Li C, Wang W, Dai Y, Niu N, Lin J (2010) **Synthesis of magnetic, up-conversion luminescent, and mesoporous core-shell-structured nanocomposites as drug carriers**, Adv. Funct. Mater. 20:1166–1172.

[101] Idris NM, Li Z, Ye L, Sim EKW, Mahendran T, Ho PCL, Zhang Y(2009) **Tracking transplanted cells in live animal using upconversion fluorescent nanoparticles**, Biomaterials 30:5104-5113.

3 Novel Multicolor Fluorescently Labeled Silica Nanoparticles for Interface Fluorescence Resonance Energy Transfer to and from Labeled Avidin

3.1 Abstract

Fluorescent silica nanoparticles (SiNPs) were prepared by covalent attachment of fluorophores to the amino-modified surface of SiNPs with a typical diameter of 15 nm. The SiNPs are intended for use in novel kinds of fluorescence resonance energy transfer (FRET)-based affinity assays at the interface between nanoparticle and sample solution. Various labels were employed to obtain a complete set of colored SiNPs, with excitation maxima ranging from 337 to 659 nm and emission maxima ranging from 436 nm to the near infrared (710 nm). The nanoparticles were characterized in terms of size and composition using transmission electron microscopy, thermogravimetry, elemental analysis, and dynamic light scattering. The surface of the fluorescent SiNPs was biotinylated, and binding of labeled avidin to the surface was studied via FRET in two model cases. In the first, FRET occurs from the biotinylated fluorescent SiNP (the donor) to the labeled avidin (the acceptor). In the second, FRET occurs in the other direction. Aside from its use in the biotin–avidin system, such SiNPs also are believed to be generally useful fluorescent markers in various kinds of FRET assays, not the least because the fluorophore is located on the surface of the SiNPs (and thus always much closer to the second fluorophore) rather than being doped deep in its interior.

3.2 Introduction

Silica nanoparticles (SiNPs) play an important role in various areas of nanotechnology[1] because they are nontoxic, commercially available, and can be easily separated from aqueoussuspensions by centrifugation due to their higher specific density. Most SiNPs are highly biocompatible, have a large specific surface that can be easily functionalized, and can be delivered into the living cell, for example for purposes of intracellular biosensing and imaging.[2,3,4] On the other side, their tendency towards aggregation (to form clusters, particularly in aqueous solution) is a severe disadvantage and is difficult to avoid, unless the surface is modified, e.g., by PEGylation.[5]

Given the widespread use of fluorescence in biophysical and bioanalytical sciences, various kinds of fluorescent SiNPs have been described so far. Bright and stable core-shell fluorescent SiNPs were made by encapsulation of organic dye molecules that were first covalently conjugated to a silica precursor in a Stöber process. Fluorophores that cover the entire UV–vis absorption and emission range were employed to result in monodisperse NPs in the size range of 20–30 nm and amenable to specific labeling of antibodies for bioimaging.[6] Dye-doped silica nanoparticles also were prepared by a water-in-oil microemulsion technique as well.[7,8] Other interesting examples include the co-encapsulation of two-photon fluorescent dye nanoaggregates as energy up-converting donors and a photosensitizing photodynamic therapy drug as an acceptor in SiNPs has been used to monitor the in vitro cytotoxic effect on tumor cells due to singlet oxygen.[9] Another group has reported on particles that comprise a fluorescein isothiocyanate-doped silica core coated with a monolayer of nanocrystalline CdTe quantum dots followed by a silica shell.[10]

Among the luminescent dopants for silica, transition metal complexes and lanthanides are frequently applied. Hybrid silica nanoparticles with a luminescent [$Ru(bpy)_3$] core (bpy=2,2′-bipyridine), and a paramagnetic monolayer coating of a silylated gadolinium complex may be applied as multimodal contrast agents for in vitro optical and magnetic resonance imaging after cell uptake.[11] A sensitive fluoroimmunoassay for recombinant human interleukin-6 with functionalized $Ru(bpy)_3$-encapsulated core-shell silica nanoparticles has been presented.[12] Core-shell SiNPs comprised of a $Ru(bpy)_3$-doped silica core and a doped silica shell were synthesized and post functionalized with encoding fluorescence for multiplex imaging.[13] Silica nanoparticles were doped with Eu^{3+} or Dy^{3+} and Au nanoparticles incorporated into their surface.[14] $Ru(bpy)_3$ immobilized on silica nanoparticles together with Au nanoparticles were reported for use in electrogenerated chemiluminescence detection.[15] Hence, there is widespread interest in such nanoparticles.

Fluorescent SiNPs have advantages over organic (fluorescent) labels in being much brighter because a single SiNP can contain hundreds of fluorophores. Moreover, the fluorophore of a SiNP is mostly contained in a benign environment, which makes it less sensitive to environmental effects (of proteins, for example) and more photostable. Hence, fluorescent NPs have been used in DNA assays[16,17] to monitor the delivery of DNA into the nucleus and for monitoring the process of gene transfection in cultured cells,[7] in immunoassays, [8,18,19,20,21] and enzymatic assays.[22] Numerous kinds of SiNPs were shown to be useful in sensor development,[23,24] drug delivery,[25,26] modification of surfaces,[22,27] and in

context with magnetic separation (based on magnetic cores inside SiNPs).[28] The group of Wang and Tan[29] has presented various kinds of fluorescent SiNPs, mainly for purposes of encoding and for detecting fluorescence resonance energy transfer (FRET) between different kinds of particles. SiNPs were prepared that are containing up to three fluorophores insider the SiNP, and FRET can occur there because the dyes are within the Förster distance (typically <10 nm). As a result, the color of emission can be varied despite the wavelength of excitation being the same in all cases. Such particles can be surface-modified with biotin and then bind to other particles (usually microparticles carrying (strept)avidin on their surface).

The FRET-based affinity system described here is entirely different in that (a) the SiNPs are labeled on the surface only (so as to remain within the Förster distance all the time), (b) the affinity interaction is occurring at the surface of a single kind of particle (rather than two kinds of particles), which makes the system more simple, and (c) FRET is occurring directly from (or to) the fluorophores at the surface to (or from) fluorescently labeled avidin, rather than from particle to particle. The rate and efficiency of energy transfer is known to depend on the negative sixth power of the distance between the donor and the acceptor, and all the fluorophores in our system are likely to be within this distance. This results in high FRET efficiency. The biotin–avidin system was chosen because it is one of the most widely used model system in the literature and has been often used in various kinds of affinity assays before.[30,31] We also are presenting here SiNPs with colors in absorption and emission that range from the UV to the near-IR so as to enlarge the spectral variability of such SiNPs for various kinds of other studies.

3.3 Experimental

3.3.1 Materials

SiNPs consisting of amorphous SiO_2 (99.5% purity), 15 nm in diameter, were purchased from Nanostructured and Amorphous Materials Inc. (www.nanoamor.com). 3-Aminopropyltriethoxy-silane (APTS) (98%), N-(3-dimethylaminopropyl)- N′-ethylcarbodiimide hydrochloride (EDC), N-hydroxysuccinimide, biotin N-hydroxysuccinimide ester, fluorescein isothiocyanate (FITC), and rhodamine B isothiocyanate (RITC) were purchased from Sigma (www. sigmaaldrich.com). Alexa Fluor 350 carboxy acid succinimidyl ester, Oregon Green 488 (2′,7′-difluorofluorescein), and fluorescein-labeled

avidin (from avidin egg white, dye-to- protein ratio 3:4:1) were purchased from Molecular Probes (www.probes.com); Chromeo 642 was from Active Motif Chromeon (www.activemotif.com); merocyanine UR-800 is from FEW Chemicals (Wolfen, Germany; www.few.de). 4-Amino-1,8-naphthalimide-N-caproic (ANIC) acid was synthesized according to literature procedures.[32] Organic solvents were of analytical quality and used as received.

3.3.2 Instrumentation

Fluorescence spectra were acquired on an Aminco-Bowman Series 2 luminescence spectrometer from SLM Inc. (www.thermoelectron.com) equipped with a 150-W cw xenon lamp as the light source. Thermogravimetric analyses were performed on a thermal analyzer (model TGA-7; from Perkin Elmer; www.perkinelmer.com) at a heating rate of 10 °C min^{-1} under nitrogen atmosphere. The specific surface area of the SiNPs was determined by the nitrogen adsorption method of Brunauer, Emmett, and Teller[33] using an instrument from Micrometrics (model ASAP 2010; www.micromertics.com). Particle sizes and zeta potentials were measured on a Malvern Zetasizer 3000 DTS 5300 Instrument (www.malvern.com) at pH 6. It can measure particle sizes ranging from 0.6 nm to 6 μm. Transmission electron microscopy was performed on a Tecnai F 30 instrument from FEI (www.fei.com).

3.3.3 Preparation of Modified SiNPs

In a typical reaction, 0.5 mL of APTS was added to 100 mg of SiNPs suspended in 25 mL of toluene under nitrogen and heating to ~95 °C for 4 h. The resulting SiNPs (type A in figure 3.1) were isolated after several cycles of centrifugation (10 min at 4,400 rpm) and washing (two times ethanol and two times acetone). The modified SiNPs were dried on air at ~60 °C in an oven for 12 h.

3.3.4 Preparation of Fluorescent SiNPs

A suspension of 5.0 mg of the amino-modified SiNPs of type A in a mixture of 3 mL of ethanol and 150 μL of a 10 mmol L^{-1} borate buffer (pH 9.3) was reacted with 127 μL of

reactive label (1 mg mL^{-1} solution) in the dark for 2 h at room temperature. The resulting NPs (type B) were isolated by four cycles of centrifugation (10 min at 4,400 rpm) and washing (two times ethanol and two times acetone).

A different procedure was carried out with Oregon Green 488. First, the carboxy group of Oregon Green dye (381 µL of a 1 mg mL^{-1} solution in ethanol) was activated in the presence of 2.0 mg EDC in 10 mL of water for 2 h at room temperature to give an active imidoester. Then, without further purification, 10.0 mg of the aminomodified SiNPs was added. The reaction was allowed to proceed for 2 h at room temperature in the dark. The resulting green-fluorescent SiNPs were isolated again by four cycles of centrifugation (10 min at 4,400 rpm) and washing (two times water and two times ethanol). The NPs were dried at ~60 °C in an oven for 12 h.

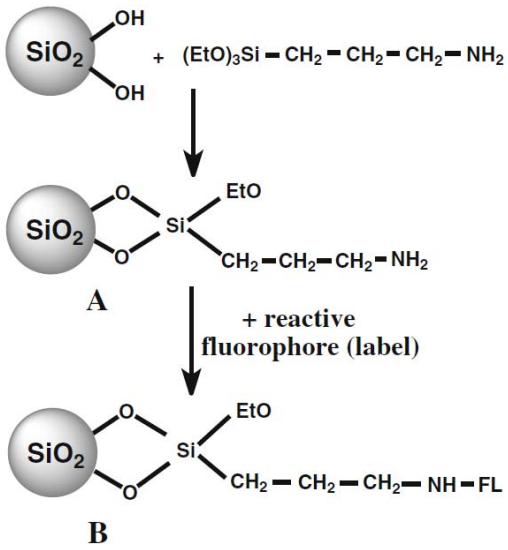

Figure 3.1 Schematic representation of the surface chemistry applied leading to amino-modified SiNPs (type A) and subsequent conjugation of a fluorophore FL to form SiNPs of type B.

3.3.5 Preparation of Fluorescent SiNPs with the Merocycanine Label UR-800

A suspension of 20 mg of amino-modified SiNPs was treated with a mixture of 250 µL of a 1 mg mL^{-1} methanol solution of the label UR-800 under nitrogen overnight at ~65 °C under magnetic stirring. The color of the resulting fluorescent NPs changed to blue. The solvents

were removed using a rotary evaporator, and the NPs deposited were washed by re-suspending them in methanol, followed by four cycles of centrifugation (10 min at 4,400 rpm) and washing (two times methanol and two times water). The NPs were dried at ~60 °C in an oven for 12 h.

3.3.6 Preparation of Biotinylated SiNPs

A suspension of 40 mg of amino-modified SiNPs (type A) in 1.5 mL of phosphate buffer (20 mmol L^{-1}) of pH 7.4 was reacted with 200 µL of biotin N-hydroxysuccinimide ester (1 mg mL^{-1} in water) for 2 h. The resulting biotinylated SiNPs were centrifuged (10 min at 4,400 rpm), washed four times with phosphate buffer to remove unbound biotin, and then dried and stored in a desiccator over diphosphorus pentoxide.

3.3.7 Preparation of Fluorescent Biotinylated SiNPs

A suspension of 30 mg of biotinylated SiNPs in 1.5 mL of phosphate buffer (20 mmol L^{-1}) of pH 7.4 was reacted with 112 µL of a 1 mg mL^{-1} aqueous solution of RITC for 2 h under stirring. The resulting fluorescent biotinylated SiNPs were purified by four cycles of centrifugation (10 min at 4,400 rpm) and washing (phosphate buffer) to remove excess label. When washing the solutions, they also were ultrasonicated to assist in the removal of any physically adsorbed fluorophores. The SiNPs were dried and stored in a desiccator over phosphorus pentoxide.

3.3.8 Preparation of Avidin Labeled with the Longwave Dye UR-800 (Av-UR-800)

A solution of 66 µL of the chlorinated merocycanine dye UR-800 (1 mg mL^{-1} in methanol) was added to an aqueous solution of 1 mg of avidin in 1 mL of phosphate buffer of pH 7.4 (20 mmol L^{-1}). The green mixture was slowly shaken in an Eppendorf thermomixer (www.eppendorf.com) overnight at ~40 °C. During this time, the color of the resulting solution changed to blue. This solution was used in further FRET experiments.

3.3.9 Energy Transfer Study using Bt-SiNP-RhB and Av-Flu

Aqueous solutions of Bt-SiNP-RhB (0.011 mmol L^{-1}) and Av-Flu (0.044 mmol L^{-1}) were mixed in ratios according to table 3.1 and were made up to a total volume of 2.5 mL with buffer of pH 7.4 (20 mmol L^{-1}). The concentration of Bt-SiNP-RhB was determined by photometry using a molar absorbance of 43,000 L (mol cm)$^{-1}$ for the conjugated dye (in water). Spectra were acquired immediately after mixing using an excitation wavelength of 430 nm.

Table 3.1 Volumes of standard solutions (in µL) applied for the FRET system between Av-Flu (0.044 mmol L^{-1}) and Bt-SiNP-RhB (0.011 mmol L^{-1}), and resulting molar ratios.

Volume of Av-Flu solution	Volume of Bt-SiNP -RhB solution	Volume of phosphate buffer	Resulting molar ratio	Associated spectrum in (figure 3.9)
40	0	2460	1 : 0	A
40	75	2385	1 : 0.48	B
40	100	2360	1 : 0.64	C
40	150	2310	1 : 0.96	D
40	200	2260	1 : 1.27	E
40	225	2235	1 : 1.44	F
40	325	2135	1 : 2.10	G
0	325	2175	0 : 1	H

3.3.10 Energy Transfer Study using Bt-SiNP-RhB and Av-UR

Aqueous solutions of Bt-SiNP-RhB (0.044 mmol L^{-1}) and of Av-UR-800 (0.011 mmol L^{-1}) were mixed in ratios according to table 3.2 and made up to a total volume of 2.5 mL with phosphate buffer of pH 7.4 (20 mmol L^{-1}). The concentration of Av-UR was determined by photometry using a molar absorbance of 174,000 L (mol cm)$^{-1}$ that was found for the model conjugate between UR-800 and isopropylamine in water solution. Spectra were acquired immediately after mixing using an excitation wavelength of 450 nm.

Table 3.2 Volumes (in µL) of standard solutions applied for the FRET system Av-UR-800 (0.011 mmol L^{-1}) and Bt-SiNP-RhB (0.044 mmol L^{-1}), and resulting molar ratios.

Volume of Bt-SiNP -RhB solution	Volume of Av-Flu solution	Volume of phosphate buffer	Resulting molar ratio	Associated spectrum in (figure 3.12)
40	0	2460	1 : 0	A
40	40	2385	1 : 0.98	B
40	80	2360	1 : 1.30	C
40	120	2310	1 : 1.96	D
40	160	2260	1 : 3.91	E
40	160	2235	0 : 1	F

3.4 Results

3.4.1 Chemical Modification of SiNPs

The surface of the SiNPs was modified using the reagent 3-APTS in toluene solvent to yield SiNPs carrying amino groups on their surface as shown as type A in figure 3.1. The presence of amino groups was proven by adding a solution of salicylaldehyde,[34,35] after which the SiNPs immediately turned yellow as a result of the formation of a colored Schiff base. In a control experiment, non-modified SiNPs gave no coloration with salicylaldehyde. Additional proof is provided by the experiments described in the following using amino-reactive labels.

3.4.2 Fluorescent Labeling of Silica Nanoparticles

The SiNPs were rendered fluorescent by covalent attachment of the following labels to their amino-modified surface: dansyl chloride (a sulfochloride), Alexa Fluor 350 (an amine-reactive N-hydroxysuccinimide (NHS) ester), FITC (containing an amino-reactive isothiocyanate group), RITC, Oregon Green (whose carboxy group first was made amino-reactive using the reagent EDC), a fluorescent aminonaphthalimide (ANIC; after first being converted into the NHS ester), and the blue (and red fluorescent) label Chromeo 642 (also an

NHS ester). The labels were directly reacted with the SiNPs in ethanol suspension in the dark for 2 h to give SiNPs of type B as shown in figure 3.1.

All kinds of reactive labels resulted in adequate labeling rates and efficiencies. The effect of non-covalent adsorption of dyes and labels varies form case to case. While some adsorption of the reactive dyes to the unmodified SiNPs can be observed in any case, a few centrifugation and washing cycles completely remove the fluorophores (as verified by fluorescence spectroscopy), while covalently labeled SiNPs could not be decolorized in this way. As centrifugation and washing procedures were used to remove excess of reactive label as well, it is assumed that the surface of the SiNPs was free of adsorbed labels.

The so-called chameleon labels represent a fairly new class of labels[36] that is characterized by the color change they undergo upon conjugation to amino groups. As a result, the conjugates can be spectrally differentiated from the unreacted label even if present in large excess. The blue pyrylium labels Py-1 (blue) and Py-5 (dark blue) were found to easily react with amino-SiNPs to yield the respective pink (Py-1) and red (Py-5) conjugates, which display a fairly strong fluorescence. Moreover, this is an additional proof for the presence of amino groups on the surface of the modified SiNPs.

SiNPs with long-wave absorption and emission are particularly interesting because all biomatter displays much less background luminescence in the long-wave part of the visible spectrum and because most biomatter is much better permeable to long- than to short-wave light. We have conjugated the chloro-substituted label UR-800 (see figure 3.2) to amino-modified SiNPs in methanol by stirring the suspension at 65°C overnight under nitrogen gas and magnetic stirring.

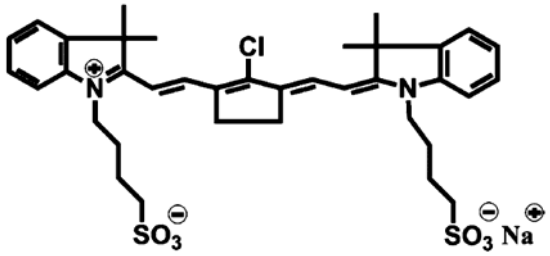

Figure 3.2 Chemical structure of the chameleon label UR-800.

The reactivity of UR-800 towards amino groups is due to an easily proceeding nucleophilic substitution of the chlorine atom in the center of the conjugated (chromophoric) π-electron system of the labels as shown in figure 3.3. This substitution reaction causes a significant

short-wave spectral shift from green (λ_{max} 800 nm) to blue (λ_{max} 659 nm). Hence, this label also may be considered as being a new kind of chameleon label. Most notably, it is virtually non-fluorescent in free form but gives a fluorescent conjugate with amines (see figure 3.4).

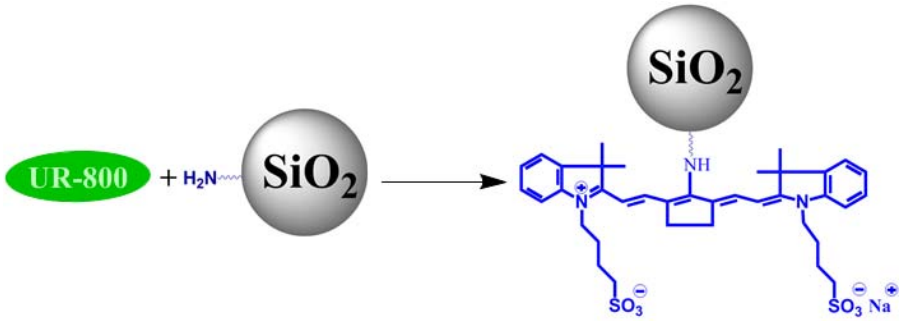

Figure 3.3 Reaction scheme for blue conjugation of UR-800 to Silica Nanoparticles

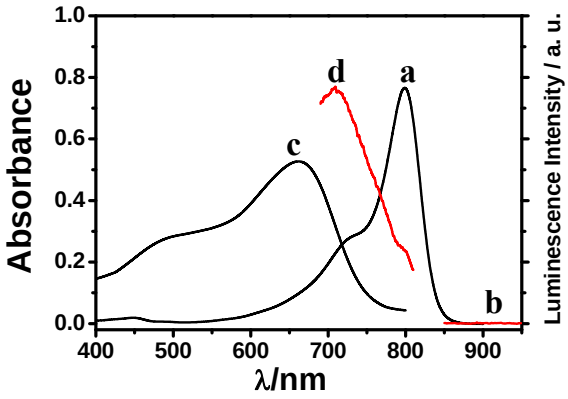

Figure 3.4 Chameleon effect of UR-800 on conjugation to amino-modified SiNPs. The absorption spectrum of UR-800 (line a) undergoes a hypsochromic shift on conjugation to amino-modified SiNPs (line c). The rather weak NIR emission of UR-800 in its nonconjugated state (line b) is spectrally well separated from the distinctly stronger red emission of the labeled SiNPs (line d).

3.4.3 Spectral Characterization of Labeled SiNPs

The spectra of the set of visible to NIR fluorescent SiNPs of type B are shown in table 3.3. They have absorption maxima that range from ~337 to 659 nm and emissions with maxima between 436 and 710 nm. The bandwidth (expressed here as BW@HM) vary to a large extent (see figure 3.5).

Table 3.3 Fluorophores used, absorption and emission maxima (in nm) of the fluorescently labeled silica nanoparticles, and spectral bandwidth of the emission band at half maximum (BW@HM) of emission band.

Fluorophore (mg)	λmax (exc.) /SiNPs	λ_{max} (em.)	BW@HM	(*w/w*) Dye (ng) /SiNPs (mg)
Conventional labels				
dansyl chloride	337	492	98	-
Alexa Fluor 350	346	436	54	-
ANIC[a]	441	520	63	-
Oregon Green 488	488	520	32	-
FITC[b]	492	525	36	193.4
RITC[c]	540	565	40	147.3
Chromeo 642	642	662	37	-
Chameleon labels				
Py-5	465	630	62	117.9
Py-1	503	602	94	174.2
UR-800[d]	659	710	64	116.8

(a) 4-amino-1,8-naphthalimide-N-caproic acid; (b) fluorescein isothiocyanate; (c) rhodamine B isothiocyanate; (d) for an overview on UR labels and their nomenclature, see http://www-analytik.chemie.uni-regensburg.de / wolfbeis/wolfbeis.htm.

The BW@HM value is a significant parameter in terms of using the particles in fluorescence energy transfer-based assays, and in multi-labeling and encoding. The Stokes' shifts range from as little as 15 nm to substantial 155 nm, which also allows some variation in the choice of labels. Furthermore, the weight ratio of the labeled dye in nanograms to SiNPs in milligrams was determined by photometry.

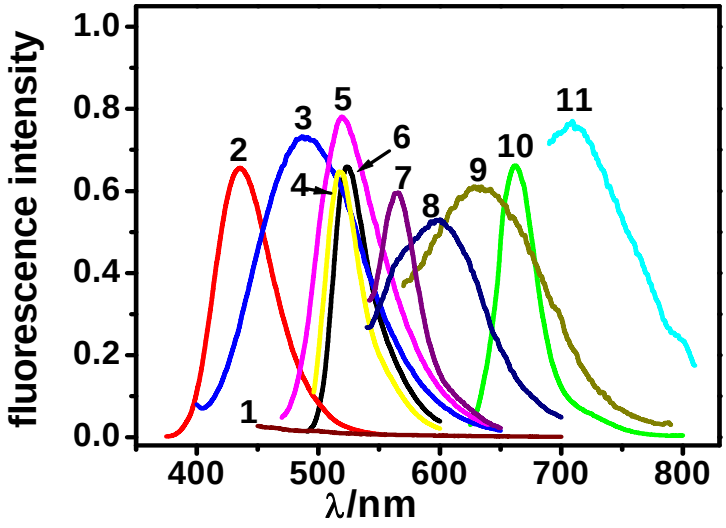

Figure 3.5 Emission spectra of (1) unmodified SiNPs; (2) Alexa Fluor 350-SiNPs; (3) dansyl chloride-SiNPs; (4) Oregon Green 488-SiNPs; (5) ANIC-SiNPs, (6) FITC-SiNPs; (7) RITC-SiNPs; (8) Py-1-SiNPs, (9) Py-5-SiNPs, (10) Chromeo 642-SiNPs, (11) UR-800-SiNPs.

It is mandatory to carefully control the quantity of label that is being conjugated onto the surface of the SiNPs. Too high loading results in self-quenching of the fluorophores and thus in reduced brightness. As a rule of thumb, it is recommended to prepare SiNPs of faint color.

3.4.4 Biotinylation of the SiNPs

Amino-modified SiNPs of type A were reacted with NHS-biotin in phosphate buffer to yield biotinylated SiNPs. Biotinylation was proven by C, H, N, and S elemental analysis and zeta potential measurements (see sections below). The remaining free amino groups on the biotinylated SiNPs can then be reacted with RITC in phosphate buffer to yield fluorescent biotinylated SiNPs that can act as both a donor and an acceptor in FRET experiments with fluorophore–avidin conjugates.

3.4.5 TEM and Zeta Potentials of SiNPs

Transmission electron microscopy (TEM) images of the SiNPs show that they are aggregated and amorphous, with particle sizes of typically 15 nm (see figure 3.6).[37] Also, TEM images of

amino-modified SiNPs show that the SiNPs have retained their size and aggregation properties.

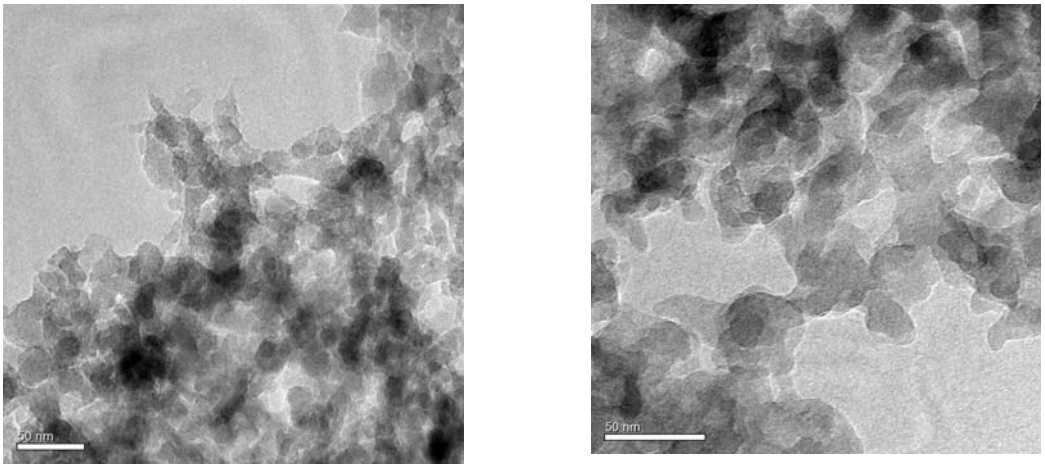

Figure 3.6 TEM pictures of SiNPs before (left) and after (right) amino-modification of the surface to yield particles of type A.

As expected, surface modification is accompanied by a change of the surface charge of the SiNPs as confirmed by measurements of zeta potentials at pH 6. Plain SiNPs are known to be negatively charged at pH 6 due to silanol groups that are dissociated. If suspended in water of pH 6, they have a zeta potential of −29.6 mV. Following modification with APTS, the potential changes to +36.1 mV due the presence of amino groups, which are positively charged at pH 6. The zeta potential of the biotinylated SiNPs is +16.1 mV, which obviously is due to a decrease in the density of amino groups on the surface, some of which will be consumed when conjugating biotin to the surface. Images of silica nanoparticles were collected on a transmission electron microscope (on a Tecnai F 30 instrument). The species were prepared by dispersing the nanoparticles in ethanol, placing a drop of it on a carbon-coated copper grid, and allowing to dry at room temperature.

3.4.6 Elemental and Thermogravimetric Analysis

The chemical composition of the surfaces of the SiNPs was investigated using conventional elemental analysis. Data are presented in table 3.4. The presence of nitrogen in the amino-modified SiNPs is clear evidence that APTS molecules have been bound to the surface. In contrast, no nitrogen was detected on the surface of the non-modified particles. The presence of a certain amount of hydrogen is due to alkyl group and also due to water bound to the unmodified SiNPs. After reacting with biotin, the detection of sulfur is proof for its successful attachment to the surface. Less than one third of the amino groups is modified with NHS-biotin (see the next section), which introduces two nitrogen atoms as well.

Table 3.4 Results of elemental analysis of SiNPs

type of SiNPs	% C	% H	% N	% S
non-modified	0.00	1.90 ± 0.030	0.00	0.00
amino-modified	6.02 ± 0.010	2.56 ± 0.043	1.98 ± 0.035	0.00
amino-modified and biotinylated	6.61 ± 0.010	2.44 ± 0.010	1.93 ± 0.020	0.52 ± 0.060

The resulting slight decrease of the nitrogen content of the biotinylated sample is well expressed by the respective C/N ratio. Regarding the content of carbon and hydrogen, the values of an elemental analysis of nanoporous materials need to be interpreted with caution due to a hardly predictable adsorption of CO2, aliphatic hydrocarbons, and water (humidity) from ambient air.

The modified SiNPs were also assessed by thermogravimetric analysis (TGA). Figure 3.7 shows the respective weight losses. The relatively small loss of plain SiNPs (plot a) is mainly due to removal of adsorbed water (whose presence also is confirmed by the result of the elemental analysis). Amino-modified SiNPs suffer from a larger weight loss, a fact that

again indicates the presence of APTS which decomposes at above 450 °C. The highest weight loss is observed for biotinylated SiNPs due to additional decomposition of biotin.

The loading of the surface with amino groups and biotin groups was quantified by using data on the calculated number of functional groups and on the specific surface area (S_{N2}) as obtained from BET measurements according to Brunauer, Emmett, and Teller.[33] The S_{N2} was determined to be 566 $m^2\ g^{-1}$, which is somewhat less than the value (640 $m^2\ g^{-1}$) given by the supplier. The density d_A of aminopropyl groups on the surface was calculated [33] using the following equation:

$$d_A(nm^{-2}) = \frac{(\Delta W_{CH} - \Delta W_{OH})N_A}{M_W S_{N_2}} \cdot 10^{-18}$$

where ΔW_{CH} and ΔW_{OH} are the ratios of weight loss for the modified and unmodified samples as measured by thermogravimetry, *Mw* is the molar mass of the aminopropyl group or biotin, S_{N2} is the BET-specific surface area as measured from the nitrogen adsorption isotherm, and NA is Avogadro's number. Using the experimental data for ΔW_{CH} and ΔW_{OH} of figure 3.7, the molecular mass of the aminopropyl group (58.1 g mol^{-1}) or biotin (227 g mol^{-1}; due to loss of the OH group on conjugation), and S_{N2} (566 $m^2\ g^{-1}$), the densities of the amino groups and the biotin groups per unit area of the surface of the SiNPs were calculated to be 0.591 and 0.195 nm^{-2}.

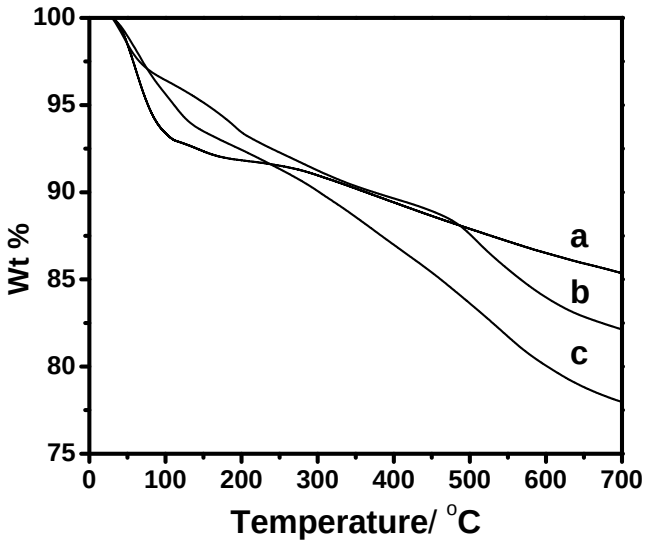

Figure 3.7 Thermogravimetric analysis of silica nanoparticles (SiNPs). (a) Non-modified SiNPs; (b) amino-modified SiNPs; (c) biotinylated SiNPs.

3.4.7 Fluorescence Resonance Energy Transfer Studies

FRET between a donor fluorophore and an acceptor fluorophore is an almost perfect tool[38,39,40,41] to detect whether two fluorescent species have a spatial proximity of less than typically 10 nm. FRET therefore is widely applied in bioanalytical sciences to study the interaction of species such as antigens and antibodies and of nucleic acid oligomers with their counterstrands, all of which display strong (non-covalent) interactions.

The biotin–(strept)avidin couple represents another kind of strong affinity binders, with a K_a as high as ~10^{14} to 10^{15} mol L^{-1}. For FRET to occur, it is mandatory to label both binding partners, usually with a donor fluorophore and an acceptor fluorophore. While this makes FRET assays more tedious than methods based on single labeling, it has the advantage of yielding two signals at two wavelengths whose intensity usually changes counterclockwise, so that the ratio of the two signals is detected.

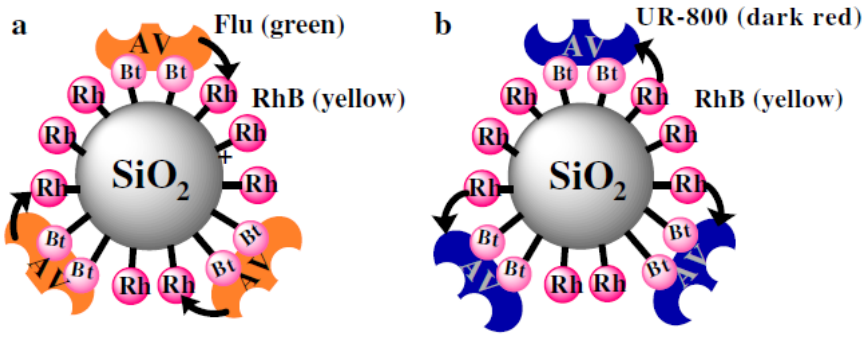

Figure 3.8 Schematic representation of the FRET model systems. A Energy transfer occurs from fluorescein-labeled avidin (the donor) to RITC-labeled biotinylated SiNPs (the acceptor). b Energy transfer occurs from RITC-labeled biotinylated SiNPs (the donor) to UR-800-labeled avidin (the acceptor).

We have investigated whether FRET may occur if avidin binds to the biotinylated SiNPs presented before. Two model systems were studied. In the first (figure 3.8a), FRET occurs from fluorescein-labeled avidin (Av-Flu) to biotinylated SiNPs labeled with rhodamine B (Bt-SiNP-RhB). In the second system (see figure 3.8b), FRET is demonstrated to occur in the reverse direction, i.e., from Bt-SiNP-RhB to avidin-labeled SiNPs with the long wave absorbing dye UR-800 (=Av-UR-800).

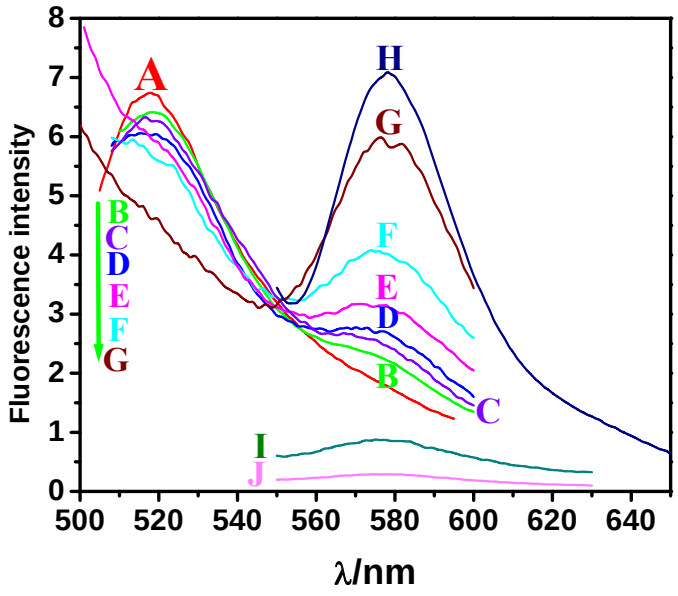

Figure 3.9 Study on the FRET between fluorescein-labeled avidin (the donor) and rhodamine-labeled biotinylated SiNPs (the acceptor). The molar ratio of rhodamine to fluorescein was varied from 1:0 (A),1:0.48 (B), 1:0.64 (C), 1:0.96 (D), 1:1.27 (E), 1:1.44 (F), 1:2.1 (G), and 0:1 (H). The emission spectra of rhodamine-labeled biotinylated SiNPs in the absence of fluorescein-labeled avidin with molar ratio of 0:0.48 (J) and 0:2.1 (I). See table 3.1

The results of a study on the (Av-Flu) to (Bt-SiNP-RhB) FRET system are shown in figure 3.9. There is a high degree of spectral overlap between the emission of fluorescein and the absorption of rhodamine B (see figure 3.10). Plot A is the (green) emission of the Av-Flu only (in the absence of Bt-SiNP-RhB), while plot H is the (yellow) emission of Bt-SiNP-RhB only (i.e., in the complete absence of Av-Flu).

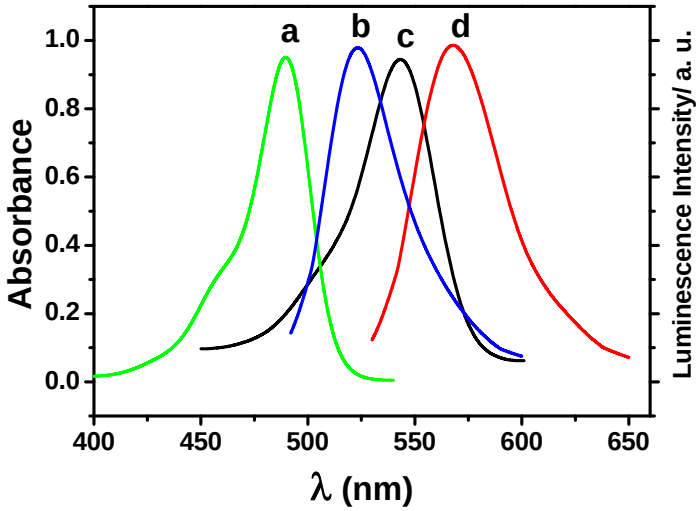

Figure 3.10 Spectra of pure FITC and RITC dyes (FRET Pair). (a) absorption spectrum of FITC, (b) emission spectrum of FITC, (C) absorption spectrum of RITC, (d) emission spectrum of RITC.

In a typical experiment, a solution of fluorescein-labeled avidin (Av-Flu) was prepared, and increasing quantities of biotinylated SiNPs labeled with RhB (Bt-SiNP-RhB) were added (details are outlined in table 3.1). As the labeled avidin is captured by the Bt-SiNP-RhB, the two fluorophores come in close proximity and FRET can occur. As a result, changes in the fluorescence spectra are found as shown in figure 3.9, where the fluorescence of Av-Flu at 520 nm decreases while that of the Bt-SiNP-RhB at 578 nm increases. The spectra clearly demonstrate efficient FRET between fluorescein and RhB on varying the molar ratio of RhB (on biotinylated NPs) from 0.48 to 2.1 (curves B to G) with respect to unit concentration of fluorescein. The effect of the concentration of rhodamine B on the efficiency of the FRET system was also studied. By comparing the fluorescence intensities of Bt-SiNP-RhB solutions (a) in the presence of Av-Flu (at ratios of 1:0.48 and 1:2.1; plots B, H) and (b) in the absence of Av-Flu but the same molar concentration of RhB (ratios of 0:0.48 and 0:2.1, respectively)

(see curves J and I in figure 3.9), one can see that the contribution caused by the increase in the concentration of RhB to the increase in FRET efficiency remains rather small.

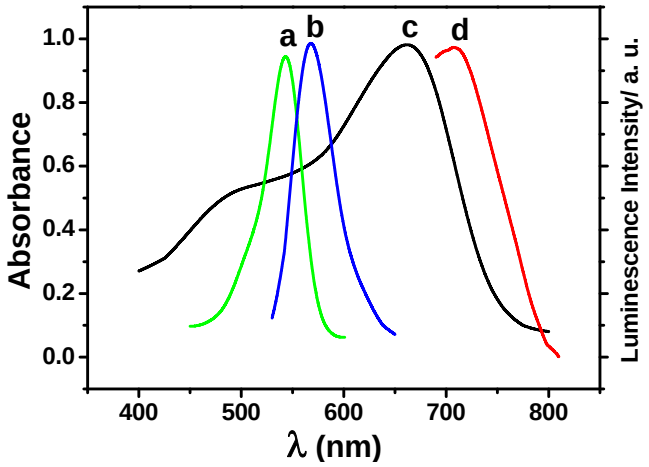

Figure 3.11 Spectra of pure RITC dye and amino modified UR-800 (FRET Pair). (a) absorption spectrum of RITC, (b) emission spectrum of RITC, (C) absorption spectrum of amino modified UR-800, (d) emission spectrum of amino modified UR-800.

In the second system studied, FRET occurs in the other direction, i.e., from the rhodamine-labeled SiNPs to avidin labeled with the long-wave dye UR-800. There is adequate spectral overlap between the emission spectra of RhB and the absorption spectra of the NIR dye (see figure 3.11), and indeed, efficient energy transfer does occur as shown in figure 3.12.
The emission of each single species of the binding couple is represented by spectra A and F. In A, the ratio is 0:1, and this results in the yellow fluorescence of rhodamine only. In F, the ratio is 1:0, and this results in the red fluorescence of UR-800 only. Increasing quantities of Av-UR-800 were added to a fixed quantity of Bt-SiNP-RhB (details in table 3.2). The increase of the fluorescence intensity of UR-800 can be seen in figure 3.12 (plots B to E). Obviously, efficient FRET occurs and results in (a) a decrease in the fluorescence intensity of biotinylated SiNPs-RhB at 578 nm and (b) an increase in the intensity of the long-wave emission at 700 nm. By comparing the fluorescence intensities of Av-UR-800 both in the presence of Bt-SiNP-RhB (at molar ratios of 1:0.98 and 1:3.91; see plots B and E) and (b) in the absence of Bt-SiNP-RhB (plots H and G in figure 3.12), one can conclude that the

contribution of the increase of concentration of the long-wave dye to the fluorescence increase is very small with respect to the efficiency of the energy transfer process.

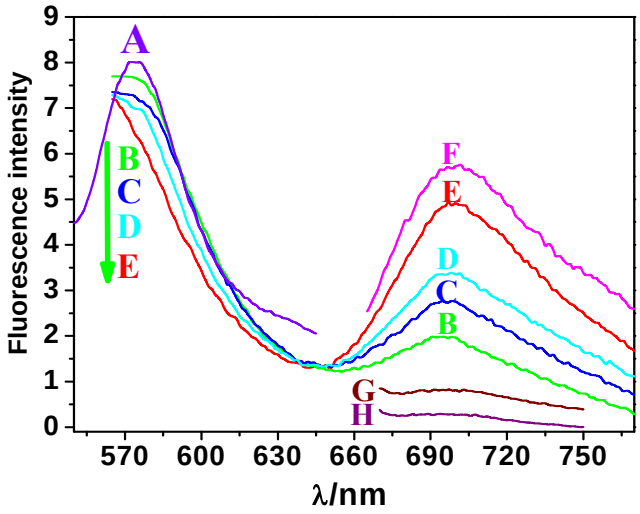

Figure 3.12 FRET study using rhodamine-labeled SiNPs (as the donor) and UR-800-labeled avidin (as the acceptor). The molar ratio of rhodamine label with biotinylated SiNPs to long-wave-avidin was varied from 1:0 (A), 1:0.98 (B), 1:1.30 (C), 1:1.96 (D), 1:3.91 (E), and 0:1 (F). The emission spectra of long-wave avidin in the absence of biotinylated SiNPs with molar ratio of 0:0.98 (H) and 0:3.91 (G). See table 3.2

3.4.8 Specificity, Interfacial Effects, and Effects of pH

In order to exclude the possibility of unspecific binding to the surface of the SiNPs, the FRET system between Av-Flu and SiNP-RhB was examined in the absence of biotin particles. Data are given in figure 3.9 and in table 3.1. They show that virtually no energy transfer is observed from the donor the acceptor (rhodamine) in the absence of biotinylated particles. This indicates that our system completely depends on the avidin–biotin affinity. The pH dependence of the affinity system based on FRET from fluorescein to rhodamine was carried out with a series of solutions with pH ranging from 6 to 9 and at an excitation wavelength of 430 nm. Nanoparticles of the type

Bt-SiNP-RhB (as an aqueous colloid) and fluorescein labeled avidin (Av-Flu; 0.044 mmol L^{-1}) were mixed in a molar ratio as described in row F in table 3.1. As was to be expected in view of the known pH dependence of the fluorescence of fluorescein, the intensity of the

fluorescein peak was found to increase with the pH of the solution, while the intensity ratio of Bt-SiNP-RhB to Av-Flu slightly decreased with increasing pH (see figure 3.13).

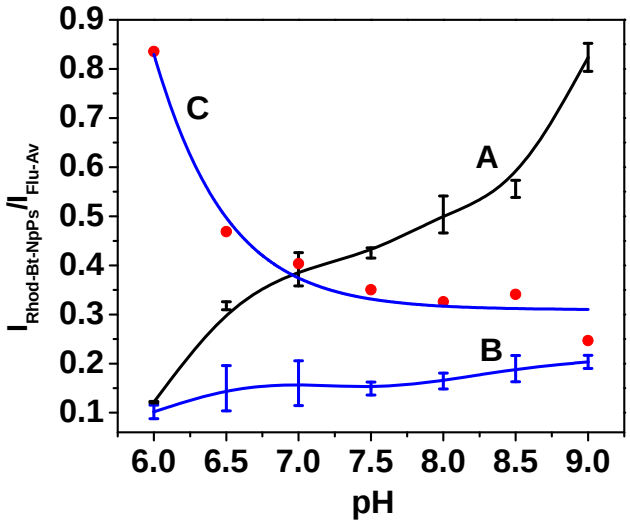

Figure 3.13 Effect of pH on (A) the luminescence intensity of the fluorescein–avidin conjugate, (B) the luminescence intensity of the rhodamine labeled biotinylated SiNPs, and (C) on the ratio of the luminescences of rhodamine-Bt-SiNP nanoparticles to fluorescein-labeled avidin (type F with molar ratio of 1.44:1 Rh/Flu; see table 3.1)

The pH dependence of system 2 (with the FRET occurring from rhodamine to the near-infrared label UR-800) was also studied with a series of solutions with pH values ranging from 6 to 9 and at an excitation wavelength of 450 nm. Avidin labeled with UR-800 (0.011 mmol L^{-1}) and Bt-SiNP-RhB (0.044 mmol L^{-1}) were mixed in the molar ratios given under D in table 3.2. Not unexpectedly (in view of the known pH independence of the fluorescence of rhodamines between 4 and 10), the intensity of the rhodamine peaks did not significantly change with the pH of solution (data not shown). The pH dependence of the fluorescence of the UR-800 labeled avidin also was measured in the absence of the donor particles (Bt-SiNP-RhB) at excitation/emission wavelengths of 659/710 nm. Both the excitation and emission peaks do not change with pH.

3.5 Discussion

We show that fluorescent labeling of the surface of aminomodified SiNPs is easily accomplished with various kinds of amine-reactive labels. These include conventional reagents such as sulfochlorides and NHS-active esters, but also reactive labels of the chameleon type. Long-wave absorbing and emitting SiNPs are certainly preferred for the reasons outlined before. We also demonstrate that the binding of biotin to avidin can be followed by FRET spectroscopy if one fluorophore is covalently linked to a SiNP. The direction of FRET is not restricted since it can occur from either a labeled protein (Av-Flu) to a biotinylated particle labeled with an acceptor, or vice versa. The (Av-Flu)-to-(Bt-SiNP-RhB) FRET system exhibits good efficiency, with an up to 6.8-fold increase of acceptor luminescence intensity. The FRET from (Bt-SiNP-RhB) to (Av-UR-800) also is efficient, with an up to 7.3-fold increase of acceptor luminescence intensity. This is also due to the fact that the distance for energy transfer is shorter, if the label is bound on the surface of the SiNP, as compared to a label that is encapsulated inside the particle. FRET-based methods like the one shown here are intrinsically self- referenced in that two signals can be measured (at two wavelengths) that change counterclockwise. Hence, the ratio of signals obtained is self-referenced and independent of variations in the intensity of the light source and the photodetector and also of geometrical factors.[42] Aggregation of the SiNPs is present according to the TEM spectra (figure 3.6) but does not seem to compromise avidin–biotin recognition and FRET. However, photoexcitation is better performed at 430 nm (in case of FITC) and at 450 nm (in case of RITC) in order to reduce the intensity of scattered light at the wavelength where emission intensity is measured. The (strept)avidin/biotin couple is one of the most widely used affinity systems. Recent applications include the avidin–biotin interactions on Fe_3O_4 nanoparticles,[43] its use in photoelectrochemical detection of biological affinity reaction,[30] in decorated core-shell nanoparticles for biorecognition studies by elastic light scattering,[44] in nanocomposites of colloidal gold particles and fatty acids,[45] in bioconjugations to Ln(III) ion-doped lanthanum trifluoride nanoparticles,[46] in superparamagnetic nanoparticles,[47] and in quantum dot biosensors for ultrasensitive multiplexed diagnostics.[48] Conceivable features of the nanoparticle-based FRET system presented here include applications in immunoassay and immunohistology, in labeling and in studies on (bio)molecular interactions at interfaces, high-throughput screening and receptor–ligand interactions, biosensing (and recognition at interfaces in general), DNA assay (that often is

based on FRET), and also other areas such as tumor targeting, "lab-on-a-particle" architectures, and intracellular delivery of drugs.

3.6 References

[1] Wang L, Wang KM, Santra S, Zhao XJ, Hilliard LR, Smith JE, Wu JR, Tan W (2006) **Watching Silica Nanoparticles Glow in the Biological World**, Anal. Chem. 78:646-654.

[2] Wang L, Zhao W, Tan W (2008) **Bioconjugated Silica Nanoparticles: Development and Applications**, Nano. Res. 1:99-115.

[3] S-Yapa MD, Phimphivong S, Coym JW, Wirth MJ, Aspinwall CA, Saavedra SS **(2007) Preparation and Characterization of Poly(lipid)-Coated, Fluorophore-Doped Silica Nanoparticles for Biolabeling and Cellular Imaging,** Langmuir 23:12624–12633.

[4] Tallury P, Payton K, Santra S (2008) **Silica-based multimodal/multifunctional nanoparticles for bioimaging and biosensing applications**, Nanomedicine 3:579-592.

[5] Xu H, Yan F, Monson EE, Kopelman R (2003) **Room-temperature preparation and characterization of poly(ethylene glycol)-coated silica nanoparticles for biomedical applications**, J. Bio. Mat. Res. 66A:870-879.

[6] Ow H, Larson DR, Srivastava M, Baird BA, Webb WW, Wiesner U (2005) **Bright and Stable Core Shell Fluorescent Silica Nanoparticles**, Nano. Lett. 5:113-117.

[7] Roy I, Ohulchanskyy TY, Bharali DJ, Pudavar HE, Mistretta RA, Kaur N, Prasad PN (2005) **Optical Tracking Of Organically Modified Silica Nanoparticles As DNA Carriers: A Nonviral, Nanomedicine Approach For Gene Delivery**, Proc. Natl. Acad. Sci. U. S. A. 102:279-284.

[8] He X, Duan J, Wang K, Tan W, Lin X, He C (2004) **A novel fluorescent label based on organic dye-doped silica nanoparticles for HepG liver cancer cell recognition**, J. Nanosci. Nanotechnol. 4:585-589.

[9] Kim S, Ohulchanskyy TY, Pudavar HE, Pandey RK, Prasad PN (2007) **Organically Modified Silica Nanoparticles Co-encapsulating Photosensitizing Drug and Aggregation-Enhanced Two-Photon Absorbing Fluorescent Dye Aggregates for Two-Photon Photodynamic Therapy**, J. Am. Chem. Soc.129:2669-2675.

[10] Kim S, Ohulchanskyy TY, Pudavar HE, Pandey RK, Prasad PN (2007) **Organically Modified Silica Nanoparticles Co-encapsulating Photosensitizing Drug and Aggregation-Enhanced Two-Photon Absorbing Fluorescent Dye Aggregates for Two-Photon Photodynamic Therapy**, J. Am. Chem. Soc.129:2669-2675.

[11] Rieter WJ, Kim JS, Taylor KM, An H, Lin W, Tarrant T, Lin W (2007) **Hybrid Silica Nanoparticles for Multimodal Imaging,** Angew. Chem. 119: 3754-3756; (2007) Angew. Chem. Int. Ed. 46:3680-3682.

[12] Hun X, Zhang Z (2007) **Functionalized fluorescent core-shell nanoparticles used as a fluorescent labels in fluoroimmunoassay for IL-6**, Biosens. Bioelectron. 22:2743-2748.

[13] Wu C, Hong J, Guo X, Huang C, Lai J, Zheng J, Chen J, Mu X, Zhao Y (2008) **Fluorescent core-shell silica nanoparticles as tunable precursors: towards encoding and multifunctional nano-probes**, Chem. Comm. 6:750-752.

[14] Petit L, Griffin J, Carlie N, Jubera V, García M, Hernández FE, Richardson K (2007) **Luminescence properties of Eu^{3+} or Dy^{3+}/Au co-doped SiO_2 nanoparticles,** Mat. Lett. 61:2879-2882.

[15] Qian L, Yang XR (2007) **One-Step Synthesis of Ru(2,2′-Bipyridine)$_3$ Cl_2-Immobilized Silica Nanoparticles for Use in Electrogenerated Chemiluminescence Detection**, Adv. Funct. Mater. 17:1353-1358.

[16] Rao KS, Rani SU, Charyulu DK, Kumar KN, Lee BK, Lee HY, Kawai T (2006) **A novel route for immobilization of oligonucleotides onto modified silica nanoparticles**, Anal. Chim. Acta. 576:177-183.

[17] Liu G, Wang J, Wu H, Lin Y, Lin Y (2007) **Nanovehicles Based Bioassay Labels**, Electroanalysis 19:777-785.

[18] Yang W, Zhang CG, Qu HY, Yang HH, Xua JG (2004) **Novel fluorescent silica nanoparticle probe for ultrasensitive immunoassays**, Anal. Chim. Acta 503:163-169.

[19] Schaertl S, Meyer-Almes FJ, Lopez-Calle E, Siemers A, Kramer J (2000) **A novel and robust homogeneous fluorescence-based assay using nanoparticles for pharmaceutical screening and diagnostics**, J. Biomol. Screen 5: 227-237.

[20] Wang FC, Yuan R, Chai YQ (2006) **Direct electrochemical immunoassay based on a silica nanoparticles/sol–gel composite architecture for encapsulation of immunoconjugate**, Appl. Microbiol. Biotechnol. 72:671-675.

[21] Santra S, Zhang P, Wang K, Tapec R, Tan W (2001) **Conjugation of Biomolecules with Luminophore-Doped Silica Nanoparticles for Photostable Biomarkers**, Anal. Chem. 73:4988-4993.

[22] Luckarift HR, Balasubramanian S, Paliwal S, Johnson GR, Simonian AL (2007) **Enzyme-encapsulated silica monolayers for rapid functionalization of a gold surface**, Colloids Surf. B 58:28-33.

[23] Burns A, Sengupta P, Zedayko T, Baird B, Wiesner U (2006) **Core/Shell Fluorescent Silica Nanoparticles for Chemical Sensing: Towards Single-Particle Laboratories**, Small 2:723-726.

[24] Slowing II, Trewyn BG, Giri S, Lin VS (2007) **Mesoporous Silica Nanoparticles for Drug Delivery and Biosensing Applications**, Adv. Funct. Mater. 17:1225-1236.

[25] Torney F, Trewyn BG, Lin VS, Wang K (2007) **Mesoporous silica nanoparticles deliver DNA and chemicals into plants**, Nature Nanotechnol. 2:295-300.

[26] Trewyn BG, Giri S, Slowing II, Lin VS (2007) **Mesoporous silica nanoparticle based controlled release, drug delivery, and biosensor systems**, Chem. Comm. 3236-3245.

[27] An Y, Chen M, Xue Q, Liu W (2007) **Preparation and self-assembly of carboxylic acid -functionalized silica**, J. Colloid Interface Sci. 311:507-513.

[28] Abou-Hassan A, Bazzi R, Cabuil V (2009) **Microfluidics in Inorganic Chemistry**, Angew. Chem. 121: 7316-7319.

[29] Wang L, Tan W (2006) **Multicolor FRET Silica Nanoparticles by Single Wavelength Excitation**, Nano. Lett. 6:84-88.

[30] Dong D, Zheng D, Wang FQ, Yang XQ, Wang N, Li YG, Guo LH, Cheng J (2004) **Quantitative Photoelectrochemical Detection of Biological Affinity Reaction: Biotin−Avidin Interaction**, Anal. Chem. 76:499-501.

[31] Hermanson GT (2008) in **Bioconjugate Techniques**, 2nd ed., Elsevier, 900-901.

[32] Link M, Schulze P, Belder D, Wolfbeis OS (2009) **New diode laser-excitable green fluorescent label and its application to detection of bovine serum albumin via microchip electrophoresis**, Microchim. Acta 166:183-188.

[33] Fuji M, Ueno S, Takei T, Watanabe T, Chikazawa M (2000) **Surface structural analysis of fine silica powder modified with butyl alcohol**, Colloid Polym. Sci. 278:30-36.

[34] Mahalingam V, Onclin S, Peter M, Ravoo BJ, Huskens J, Reinhoudt DB (2004) **Directed self-assembly of functionalized silica nanoparticles on molecular printboards through multivalent supramolecular interactions**, Langmuir 20:11756-11762.

[35] Schiestel T, Brunner H, Tovar GE (2004) **Controlled Surface Functionalization of Silica Nanospheres by Covalent Conjugation Reactions and Preparation of High Density Streptavidin Nanoparticles**, J. Nanosci. Nanotech. 4:504-511.

[36] Wetzl BK, Yarmoluk SM, Craig DB, Wolfbeis OS (2004) **Chameleon Labels for Staining and Quantifying Proteins**, Angew. Chem. 116:5515-5517; (2004) Angew. Chem. Int. Ed. 43:5400-5402.

[37] Nanostructured & Amorphous Materials, Inc. (2009) http://www.nanoamor.com/inc/pdetail?v=1&pid=260. Accessed October 2009

[38] Miller JN (2005) **Fluorescence energy transfer methods in bioanalysis**, Analyst 130:265–270.

[39] Medintz IL, Clapp AR, Mattoussi H, Goldman ER, Fisher B, Mauro JM (2003) **Self-assembled nanoscale biosensors based on quantum dot FRET donors**, Nat. Mater. 2:630-638.

[40] Tong AK, Jockusch S, Li ZM, Zhu HR, Akins DL, Turro NJ, Ju JY (2001) **Triple Fluorescence Energy Transfer in Covalently Trichromophore-Labeled DNA**, J. Am. Chem. Soc. 123:12923-12924.

[41] You X, Nguyen AW, Jabaiah A, Sheff MA, Thorn KS, Daugherty PS (2006) **Intracellular protein interaction mapping with FRET hybrids**, Proc. Natl. Acad. Sci. U. S. A. 103:18458-18463.

[42] Schaeferling M, Duerkop A in **Standardization and Quality Assurance in Fluorescence Measurements I: Techniques** (Springer Series on Fluorescence), Vol. 5 (Ed.: U. Resch-Genger, Springer, Berlin Heidelberg, 2008, pp. 373-414.

[43] Hirata N, Tanabe K, Narita A, Tanaka K, Naka K, Chujo Y, Nishimoto S (2009) **Preparation and fluorescence properties of fluorophore-labeled avidin–biotin system immobilized on Fe_3O_4 nanoparticles through functional indolequinone linker**, Bioorgan. Med. Chem. 17:3775-3781.

[44] Prosperi D, Morasso C, Tortora P, Monti D, Bellini T (2007) **Avidin decorated core-shell nanoparticles for biorecognition studies by elastic light scattering,** Chembiochem 8:1021-1028.

[45] Lala N, Sastry M (2000) **Nanocomposites of colloidal gold particles and fatty acids formed by the high-affinity biotin–avidin interaction**, Phys. Chem. Chem. Phys. 2: 2461-2466

[46] Diamente PR, Burke RD, van Veggel FCJM (2006) **Bioconjugation of Ln^{3+}-Doped LaF_3 Nanoparticles to Avidin**, Langmuir 22:1782-1788

[47] Park JA, Lee JJ, Kim IS, Park BH, Lee GH, Kim TJ, Ri HC, Kim HJ, Chang YM (2008) **Magnetic and MR relaxation properties of avidin–biotin conjugated superparamagnetic nanoparticles**, Colloid Surface A 313:288-291

[48] Geissler D, Charbonniere LJ, Ziessel RF, Butlin NG, Lohmannsröben HG, Hildebrandt N (2010) **Quantum Dot Biosensors for Ultrasensitive Multiplexed Diagnostics**, Angew. Chem. Int. Edit. 49: 1396-1401.

4 Detection of Biotin-Avidin Affinity Binding by Exploiting a Self-Referenced System Composed of Upconverting Luminescent Nanoparticles and Gold Nanoparticles

4.1 Abstract

We demonstrate an affinity system based on the interaction of two types of nanoparticles. The first type consists of upconverting $NaYF_4$:Yb,Er nanoparticles (UCLNPs) with a size of 40 – 100 nm, absorbing light in the infrared and showing green luminescence at 521 and 543 nm and red luminescent at 657 nm. The second type consists of gold nanoparticles (Au-NPs) with a size of about 50 nm absorbing the green luminescence of the UCLNPs. By labeling the UCLNPs with avidin and the AuNPs with biotin we established a model system for a self referenced affinity system applicable to sensing in biological samples. In the presence of avidin-modified UCLNPS, the biotinylated Au-NPs can be detected in the range from 12 to 250 $\mu g \cdot mL^{-1}$ by rationing the intensity of the red (analyte-independent) emission band to that of the green (analyte-dependent) emission band. All nanoparticles were characterized in terms of size and composition using transmission electron microscopy, thermo-gravimetry, and FTIR spectroscopy.

4.2 Introduction

The avidin/biotin system is w5-affinity and non-covalent coupling system and widely used for non-covalent conjugation.[1,2,3] Its unusual affinity (with a Ka of > 10-12) has made it quite useful in specific targeting applications including immuno-assays,[4,5] high-throughput screening,[5,6,7,8] detection and immobilization of DNA,[9,10,11,12] and biofunctionalization,[13] *in vitro* cytotoxicity,[14] to mention only a few. The fair ease of biotinylating biomolecules without compromising their function has further contributed to its popularity.

In order to make nanoparticles (NPs) useful for purposes of biosensing, their surface has to be (bio)chemically modified. Typical examples include labeling of NPs with species such as biotin, avidin, proteins (such as antibodies), or DNA. Various kinds of NPs have been modified in this way, for example those made from silica,[15] carbon nanotubes,[16,17] or semiconductor inorganic NPs of the zinc oxide type.[18] Gold NPs are particularly often used in

biophysical and bioanalytical sciences because they are nontoxic and their surface can be easily modified with various types and modifications of alkyl thiols[19] and with polymer that previously have been end-capped with specific biomolecules.[20] Gold NPs modified with biomolecules such as biotin were used in nummerous bioapplications including immunosensing[21] and in nanomedicine.[22]

Infrared-to-visible upconverting nanoparticles (UCLNPS) are capable of converting near-infrared (NIR) light into visible luminescence. They often are based on the matrix material $NaYF_4$ that is doped with trivalent lanthanide ions such as ytterbium or erbium which determine the color of emission. UCLNPS have found numerous applications including sensing ,[23,24] labeling of biomolecules[25,26,27] and in enzymatic and affinity assays.[28,29] Compared to organic labels or classical (luminescent) nanoparticles,[30] they display fairly high quantum yield, tunable emission wavelengths, lack of blinking, and photostability. Auto-fluorescence from biomaterial and Raman scatter are completely absent in the visible part of the spectrum because luminescence is excited by NIR laser light, typically at 980 nm. It is noted here that 980-nm light can be generated with low-cost and battery-powered diode lasers of the laser pointer type, whilst most luminescent nanoparticles (including the so-called quantum dots) requite shortwave (or even UV) light sources which are more expensive. The use of UCNP type of labels leads to higher signal-to-noise ratios and thus to improved performance in bioassays,[31,32] imaging,[33,34] and in terms of detection limits. Moreover, NIR light is safe to tissue which it can penetrate to a depth of up to several mm.[35,36]

Given this, there have been substantial efforts in order to functionalize the surface of such NPs with respect to bioconjugation, [34,37,38] among others. Recently, UCLNPS have been shown to be useful in energy transfer-based sandwich immune assays.[39,40,41] In these systems, the emission of the UCLNPS is reabsorbed by the fluorescently labeled biomolecules on the UCNP. Interestingly, it is stated that the effects are based on fluorescence energy transfer (FRET) even though distances are longer – at the average – than the typical distances (up to 10 nm) over which FRET can occur.

It is a most welcome coincidence that the bands of the green luminescence of UCLNPS of the type $NaYF_4$:Yb,Er (with emission maxima at 521 and 543 nm) match the absorption band of gold nanoparticles (Au-NPs) that are red or pink (depending on size)[42] and in our case have an absorption maximum at 541 nm as seen in figure 4.1 . We perceived that if Au-NPs are attached to green emitting UCLNPS, the green fluorescence of the latter will be screened off by an inner filter effect. Wang et al.[23] have studied the interaction used biotinylated Au-

NPs along with biotinylated UCLNPS. On addition of avidin, the two types of particles come in close proximity, and this was said to result in FRET which however cannot be the only reason for the reduction in the intensity of the emission of the UCLNPS simply because of the size of the particles compared to the maximal distance (7 to 10 nm) over which FRET can occur according to the Förster equation.[43,44] The model system they chose (two types of biotinylated particles) is rather unrealistic from a bioanalytical point of view because in most practical situations (from high-throughput screening to immunoassays and gene assays) it is the interaction of a biotinylated species with an avidin conjugated species that is to be detected, rather than the interaction of two biotinylated species.

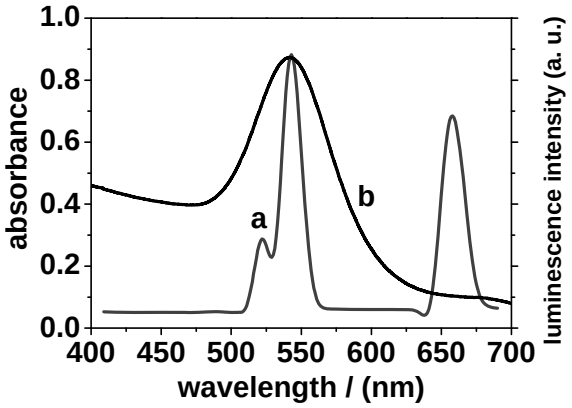

Figure 4.1 (a) Emission spectrum of avidin labeled UCLNPS following photo-excitation with a diode laser at 980 nm; (b) absorption spectrum of the biotinylated 50-nm gold nanoparticles

In another report,[45] the interaction between UCLNPS and Au-NPs was used in a sandwich-type of immunoassay. The system is based on the interactions of (a) an antibody conjugated to an UCNP; (b) a secondary antibody, and an (c) antigen linked to AuNPs. Equilibration typically takes more than 1 h. Luminescence resonance energy transfer (LRET) was again invoked as the mechanism for quenching. This is, however, unlikely to be the cause for the reduction in intensity ("quenching") for the reasons outlined before. Rather, we believe that the effect is caused by an inner filter effect in that the green emission of the UCLNPS is absorbed by the red (or pink) gold NPs. The system presented here is based on silica-coated UCLNPS ($NaYF_4$ nanocrystals doped with Yb^{3+} and Er^{3+}) which are more biocompatible than uncoated UCLNPS. It was designed in order to be useful in all the typical bioassay formats

where the high-affinity interaction between biotin and avidin is exploited. We also demonstrate that the dual emission of most UCLNPS has a beneficial feature by enabling rationed measurements because only one of the two emission bands is analytically sensitive, whilst the second one is inert and represents a most useful reference signal.

4.3 Materials and Methods

4.3.1 Materials

Yttrium(III) chloride hexahydrate (99.99%), ytterbium(III) chloride hexahydrate (99.99%), Erbium(III) chloride hexahydrate (99.99%), tetraethoxysilane (TEOS), ammonium hydroxide solution (28% in water) and avidin (from egg white) were purchased from Sigma (www.sigmaaldrich.com). Hydrogen tetrachloroaurate(III) hydrate (49% Au) was purchased from Chempur (www.chempur.de), trisodium citrate dihydrate and ethylene-diaminetetraacetic acid (EDTA) from Merck (www.merck-chemicals.de), hydroxylamine hydrochloride from Alfa Aesar (www.alfa.com), 3-(glycidyloxypropyl)-trimethoxysilane (98% purity) from ABCR (www.abcr.de), and biotin terminated undecylthiol (HS-$(CH_2)_{11}$-NH-CO-biotin) from Prochimia (www.prochimia.com). The phosphate buffer used (20 mM) had a pH of 7.4.

4.3.2 Instrumentation

Luminescence spectra of particles were recorded on a Cary Eclipse fluorometer (from Varian; www.varianinc.com). A 980-nm fiber optic diode laser with power regulation (max. 5 W cw; from Roithner Lasertechnik; www.roithner-laser.com) was used as the light source for upconversion photoexcitation. Transmission electron microcopy images were acquired using a 120-kV Zeiss (www.smt.zeiss.com) instrument (type Leo 912AB) equipped with a Proscan CCD (www.proscan.de) camera. DR-FTIR spectra were acquired on a FT/IR – 6100 IR spectrometer distributed by Jasco (www.jascoinc.com). A diffuse reflectance accessory (EasiDiff) provided by Pike Technologies (www.piketech.com) was used for sample preparation. Thermogravimetric analyses were performed on a thermal analyzer (model TGA-7; from Perkin-Elmer; www.perkinelmer.com) device at a heating rate of 10 °C min-1 under

nitrogen atmosphere. Particle sizes and zeta potentials were measured on a Malvern Zetasizer 3000 DTS 5300 instrument (www.malvern.com) at pH 6. It can measure particle sizes ranging from 0.6 nm to 6 μm.

4.3.3 Synthesis of $NaYF_4$:Yb,Er Upconverting Nanoparticles

$NaYF_4$:Yb,Er UCLNPS were prepared using the coprecipitation method.[46] In a typical procedure, solutions of 16 mL of 0.2 M of YCl_3, 3.4 mL of 0.2 M $YbCl_3$ and 0.6 mL of 0.2 M $ErCl_3$ were mixed with 20 mL of a 0.2 M EDTA solution in order to form the respective EDTA complex. This solution was quickly injected into 60 mL of a 0.05 mol solution of sodium fluoride, and the mixture stirred for 1 h at room temperature. The resulting precipitate was centrifuged, washed three times with water and once with ethanol. The precipitate was then dried in a drying furnace and under vacuum. Annealing of the nanoparticles was carried out in an atmosphere of argon by heating them to 400 ºC at a rate of 20 ºC per min, maintaining this temperature for 5 h, and cooling to room temperature under the same atmosphere. The resulting (partial) conversion of the cubic into the hexagonal phase[46] yields particles with higher upconversion efficiencies.

4.3.4 Synthesis of silica shell $NaYF_4$:Yb,Er Upconverting Nanoparticles

The above nanoparticles were covered with a silica shell that was created by the hydrolysis of tetraethyl orthosilicate.[47] In a typical procedure, 40 mg of the UCLNPS were stirred in 25 mL ethanol for 30 min. Then, 500 μL of water, 300 μL of ammonium hydroxide and 325 μL of TEOS were added to the solution, the mixture heated to 40 °C and then gently stirred for 30 min. Finally, 15 μL of 3-(glycidyloxypropyl)trimethoxysilane were added and the mixture stirred for another 2 h. The modified UCLNPS were isolated after several cycles of centrifugation (10 min at 4400 rpm) and washing (two times ethanol, two times water).

4.3.5 Preparation of Avidin-Labeled $NaYF_4$:Yb,Er Upconverting Nanoparticles

A solution of 25 mg of silica-modified UCLNPS was dispersed in 1.5 mL of the pH 7.4 buffer by ultrasonication for 20 min. Then, 1 mg of avidin was added to react with the surface epoxy

groups. The mixture was shaken in an Eppendorf thermomixer (www.eppendorf.com) overnight at room temperature to allow for the reaction to complete. UCLNPS were isolated after several cycles of centrifugation (10 min at 6000 rpm) and washing (three times with buffer of pH 7.4). The avidin labeled UCLNPS were redispersed in 10 mL of buffer, sonicated, and stored at 4 °C. This solution was used in further experiments. The following scheme (figure4.1) shows the modification procedure of the UCLNPS.

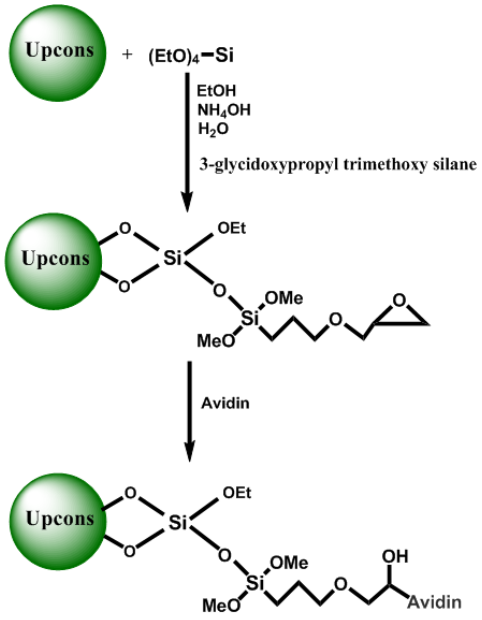

Figure 4.1. Surface chemistry leading to epoxy-modified silica shell UCLNPS, and subsequent conjugation of avidin to the surface.

4.3.6 Synthesis of 20-nm Gold Nanoparticles (Au-NPs)

The colloidal gold nanoparticles were synthesized as described by Turkevich[48] et al. In a typical experiment, a volume of 47.5 mL of a solution of 5 mg of chloroauric acid ($HAuCl_4$) were brought to reflux, and 2.5 mL of a 1% sodium citrate solution added to the boiling solution. The reduction of the gold ions by the citrate ions is complete after 5 min. The red solution (refered to as solution A) was further boiled for 30 min and then left to cool to room temperature. This method yields spherical particles with an average diameter of about 20 nm.

4.3.7 Synthesis of 50-nm Gold Nanoparticles (Au-NPs)

The 20-nm colloidal gold solution was used as seed solution for growth of the larger spheres of 50 nm. These nanoparticles were obtained by the reduction of fresh $HAuCl_4$ with hydroxylamine in the presence of 20 nm gold nanoparticles as described by Turkevich[49]et al. Solution A (0.9 mL) was treated with 15 mL of a solution of chloroauric acid (containing 1.5 mg of $HAuCl_4$) then with 2 mg of solid hydroxylamine hydrochloride. The resulting solution was left to stay for at least 30 min so to allow for particle growth to give a red suspension of gold nanoparticles (refered to as solution B). The volume of the seed solution was estimated with the Turkevich equation.[50]

4.3.8 Synthesis of Biotinylated Gold Nanoparticles

A solution of 8 mL of biotin-terminated undecylthiol (100 µM in water:ethanol; 50% v/v) was added to 15.9 mL of solution B. The vial is left to stay overnight. The resulting red nanoparticles were isolated and purified by several cycles of centrifugation (10 min at 14000 rpm) and washing (three times with phosphate buffer of pH 7.4). The biotinylated gold NPs were redispersed in 5 mL buffer, sonicated, and stored at 4 °C. This stock solution (refered to as solution C) was used in further experiments.

4.3.9 Study on the Interaction Between Avidin labeled UCLNPs and Biotinylated Au-NPs

The affinity interactions of the avidin labeled UCLNPS and the biotinylated Au-NPs was investigated by luminescence spectroscopy. In a typical procedure, aqueous solutions (200 µL of a 1 mg L^{-1} solution of avidin-labeled UCLNPS) was mixed, in increasing ratios (0 - 500 µL), with an aqueous solution of 0.5 mg mL^{-1} of biotinylated Au-NPs (after centrifugation and resuspension), and made up to a total volume of 2.0 mL with buffer of pH 7.4. Luminescence spectra were acquired immediately after mixing.

4.4 Results and Discussion

The epoxy-functionalized UCLNPS can be easily dispersed in water to form a colloidal solution. The TEM picture given in figure 4.2 shows that the UCLNPS are coated with a layer of silica and spherical in shape, with a size distribution ranging from 120 to 170 nm.

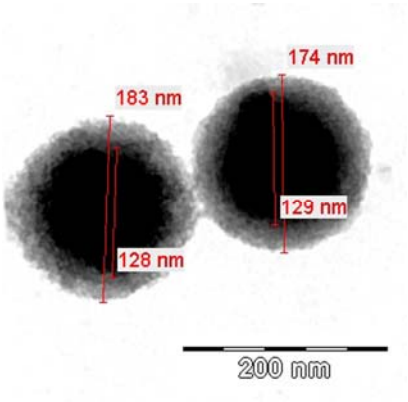

Figure 4.2 Transmission electron microscopy image of silica-coated upconverting nanoparticles showing a core consisting of UCLNPS and the (epoxy-modified) silica coating. Scale bar: 200 nm.

UCLNPS were first characterized by thermogravimetric analysis (TGA). Plain UCLNPS display a rather small loss which is due to evaporation of adsorbed water. Epoxy-modified UCNP suffer from a larger weight loss due to the presence of (3-glycidyloxy-propyl)trimethoxysilane which decomposes at above 450 °C. The highest weight loss is observed for avidin labeled UCNP due to additional decomposition of avidin. The differences in weight loss between the unmodified UCLNPS, epoxy modified UCLNPS, and avidin-labeled UCLNPS are good proof for surface modification (see figure 4.3).

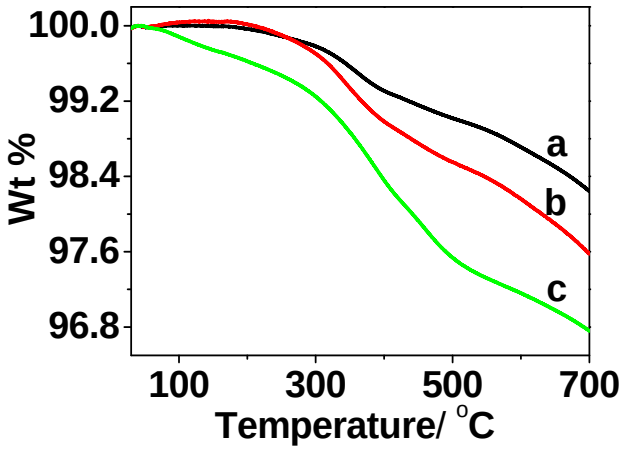

Figure 4.3. Thermogravimetric analysis of UCLNPS. (a) plain UCLNPS; (b) epoxy-modified silica shell UCLNPS, (c) avidin-labeled silica shell UCLNPS.

4.4.1 FTIR Spectra of Epoxy-Modified UCLNPs with a Silica Shell, and of Biotinylated Gold NPs

The surface modification of the UCLNPS and Au-NPs was assessed by FTIR spectroscopy of the epoxy-modified UCLNPS with a silica shell, and of the biotinylated gold NPs. The characteristic IR absorption signals for modified samples are given in figure 4.4. the FTIR spectrum which displays a sharp band peaking at ~940 cm^{-1} (epoxy groups) and C–H stretching vibrations at 2920 cm^{-1} and 2840 cm^{-1}. The spectra of the gold NPs show two characteristic peaks at 2943 cm^{-1} and 2880 cm^{-1} that can be attributed to CH_2 stretching modes. These peaks clearly demonstrate the presence of alkyl chains. The peak at 1650 cm^{-1} is attributed to the biotin amide carbonyl group.

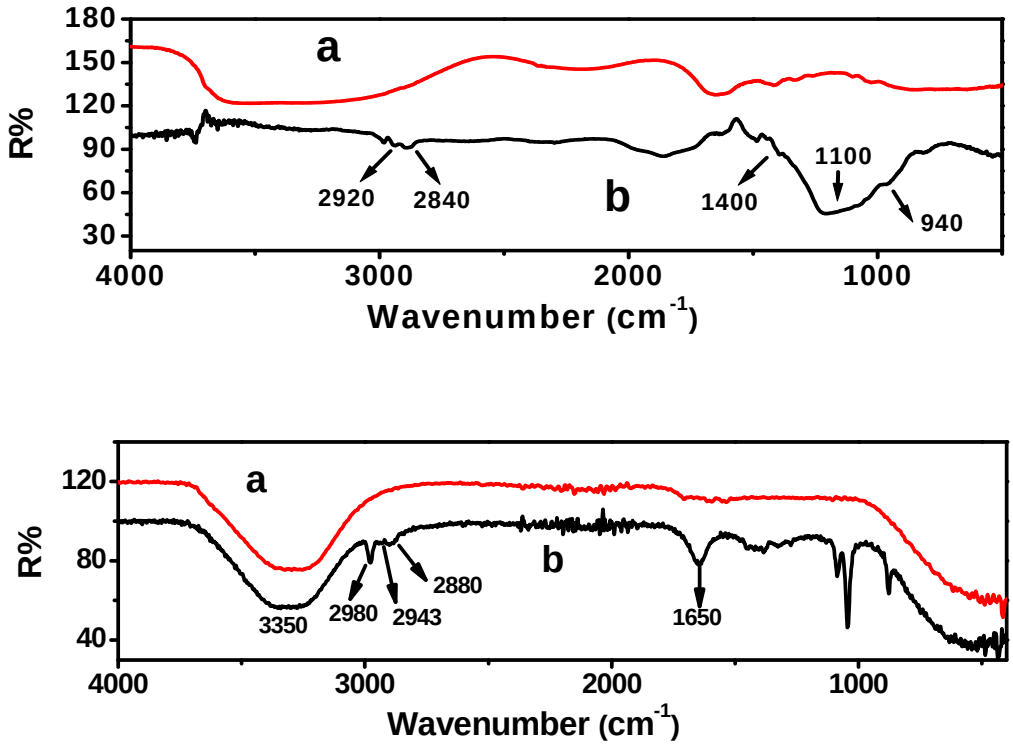

Figure 4.4 FTIR spectra of UCLNPS (top). (a): plain particles; (b): epoxy/silica modified particles), and Au-NPs (bottom) (a): plain particles, (b): biotinylated Au-NPs.

.

The colloidal gold nanoparticles have an average diameter of about 20 nm figure 4.5. Such Au-NPs have absorption maxima at 523 nm which is not a perfect match with respect to the green emission of the UCLNPS. In order to obtain a better spectral match, the 20 nm Au-NPs were used as a seed to grow the spheres to a size of ~50 nm (figure 4.5) which shifts the absorption maximum to 534 nm. The Au-NPs where characterized in terms of TEM and DLs as show in figures 4.5 and 4.6.

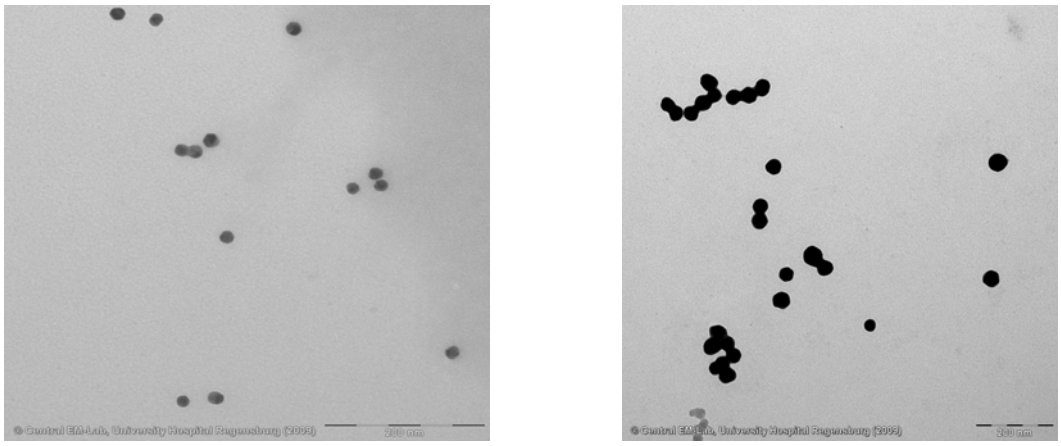

Figure 4.5 TEM images of gold nanoparticles (Au-NPs). The picture on the left shows the 20-nm Au-NPs that were used as seeds for the 50-nm Au-NPs shown on the right. Scale bars: 200 nm).

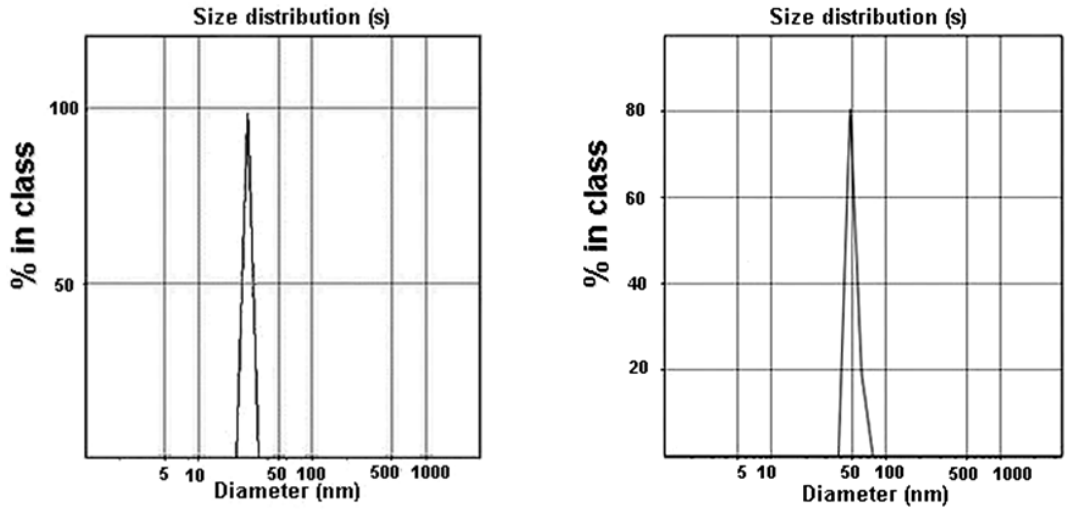

Figure 4.6 Dynamic light scattering spectra. of the Au-NPs with an average diameter of about 20 nm (left) and of about 50 nm (right).

The surface of gold nanoparticles can be easily modified by reaction with thiols.[51] We are using a biotinylated undecylthiol of the chemical structure HS-$(CH_2)_{11}$-NH-CO-biotin whose thiol group readily reacts with the surface of the Au-NPs. This is accompanied by a change in the zeta potential ζ of the particles from -20.6 mV to -2.4 mV due to the replacement of the citrate ligands on the surface of AuNPs by biotinylated undecylthiol.

Interestingly, an additional red-shift to 541 nm is observed following surface modification

(see figure 4.7). The spectrum of the resulting pink solution now perfectly overlaps the 543-nm emission band of the UCLNPS.

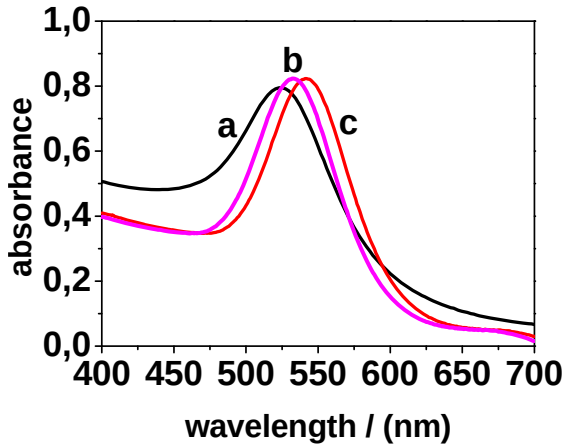

Figure 4.7 Absorption spectra of (a) 20-nm seed solution of gold NPs, (b) 50-nm NPs and (c) biotinylated gold nanoparticles in water.

The detection scheme for the bioaffinity assay is straightforward and schematically outlined in figure 4.8. The biotinylated Au-NPs have a high affinity for the avidin modified UCLNPS of the type $NaYF_4$:Yb,Er. On binding, the gold nanoparticles form a kind of coating on the surface of the UCLNPS whose green emission bands (peaking at 521 and 543 nm) then will be absorbed by the Au-NPs. We have intentionally chosen UCLNPS that display a strong second emission band at 657 nm which however is not screened off and thus can serve as a reference signal. The analytical information of the system is obtained by rationing the intensity of the red (analyte-independent) emission and the green (analyte-dependent) emission. This option makes the assay particularly attractive because referenced fluorometric methods are independent of fluctuations of light sources and geometrical as well as other factors, and thus are more robust[52] than assays based on measurement of intensities at identical wavelengths.

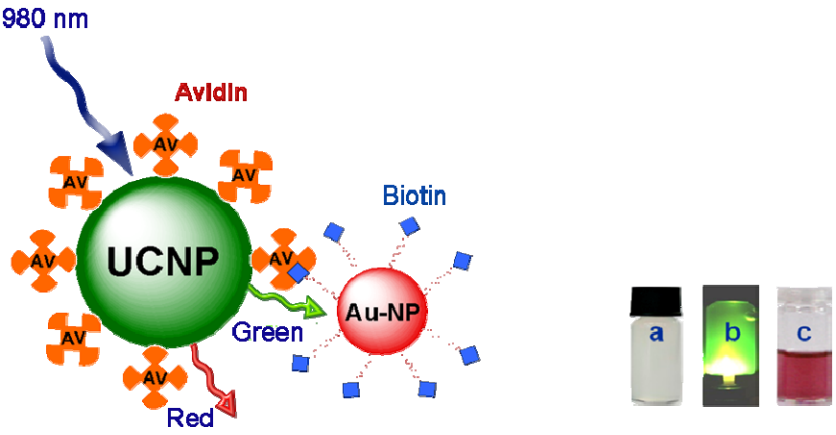

Figure 4.8 Schematic of the binding of biotinylated gold nanoparticles to avidinylated upconverting nanoparticles. The green emission of the UCLNPS is absorbed by the biotinylated gold nanoparticles. The red emission of the UCLNPS, in contrast, is not absorbed and may serve as a reference signal. Photographs: (a) colorless suspension of UCNP under visible light; (b) UCLNPS with green luminescence following 980-nm laser excitation; (c), red gold NPs under visible light.

In order to demonstrate the affinity assay to work, varying concentrations of biotinylated Au-NPs were added to a fixed quantity of avidin-labeled UCNP. The luminescence of the UCNP at 541 nm was measured following each addition of aliquots. Figure 4.9 shows that the intensity at 541 nm (I_1) is strongly reduced in the presence of Au-NPs, whilst that of the (red) reference band at 657 nm (I_2) remains virtually unchanged.

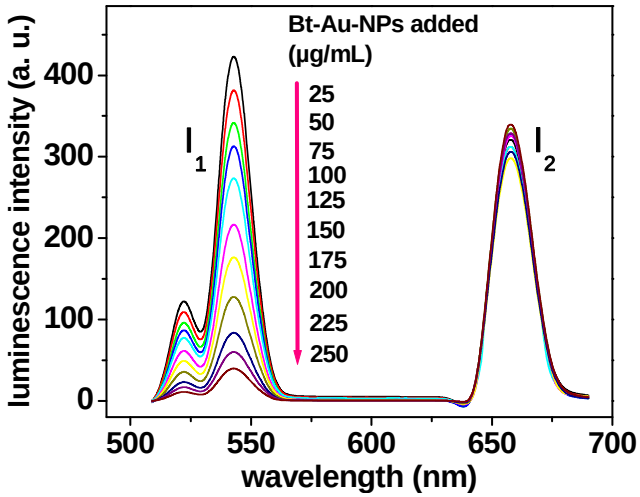

Figure 4.9 Luminescence of the UCLNPS (photo-excited at 980 nm) after addition of different concentrations of biotinylated gold nanoparticles.

Similar experiments were carried out by titrating (a) non-labeled UCLNPS with non-biotinylated Au-NPs, (b) non-labeled UCLNPS with biotinylated Au-NPs (see figure 4.5, left part), and (c) labeled UCLNPS with non-biotinylated Au-NPs (see figure 4.10, right part). No reduction in luminescence is observed in either of these cases which is excellent proof for (a) the specificity of this affinity system, and (b) the absence of unspecific binding of proteins or particles to surfaces.

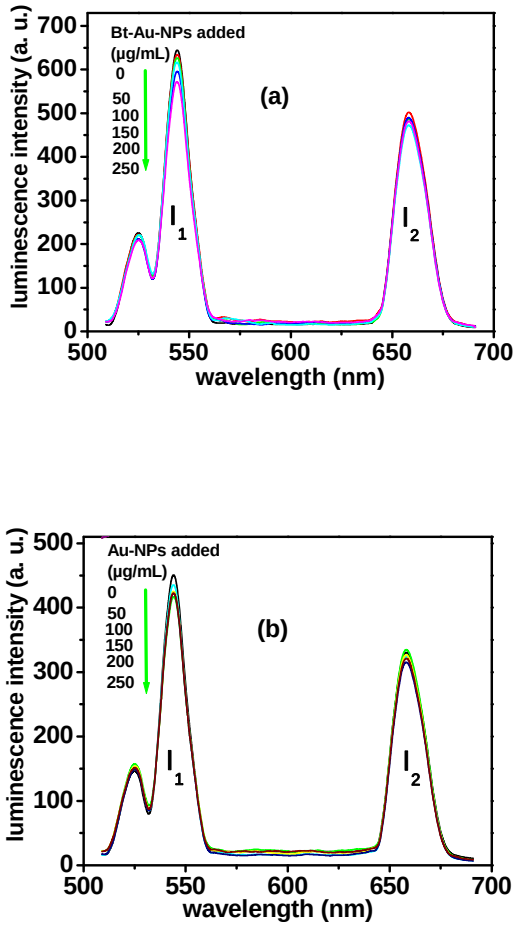

Figure 4.10 (a) Upconversion luminescence spectra of UCLNPS without avidin at different concentrations of biotinylated gold nanoparticles. (b) Relationship between I_2/I_1 and the concentration of biotinylated gold **(**left). Upconversion luminescence spectra of avidinylated UCLNPS at different concentrations of 50-nm Au-NPs without biotin upon diode laser excitation at 980 nm. (d) Relationship between I_2/I_1 and the concentration of the gold nanoparticles (right).

Calibration plots for determining the concentration of Au-NPs based on (a) the intensity of the luminescence of the UCNP (I_1), and (b) the ratio between the relative intensities of the luminescence of the UCLNPS at two wavelengths (I_1/I_2) are shown in figure 4.11. The dynamic response ranges from around 12 to 250 µg of biotinylated Au-NPs per mL of sample solution.

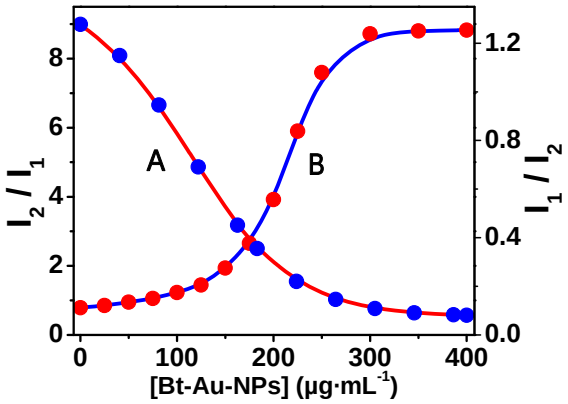

Figure 4.11 Left: Relationship between the intensity of luminescence and the concentration of biotinylated gold NPs. I_2 and I_1, respectively, are the intensities of the luminescence of the 657-nm (red) peak and the 543-nm (green) peak; (right) relationship between the concentration of biotinylated gold NPs and the rationed intensities of luminescence (I_2/I_1; left), I_1/I_2 (right).

4.4.2 Ratio of the Intensities of the Two Bands of UCLNPs in Presence of Gold NPs for the Situation Where one kind of Particles is not Containing the Affinity Partner.

In one set of experiments, non-labeled UCLNPS with biotinylated Au-NPs (see figure 4.5) to give plot c in the figure below. In the second set of experiments, avidinylated UCLNPS were titrated with non-biotinylated Au-NPs (see figure 4.12, right part) to result in plot (d) in the figure below.

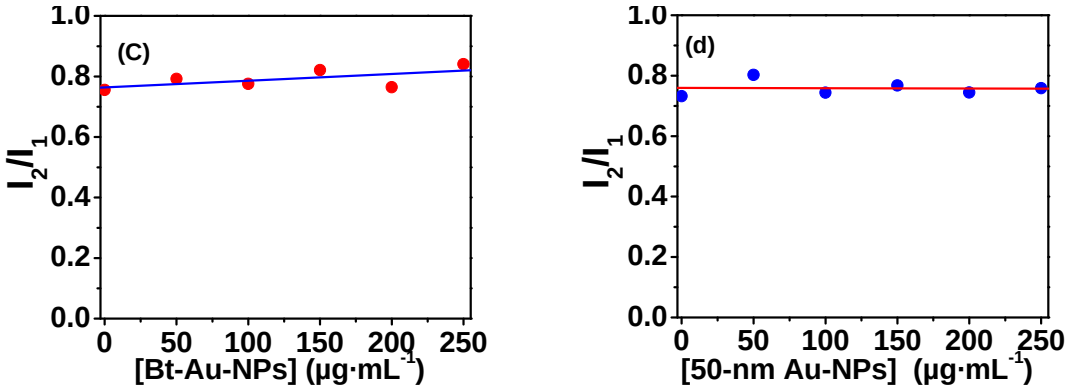

Figure 4.12 Ratio between the intensities of the emissions at 657 nm (I_2) and 541 nm (I_1) versus (c) the concentration of biotinylated gold nanoparticles in presence of no-unlabeled UCLNPS (left plot); and (d) versus the concentration of non-labeled 50-nm gold NPs in presence of biotinylated UCLNPS (right side plot). Also see Figure 4.10.

Wang et al.[45] have presented an UCNP-based immunoassay using a material that has a very weak emission in the red (665 nm) and which is not suitable for self-referencing, which is a major aspect of the work presented here. The analytical information in their method is the ratio between the analyte-dependent intensity of the green emission (I) and the "unquenched" green intensity (I_0). This ratio is, however, prone to the usual interferences of fluorometry because the two intensities cannot be determined simultaneously (unlike the intensities of the red and the green emission in our case). Moreover, FRET (and LRET) based methods (as claimed by the authors) are sensitive to even minute changes in the distance of the two luminophores involved due to the dependence on the inverse 6th power of the efficiency of FRET.

4.5 Conclusion

We demonstrate here a new kind of affinity scheme based on the strong interaction between avidin and biotin. It is based on the spectral overlap between the luminescence of the $NaYF_4$:Yb,Er upconversion nanoparticles (UCLNPS) and the absorption band of the gold nanoparticles. If placed in close spatial proximity via biotin-avidin binding, an inner filter effect is observed that leads to an apparent decrease in the quantum yield as a result of the re-absorption of light emitted by the UCLNPS. The effect can be used to detect binding between avidin and biotin. The method represents an attractive alternative to systems where organic labels are applied and where the efficiency of FRET between two (organic) fluorophores

yields the analytical signal. One very attractive feature of this system relies on the fact that it is displaying two emission bands. One is affected by the biotinylated gold particles, but the other not, thus leading to a self-referenced signal. Specific other features include NIR photoexcitation, lack of blinking, exceptional photostability, good solubility of the nanoparticles in aqueous solution, and facile biofunctionalization of surfaces. We expect this system to be applicable to wherever the avidin-biotin system is being employed, for example to study protein-proteins interactions, ligand-receptor interactions, the formation of DNA duplexes, and in high-throughput screening as outlined in the introduction. Conceivably, it can be extended to the interaction of other species (such as antigens and antibodies; or oligomers and their counterstrands) if one species is linked to the Au-NPs, and the other to UCLNPS. It therefore is believed to have wide applicability.

4.6 Reference

1 Hermanson GT (2008) **Bioconjugate Techniques**, 2nd edn. Elsevier, pp 900.

2 Diamandis EP, Christopoulos TK (1991) **The Biotin-(Strept)Avidin System: Principles and Applications in Biotechnology**, Clin. Chem. 37:625-638.

3 Krishan VV, Khan IH, Luciw PA (2009) **Multiplexed immunoassays by flow cytometry for molecular profiling: Basic concepts and proteomic applications**, Crit. Rev. Biotechnol. 29:29-43.

4 Klein G, Humbert N, Gradinaru J, Ivanova A, Gilardoni F, Rusbandi U E, Ward TR (2005) **Tailoring the Active Site of Chemzymes Using a Chemogenetic Optimization Procedure: Towards Substrate-Specific Artificial Hydrogenases Based on the Biotin-Avidin Technology**, Angew. Chem. Int. Ed. 44: 7764-7767.

5 Wang L, Zhao WJ, O'Donoghue MB, Tan WH (2007) **Fluorescent nanoparticles for multiplexed bacteria monitoring**. Bioconjugate Chem. 18:297-301.

6 Asai T, Trinh R, Ng PP, Penichet ML, Wims LA, Morrison SL (2005) **A human biotin acceptor domain allows site-specific conjugation of an enzyme to an antibody-avidin fusion protein for targeted drug delivery**, Biomol. Eng. 21:145-55.

7 Mei, HY, Cui M, Sutton ST, Truong HN, Chung FZ, Czarnik AW (1996) **Inhibition of self-splicing group I intron RNA: high-throughput screening assays**, Nucleic Acids Res. 24:5051-5053.

8 Sun LN, Peng HS, Stich MIJ, Achatz D, Wolfbeis OS (2009) **pH sensor based on upconverting luminescent lanthanide nanorods**. Chem. Comm. 5000-5002.

9 Bonanni A, Pividori MI, del Valle M (2007) **Application of the avidin–biotin interaction to immobilize DNA in the development of electrochemical impedance Genosensors**, Anal. Bioanal. Chem . 389:851-861.

10 Masarik M, Kizek R, Kramer KJ, Billova S, Brazdova M, Vacek J, Bailey M, Jelen F, Howard JA (2003) **Application of avidinbiotin technology and adsorptive transfer stripping square-wave voltammetry for detection of DNA hybridization and avidin in transgenic avidin maize**, Anal. Chem. 75:2663-2669.

[11] Mao X, Xu H, Zeng QX, Zeng LW, Liu GD (2009) **Molecular beacon-functionalized gold nanoparticles as probes in dry-reagent strip biosensor for DNA analysis,** Chem. Commun. 3065-3067.

[12] Morais S, Marco-Moles R, Puchades R, Maquieira A (2006) **DNA microarraying on compact disc surfaces. Application to the analysis of single nucleotide polymorphisms in Plum pox virus**, Chem. Comm.2368-2370.

[13] Wang GP, Song EQ, Xie HY, Zhang ZL, Tian ZQ, Zuo C, Pang DW, Wu DC, Shi YB (2005) **Biofunctionalization of fluorescent-magnetic-bifunctional nanospheres and their applications**, Chem. Comm. 4276-4278.

[14] Zeng X, Sun YX, Qu W, Zhang XZ, Zhuo RX (2010) **Biotinylated transferrin/avidin/biotinylated disulfide containing PEI bioconjugates mediated p53 gene delivery system for tumor targeted transfection**, Biomaterials 31:4771-4780.

[15] Saleh SM, Rainer M, Heike SM, Duerkop A, Wolfbeis OS (2010) **Novel multicolor fluorescently labeled silica nanoparticles for interface fluorescence resonance energy transfer to and from labeled avidin**, Anal. Bioanal. Chem. 398:1615-1623.

[16] Kim YS, Cho JH, Ansari SG, Kim HI, Dar MA, Seo HK, Kim GS, Lee DS, Khang G, Shin HS (2006) **Immobilization of avidin on the functionalized carbon nanotubes,** Synthetic. Met. 156:938-943.

[17] Wahab R, Ansari SG, Kim YS, Mohanty TR, Hwang IH, Shin HS (2009) **Immobilization of DNA on nano-hydroxyapatite and their interaction with carbon nanotubes**, Synthetic. Met. 159:238-245.

[18] Wahab R, Kim YS, Hwang IH, Shin HS (2009) **A non-aqueous synthesis, characterization of zinc oxide nanoparticles and their interaction with DNA,** Synthetic. Met. 159:2443-2452.

[19] Lala N, Chittiboyina AG, Chavan SP, Sastry M (2002) **Biotinylation of colloidal gold particles using interdigitated bilayers: a UV-visible spectroscopy and TEM study of the biotin-avidin molecular recognition process**, Colloid Surface A 205:15-20.

[20] Aqil A, Qiu HJ, Greisch JF, Jerome R, De Pauw E, Jerome C (2008) **Coating of gold nanoparticles by thermosensitive poly(N-isopropylacrylamide) end-capped by biotin**, Polymer 49:1145-1153.

[21] Lin CC, Chen LC, Huang CH, Ding SJ, Chang CC, Chang, HC (2008) **Development of the multi-functionalized gold nanoparticles with electrochemical-based immunoassay for protein A detection**, J. Electroanal. Chem. 619:39-45.

[22] Daniel MC, Astruc D (2004) **Gold nanoparticles: Assembly, supramolecular chemistry, quantum-size- related properties, and applications toward biology, catalysis, and nanotechnology**, Chem. Rev. 104:293–346.

[23] Wang LY, Yan RX, Hao ZY, Wang L, Zeng JH, Bao H, Wang X, Peng Q, Li YD (2005) **Fluorescence Resonant Energy TransferBiosensor Based on Upconversion-Luminescent Nanoparticles**, Angew. Chem. Int. Ed. 44:6054- 6057.

[24] Sun HY, Tan LP, Gao LQ, Yao SQ (2009) **High-throughput screening of catalytically inactive mutants of protein tyrosine phosphatases (PTPs) in a phosphopeptide microarray**. Chem. Comm. 677-679.

[25] Wang F, Liu XG (2008) **Upconversion Multicolor Fine-Tuning: Visible to Near-Infrared Emission from Lanthanide-Doped $NaYF_4$ Nanoparticles**, J. Am. Chem. Soc. 130:5642-5643.

[26] Sivakumar S, Diamente PR, van Veggel FC (2006) **Silica-Coated Ln^{3+}-Doped LaF_3 Nanoparticlesas Robust Down- and Upconverting Biolabels**, Chem. Eur. J. 12:5878-5884.

[27] Kong DY, Quan ZW, Yang J, Yang PP, Li CX, Lin J (2009) **Avidin conjugation to up-conversion phosphor $NaYF_4$: Yb^{3+}, Er^{3+} by the oxidation of the oligosaccharide chains**, J. Nanopart. Res. 11:821-829.

[28] Rantanen T, Jarvenpaa ML, Vuojola J, Kuningas K, Soukka T (2008) **Fluorescence-Quenching-Based Enzyme-Activity Assay by Using Photon Upconversion**, Angew. Chem. Int. Ed. 47;3811-3813.

[29] Morgan CG, Dad S, Mitchell AC (2008) **Present status of, and future prospects for, upconverting phosphors in proximity-based bioassay**, J. Alloy Compd. 451:526-529.

[30] Resch-Genger U, Grabolle M, Cavaliere-Jaricot S, Nitschke R, Nann T (2008) **Quantum dots versus organic dyes as fluorescent labels**, Nat. Methods**.** 5:763-775.

[31] Soukka T, Rantanen T, Kuningas K (2008) **Photon Upconversion in Homogeneous Fluorescence-based Bioanalytical Assays**, Fluorescence Methods and Applications: Spectroscopy, Imaging, and Probes 1130:188-200.

[32] Medintz IL, Uyeda HT, Goldman ER, Mattoussi H (2005) **Quantum dot bioconjugates for imaging, labelling and sensing**, Nat. Mater. 4:435-446.

[33] Jiang S, Zhang Y, Lim KM, Sim EK, Ye L (2009) **NIR-to-visible upconversion nanoparticles for fluorescent labeling and targeted delivery of siRNA**. Nanotechnol. 20.

[34] Mader H S, Kele P, Saleh SM, Wolfbeis OS (2010) **Upconverting luminescent nanoparticles for use in bioconjugation and bioimaging**, *Curr. Opin. Chem. Biol.* 14:582-596.

[35] Jalil RA, Zhang Y (2008) **Biocompatibility of silica coated NaYF(4) upconversion fluorescent nanocrystals**, Biomat. 29:4122-4128.

[36] Wang M, Mi CC, Zhang YX, Liu JL, Li F, Mao CB, Xu SK (2009) **NIR-Responsive Silica-Coated $NaYbF_4$:Er/Tm/Ho Upconversion Fluorescent Nanoparticles with Tunable Emission Colors and Their Applications in Immunolabeling and Fluorescent Imaging of Cancer Cells**, J. Phys. Chem. C 113:19021-19027.

[37] Li ZQ, Zhang Y (2006) **Monodisperse Silica-Coated Polyvinylpyrrolidone/ $NaYF_4$ Nanocrystals with Multicolor Upconversion Fluorescence Emission**. Angew. Chem. Int. Ed. 45:7732-7735.

[38] Li ZQ, Zhang Y, Jiang S (2008) **Multicolor Core/Shell-Structured Upconversion FluorescentNanoparticles**, Adv. Mater. 20:4765-4769.

[39] Kuningas K, Pakkila H, Ukonaho T, Rantanen T, Lovgren T, Soukka T (2007) **Upconversion Fluorescence Enables Homogeneous Immunoassay in Whole Blood**, Clin. Chem .53:145-146.

[40] Zhang P, Rogelj S, Nguyen K, Wheeler D (2006) **Design of a Highly Sensitive and Specific Nucleotide Sensor Based on Photon Upconverting Particles**, J. Am. Chem. Soc. 128:12410-12411.

[41] Kuningas K, Ukonaho T, Pakkila H, Rantanen T, Rosenberg J, Lovgren T, Soukka T (2006) **Upconversion Fluorescence Resonance Energy Transfer in a Homogeneous Immunoassay for Estradiol**, Anal. Chem. 78:4690-4696.

[42] Link S, El-Sayed M A (1999) **Size and Temperature Dependence of the Plasmon Absorption of Colloidal Gold Nanoparticles**, J. Phys. Chem. B 103:4212-4217.

[43] Miller JN (2005) **Fluorescence energy transfer methods in bioanalysis**, Analyst 130:265-270.

[44] Lakowicz JR, Malicka J, Gryczynski I, Gryczynski Z, Geddes CD (2003) **Radiative decay engineering: the role of photonic mode density in biotechnology**, J. Phys. D. Appl. Phys. 36:R240-R249.

[45] Wang M, Hou W, Mi CC, Wang WX, Xu ZR, Teng HH, Mao CB, Xu SK (2009) **Immunoassay of Goat Antihuman Immunoglobulin G Antibody Based on Luminescence Resonance Energy Transfer between Near-Infrared Responsive $NaYF_4$:Yb, Er Upconversion Fluorescent Nanoparticles and Gold Nanoparticles**, Anal. Chem. 81:8783-8789.

[46] Yi GS, Lu HC, Zhao SY, Yue G, Yang WJ, Chen DP, Guo LH (2004) **Synthesis, Characterization, and Biological Application of Size-Controlled´Nanocrystalline $NaYF_4$:Yb,Er Infrared-to-Visible Up-Conversion Phosphors**, Nano. Lett. 4:2191-2196.

[47] Stöber W, Fink A (1968) **Controlled Growth of Monodisperse Silica Spheres in the Micron Size Range**, J. Colloid. Interf. Sci. 26, 62-69.

[48] Turkevich J, Stevenson PC, Hillier J (1951) **A study of the nucleation and growth processes in the synthesis of colloidal gold**, Discuss. Faraday Soc. 11:55-75.

[49] Turkevich J, Garton G, Stevenson PC (1954) **The Color of Colloidal Gold**, J. Colloid Sci. 9:S26-S35.

[50] Turkevich J (1985) **Colloidal Gold Part II**, Gold Bull. 18:125-131.

[51] Nath N, Chilkoti A (2002) **A Colorimetric Gold Nanoparticle Sensor To Interrogate Biomolecular Interactions in Real Time on a Surface**, Anal. Chem. 74:504-509.

[52] Schaeferling M, Duerkop A (2008) **In: Standardization and Quality Assurance in Fluorescence Measurements I: Techniques, Springer Ser Fluorescence**, Ed: U. Resch-Genger, Springer, Berlin 5, pp 373.

5 Preparation of Nanoparticles Labeled with Longwave Absorbing and Emitting Chameleon Labels, and a Method for Detecting Amino Groups on Surfaces

5.1 Abstract

Nanoparticles carrying longwave absorbing and emitting fluorescent labels were prepared by conjugating reactive dyes to the surface of amino-modified particles. The dyes have a reactive chloro group capable of reacting with amino groups and thereby undergoing a change in color, typically from green to blue. Specifically, we report in particles made from silica, polystyrene, and from lanthanide-doped $NaYF_4$ nanocrystals. The latter show the effect of upconversion in that near-infrared laser light is converted into visible luminescence. They also show the unusual property of displaying dual emission, depending on whether their luminescence is photoexcited with visible light or near-infrared light. All particles are characterized in terms of size and spectra. The chameleon effect (i. e., the color change from green to blue) can be used to detect the presence of amino groups on the surface of nanoparticles.

5.2 Introduction

Fluorescently labeled nanoparticles have found substantial interest in recent years. They are typically made from materials such as silica,[1,2,3,4,5,6,7] polystyrene [8,9,10] or polyacrylonitrile, [11,12,13] nanocrystals,[14] and quantum dots.[15] Applications of fluorescent nanoparticles include the labeling of biomaterials such as proteins,[16] antibodies,[17] oligomers,[18] and even stem cells,[19] in FRET studies,[20] and the like. Other than conventional labels, they are carrying thousands of fluorophores per single particle and thus can render biomolecules much more fluorescent. Labeled microparticles, on the other side, have been used in cytometry,[21,22,23] bioanalysis in general, [24,25] screening,[26,27] imaging and fluorescence-activated cell sorting.[28,29]

We are reporting here on deeply colored and fluorescent nanoparticles tagged with a new class of longwave labels. These show the interesting property (refered to as the chameleon effect) of undergoing a color change on conjugation to an amino group, typically from green to blue. The

chameleon labels presented here complement previous labels of that kind whose color changes from blue to red on conjugation.[30] Longwave labeled nanoparticles are of particular

interest in biosciences because red and NIR light causes much less fluorescence background of biological matter than light of wavelengths of below 500 nm, and because biomatter is much better penetrated by longwave light than by shortwave light.[31] The new particles are considered to represent attractive alternatives to those used so far. Moreover, the change in the color of the labels from green to blue on reaction with amino-modified nanoparticles is shown to be useful for detecting the presence of amino groups on such particles.

5.3 Experimental

5.3.1 Materials

Silica nanoparticles consisting of amorphous SiO_2 (99.5% purity; 15 nm in diameter) were purchased from Nanostructured and Amorphous Materials Inc. (www.nanoamor.com). Amino-modified polystyrene nanoparticles, 100 nm in diameter, were from Polysciences Inc. (www.polysciences.com). APTS (3-aminopropyl) triethoxysilane (98%) and the lanthanide chlorides were acquired from Sigma (www.sigmaaldrich.com), EDTA from Merck (www.merck-chemicals.de), and the merocyanines S-0121, S-0306, S-0378, S-0749 from FEW Chemicals (www.few.de).

5.3.2 Instrumentation

Fluorescence spectra were acquired on an FP-6300 High Sensitivity Fluorescence Spectrometer from Jasco, UK (www.jasco.co.uk). Luminescence spectra of the UCLNPs were recorded on a Cary Eclipse fluorometer (from Varian; www.varianinc.com). A 980-nm fiber-optic diode laser (maximally 5 mW cw; from Roithner Lasertechnik; www.roithner-laser.com) was used as the light source for upconversion photoexcitation. The specific surface area of the silica NPs was determined by the nitrogen adsorption method of Brunauer, Emmett and Teller (BET)[32] using the ASAP 2010 system of Micrometrics (www.micrometrics.com).

5.3.2 Preparation of Amino-Modified Silica Nanoparticles (SiNPs)

In a typical reaction, 0.5 mL of APTS was added to 100 mg of the SiNPs suspended in 25 mL of toluene, and the mixture heated to 95 °C for 4 h. The resulting NPs were isolated by centrifugation (10 min and 4400 rpm) and washing cycles using two times ethanol and two

times acetone. The amino-modified SiNPs were dried at ~60 °C for 12 h and stored in a dry atmosphere.

5.3.3 Preparation of Labeled SiNPs

A suspension of 20 mg of the amino-modified SiNPs was treated with a mixture of 250 µL of a 1 mg mL^{-1} methanol solution of the merocycanine labels. Then, 200 µL of a 10 mM borate buffer solution of pH 9.3 was added and the mixture stirred under nitrogen overnight at ~ 65 °C. The color of the green colloidal suspension changed to blue. The solvent was removed using a rotary evaporator, and the blue NPs deposited were washed by re-suspending them in methanol, followed by four cycles of centrifugation (10 min at 4400 rpm) and washing (two times methanol and two times water). The NPs were dried at ~60 °C in an oven for 12 h and stored in an Eppendorf cup.

5.3.4 Preparation of Fluorescently Labeled Polystyrene Nanoparticles

In a typical reaction, a solution of 100 µL amino-modified polystyrene nanoparticles (PSNPs; diameter 100 nm; a 2.5% suspension in water) was treated with a mixture of 165 µL of a 1 mg mL^{-1} ethanol solution of the respective label in an Eppendorf vial and subsequent stirring in a thermomixer (at 950 rpm and 60 °C) for 12 h (2 h only in case of the more reactive label S-0378). The green color of the colloidal solution changed to blue. The solvents were removed, and the particles were purified via four cycles of centrifugation (10 min at 4400 rpm) and washing (two times ethanol and two times water). They were dried at ~60 °C in an oven for 12 h.

5.3.4 Synthesis of the $NaYF_4$:Yb,Er Upconverting Luminescent Nanoparticles (UCNLPs)

These were prepared by the coprecipitation method.[33] In a typical procedure, 16 mL of a 0.2 M solution of YCl_3, 3.4 mL of 0.2 M $YbCl_3$, and 0.6 mL of 0.2 M $ErCl_3$ were mixed with 20 mL of a 0.2 M EDTA solution in order to form the respective EDTA complexes. This solution was quickly injected into 60 mL of a 0.05 mol solution of sodium fluoride, and the mixture

stirred for 1 h at room temperature. The resulting precipitate was centrifuged, washed three times with water and once with ethanol. The precipitate was then dried in a drying furnace and under vacuum. The nanoparticles thus prepared are rather weak upconverters when illuminated with 980-nm light, but their efficiency is distinctly enhanced if they are annealed at high temperatures upon which they undergo a transformation from the mainly cubic phase to a hexagonal phase. Annealing of the nanoparticles was carried out in an atmosphere of argon by heating them to 400 ºC at a rate of 20 ºC per min, maintaining this temperature for 5 h, and cooling to room temperature under the same atmosphere. The resulting (partial) conversion of the cubic into the hexagonal phase yields particles with higher upconversion efficiency.

5.3.5 Preparation of Amino-Modified UCLNPs

The respective UCLNPs (150 mg) were suspended in 25 mL of dry toluene in a 100 mL Schlenk flask and flushed with dry nitrogen. APTS (0.5 mL) was added and the mixture stirred for 4 h at 90 °C. The mixture was allowed to cool. The particles were separated by centrifugation (20 min at 4000 rpm), washed several times with ethanol and acetone (via centrifugation/washing cycles), dried in a furnace at 60 °C, and stored in an Eppendorf cup.

5.3.6 Labeling of UCLNPs

(A) In water/methanol using labels S-0378 or S-0121: A solution of 100 µL of a 1 mg mL^{-1} methanol solution of the respective merocycanine was added to a mixture of 20 mg of amino-modified UCLNPs suspended in 5 mL of methanol and 200 µL of a 10 mM borate buffer solution of pH 9.3. The mixture was stirred overnight at ~ 65 °C using a magnetic stirrer. The color of the resulting nanoparticles changed to blue. The solvent was removed using a rotary evaporator, and the deposited NPs were purified by four cycles of centrifugation (10 min and 4400 rpm) and washing using two times methanol and two times water. The NPs were dried at ~60 °C for 12 h.

(B) In toluene (using label S-0749): The amino-modified UCLNPs (20 mg) were suspended in 5 mL of toluene and treated with 100 µL of a 1 mg mL^{-1} toluene solution of S-0749. The mixture was stirred under nitrogen overnight at ~65 °C. Toluene was removed using a rotary

evaporator, and the blue NPs deposited were washed by re-suspending them in toluene, followed by four cycles of centrifugation (10 min at 4400 rpm) and washing (two times toluene and two times water). The NPs were dried at ~60 °C in an oven for 12 h.

5.4 Results

5.4.1 Choice of Labels, and Mechanism of the Chameleon Effect

Figure 5.1 gives the chemical structures of the (known) exemplary dyes that have been investigated for their reactivity towards particles carrying amino groups on their surface. Figures 5.2 and 5.3 show the absorption and emission spectra of the free longwave dyes before their reaction with amines. All labels have a fairly reactive chloro group in the center of the chromophore. The dyes carrying sulfo groups are water soluble (to a varying extent), while S-0749 lacks such groups and is soluble in organic solvents such as methanol, dimethylformamide, acetone or toluene only.

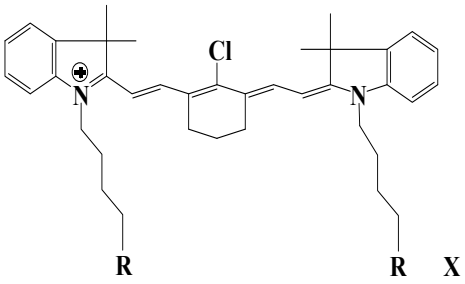

S-0121: R = SO_3^- X = Na^+

S-0749: R = H X = PF_6^-

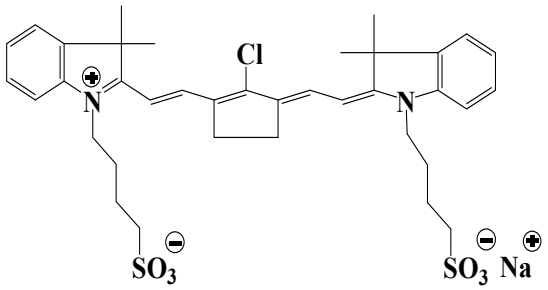

S-0378

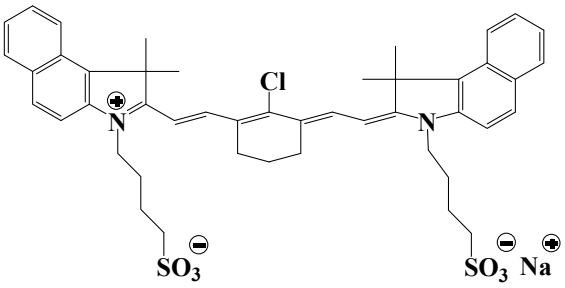

S-0306

Figure 5.1 Chemical structures of the cyanine type chameleon labels.

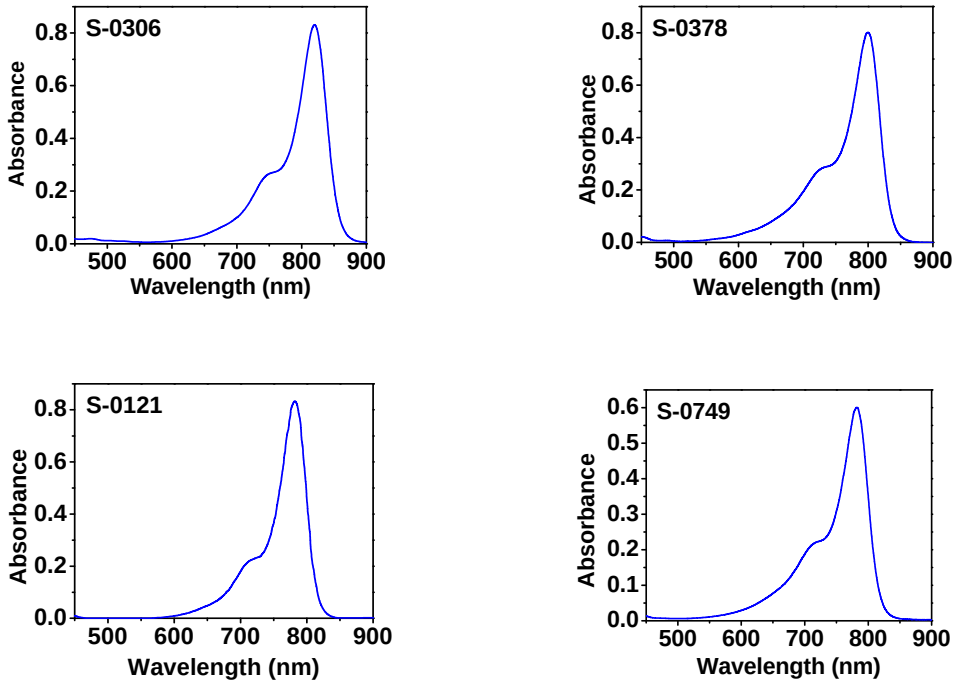

Figure 5.2 Absorption spectra of four chameleon dyes in methanol (before conjugation)

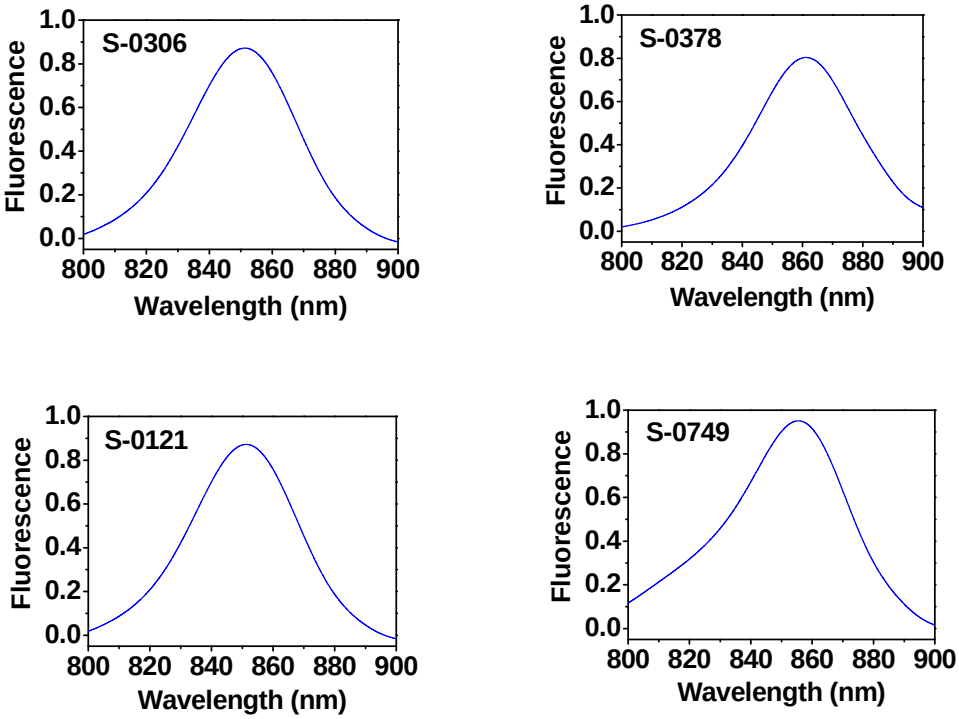

Figure 5.3 Fluorescence emission spectra of four chameleon dyes in methanol (before conjugation)

The dyes (labels) undergo facile nucleophilic substitution by amines in organic and – in case of labels with sulfo groups – aqueous solution at typically 40 – 60 °C as shown in Scheme 1. This is accompanied by a hypsochromic color change (from green to blue) to which we refer to as chameleon effect. With the exception of the so-called Py dyes,[30,34] practically all fluorescent labels do not undergo a significant color change on conjugation. The color change observed here is in accordance with color theory[35] because the strongly electron-withdrawing chloro substituent is being replaced by the electron-donating amino group. Label S-0378 is particularly reactive, probably because the chloro atom is located at a 5-membered ring. It reacts smoothly (within 2 h at ~40 °C) with amino-modified particles as shown in Scheme 5.1.

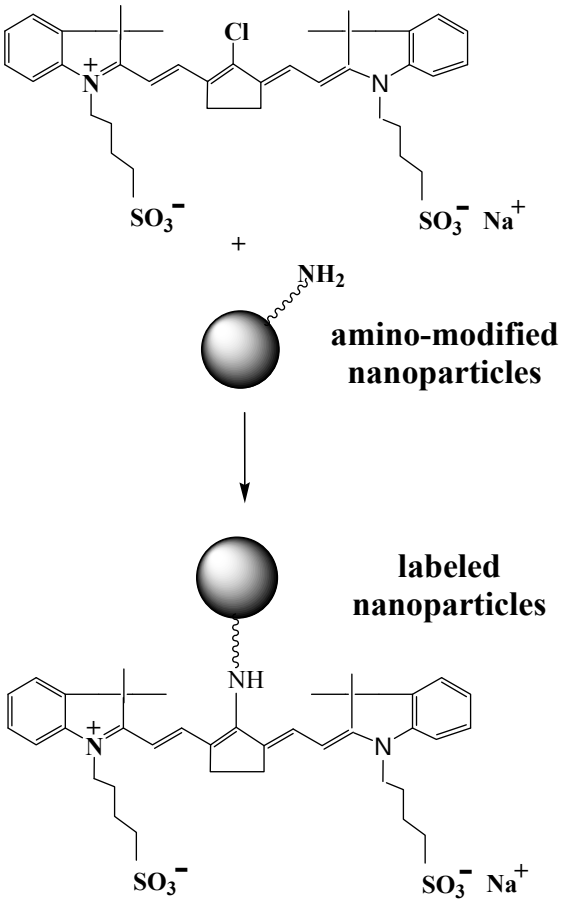

Scheme 5.1 Schematic representation of the reaction of an amino-modified particle with a chloro-reactive chameleon label.

5.4.2 Labeled Silica Nanoparticles

The amino-modified silica nanoparticles (SiNPs) were modified with the reagent 3-(aminopropyl)triethoxysilane (APTS) by an established procedure.[5] The resulting particles were characterized by thermogravimetric analysis, the results of which are shown in figure 5.4. The loading of the SiNPs with amino groups can be adjusted by varying the quantity of reagents employed. The relatively small loss of plain SiNPs or UCLNPs is mainly due to removal of adsorbed water. Amino-modified NPs suffer from a larger weight loss a fact that again indicates the presence of APTS which decomposes at above 450 °C. Further, surface modification is accompanied by a change of the surface charge of the SiNPs as confirmed by measurements of zeta potentials at pH 6. Plain SiNPs are known to be negatively charged at pH 6 due to silanol groups that are dissociated. If suspended in water of pH 6, they have a zeta potential of -29.6 mV. Following modification with APTS, the zeta potential changes to +36.1 mV due the presence of amino groups which are positively charged at pH 6.

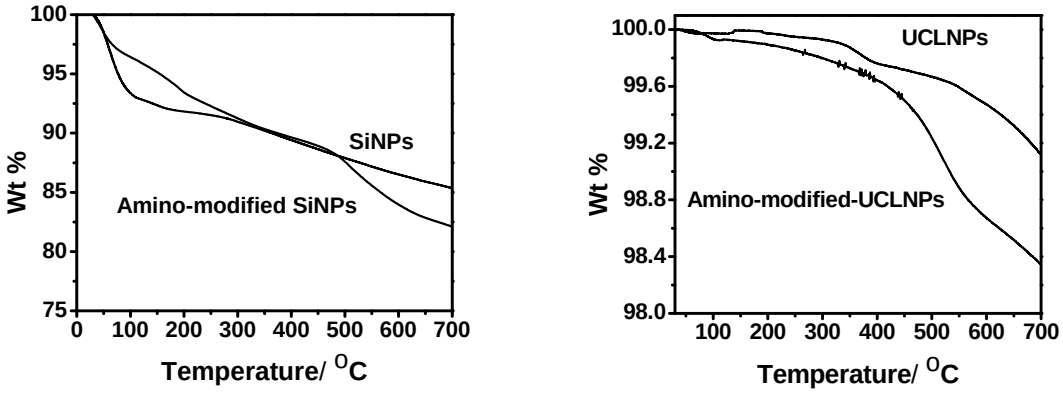

Figure 5.4 Thermogravimetric analyses of silica nanoparticles (SiNPs; left) and of upconverting nanoparticles (UCLNPs; right).

We find a loading with 0.6 amino groups per nm^{-2} of the surface (as determined by thermogravimetry and BET according to ref.[36] to be best in terms of reproducibility and small self-quenching of the labels. The amino-modified SiNPs were labeled with all four dyes. Those carrying sulfo groups were applied in methanol solution and S-0749 in toluene

solution. The resulting SiNPs, after isolation by centrifugation and several wash cycles, display blue color and dark red luminescence. The supernatant, in contrast, remains more or less green (depending on the excess of label applied). Figure 5.5 gives a picture of the color change observed.

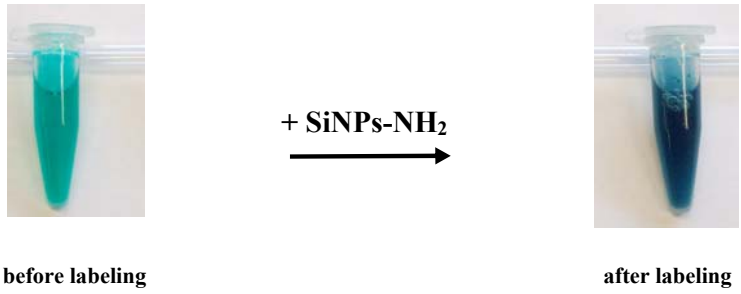

Figure 5.5 Schematic representation of the color change from green (left) to blue (right) on labeling amino-modified silica nanoparticles with label S-0378.

5.4.3 Labeled Polystyrene Nanoparticles

To explore the scope of the method, we also have labeled other types of nanoparticles. Amino-modified polystyrene nanoparticles (PSNPs) are commercially available. Labeling of these particles with dyes S-0121 and S-0378 in methanol solution proceeds with the same ease as in case of the SiNPs. A typical protocol is given in the Exptl. Part.

5.4.4 Labeled Upconverting Luminescent Nanoparticles

Upconverting luminescent nanoparticles (UCLNPs) are capable of upconverting longwave light (>800 nm) into visible luminescence.[37,38] They usually are based on a $NaYF_4$ structure that is doped with rare earth elements such as the trivalent ions of Eu, Tb, Yb, or Er. The particles used here have sizes ranging from 50 to 90 nm as shown by TEM (see figure 5.6). They were surface-modified in toluene solution using the reagent APTS by exploiting the fact that $NaYF_4$ nanocrystals (like many other crystals) carry hydroxy groups on their surface that undergo chemical reactions with triethoxysilanes such as APTS. The resulting particles were characterized by thermogravimetric analysis, the results of which are shown in figure 5.4. Labeling of the amino-modified UCLNPs with S-0121, S-0749 and S-0378 gave the particles

whose spectral properties are given in table 5.1.

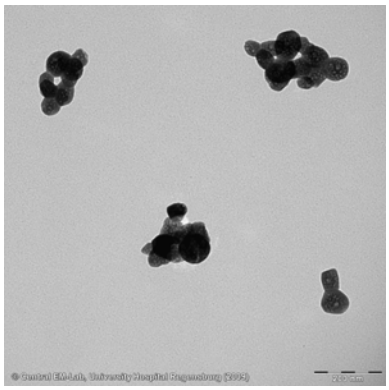

Figure 5.6 TEM pictures of the UCLNPs with 50-90 nm particle size, Scale bar: 200 nm.

5.4.5 Absorption and Emission Spectra of the Nanoparticles

The absorption and emission spectra of the SiNPs labeled with S-0378 are given in figure 5.7. The loading of the SiNPs and UCLNPs with amino groups can be governed by the quantity of reagents employed. Typical absorption and emission spectra of the SiNPs labeled with S-0121, S-0749, and S-0378 are given in figure 5.8, and those of the PSNPs in figure 5.9. Table 5.1 summarizes the spectral properties of all particles.

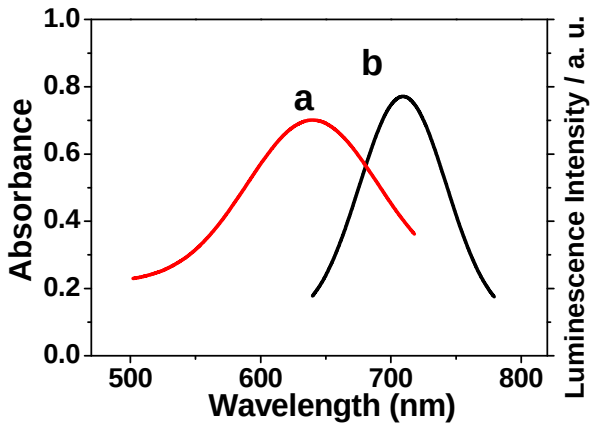

Figure 5.7 Normalized absorption spectrum (a) and emission spectrum (b) of SiNPs labeled with S-0378.

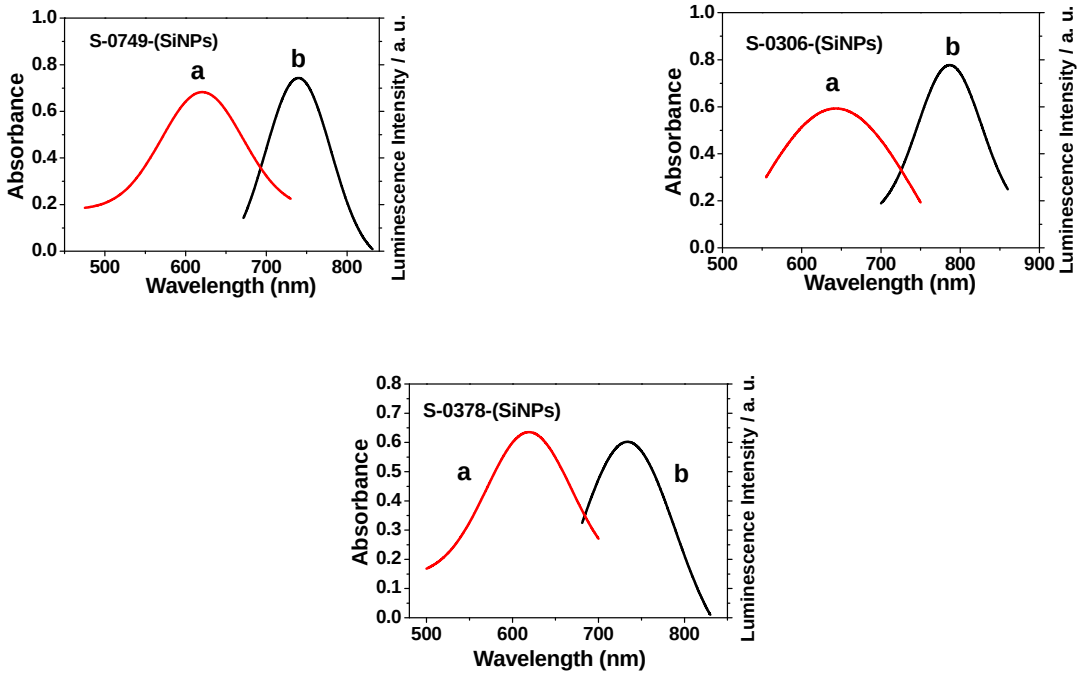

Figure 5.8 Normalized absorption (a) and fluorescence (b) spectra of SiNPs labeled with chameleon dyes.

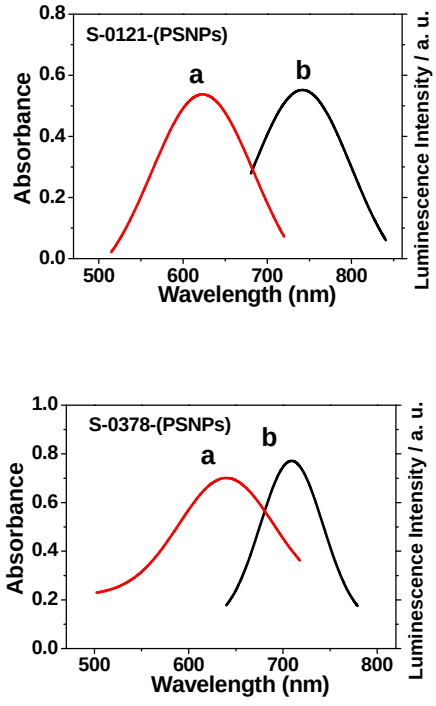

Figure 5.9 Absorption spectra (a) and emission spectra (b) of PSNPs labeled with UR- chameleon dye.

Table 5.1 Fluorophores used and absorption and emission maxima (in nm) of the labeled silica nanoparticles(SiNPs), upconverting luminescent nanoparticles (UCLNPs), and polystyrene nanoparticles (PSNPs), and spectral bandwidths of the emission bands at half maximum.

Fluorophore/nanoparticle	λ_{max} *(abs.)*[(a)]	λ_{max} *(em.)*[(a)]	*band width*[(a)]
S-0378-(SiNPs) [(b)]	641	708	105
S-0121-(SiNPs) [(b)]	618	734	120
S-0749-(SiNPs) [(b)]	622	739	82
S-0306-(SiNPs) [(b)]	644	786	90
S-0121-(PSNPs) [(c)]	623	743	122
S-0378-(PSNPs) [(c)]	641	708	125
S-0121-(UCLNPs) [(d)]	624	738	102
S-0749-(UCLNPs) [(d)]	621	739	80
S-0378-(UCLNPs) [(d)]	642	707	92

[(a)] after conjugation; [(b)] average size 10 nm; [(c)] average size 100 nm; [(d)] average size 50-90 nm.

It is virtually impossible to determine the molar absorbances of surface-immobilized labels. Therefore, we have reacted the labels S-0378, S-0306 and S-0121 with n-propylamine to obtain model compounds whose molar absorbances were determined. The respective values are 174,000, 165,000 and 170,000 cm M^{-1}. The molar absorbances of the (blue) conjugates are smaller than those of the (green) labels which are higher by typically 40%.

The labeled UCLNPs display a most interesting property. If excited with visible light at ~ 620 nm, the typical deep red fluorescence of the chameleon label is visible. If excited with 980-nm laser light, the upconverted luminescence (green and red; two bands) can be seen. Such particles are of substantial interest in terms of encoding trade named products, in the authentication of documents or banknotes, and in security and anti-terror technology.[39] Figure 5.10 shows spectra of the UCLNPs labeled with S-0121 under 620 nm and 980 nm excitation, respectively. Compared to unlabeled UCLNP (see figure 5.10, right panel), the typical green and red emission of the UCLNPs can be seen, but the intensity of the red peak is reduced in the labeled UCLNPs (plot d) due to an inner filter effect caused by the longwave label on their

surface. Typical absorption and emission spectra of the UCLNPs labeled with S-0749, and S-0378 are given in figure 5.11.

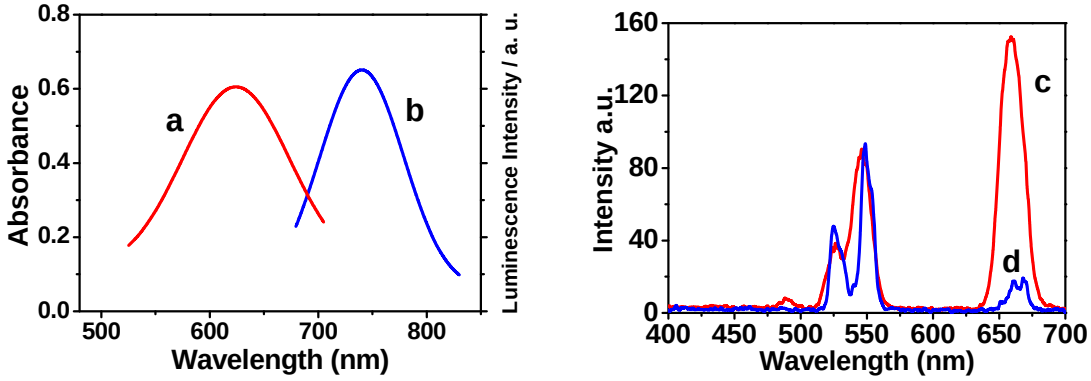

Figure 10. *Left panel*: Absorbance spectra (a) and emission spectra (b) of UCLNPs labeled with S-0121 under 620-nm excitation. *Right panel*: Fluorescence spectra of UCLNPs before (c) and after (d) labeling with S-0121 at 980-nm laser diode excitation. The intensity of the red band is screened off in the presence of the label.

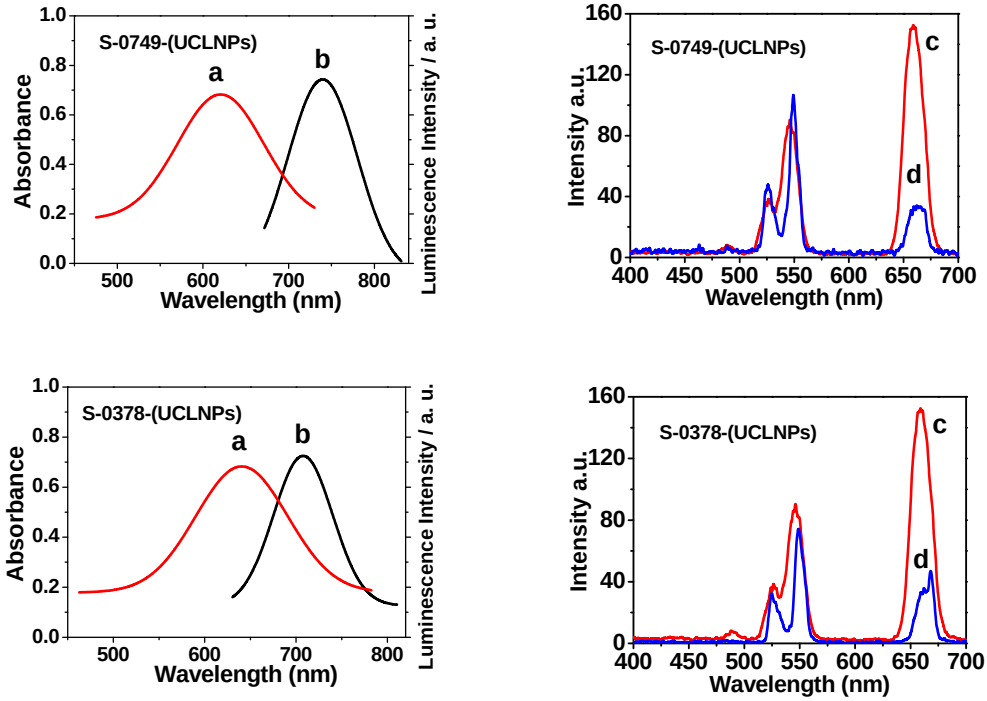

Figure 5.11 *Left panel:* Absorbance spectra (a) and emission spectra (b) of UCLNPs labeled with UR- chameleon dyes S-0749 and S-0378 under 620-nm excitation. *Right panel:* Fluorescence spectra of UCLNPs before (c) and after (d) labeling with the two chameleon dyes. Excitation at 980 nm using a laser diode.

5.4.6 Detecting Amino Groups on the Surface of Nanoparticles

The color changes associated with the conjugation of such chameleon labels also enable the visual detection of free amino groups. The method is simple in that a dilute (green) solution of label S-0378 in methanol is added to the solid or suspended amino-modified NPs. After a reaction time of 2 h at 40 – 50 °C, the NPs are separated by centrifugation and washed with methanol. NPs carrying amino group assume a blue color, while NPs without amino groups remain colorless. This is shown in Figure 5.12.

While some adsorption of the reactive dyes to the unmodified NPs can be observed in all dyes, a few centrifugation and washing cycles completely remove the fluorophores (as verified by fluorescence spectroscopy), while covalently labeled SiNPs cannot be decolorized in this way.

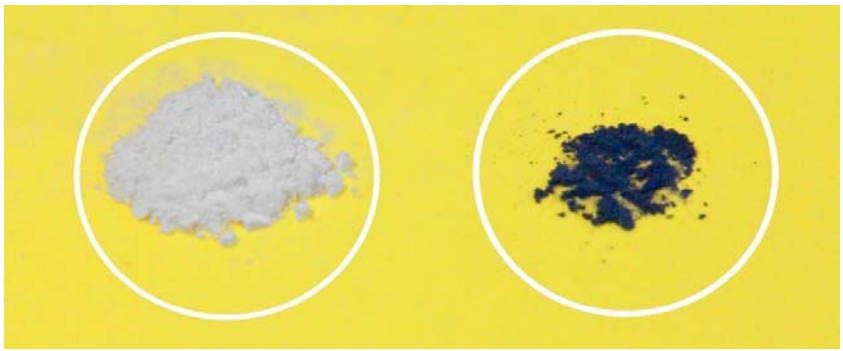

Figure 5.12 Photographs of silica nanoparticles (SiNPs) reacted with label S-0378. *Left*: SiNPs without amino groups. *Right*: SiNPs containing amino groups on the surface.

5.5 Discussion

The chloro groups in the labels shown in figure 5.1 are known to easily react with amines and sulfides.[40,41,42] Most notably, this reaction is accompanied by a large shortwave spectral shift and typically proceeds smoothly at temperatures between 30 to 80 °C to give particles that will be described in the following. The dyes used here have been used by Patonay et al.[40] as the starting material in the synthesis of amino-reactive labels by first reacting them at the

chloro substituent with thiophenols, this followed by modification to end up – in several steps – with a label for amines. Our protocol, as applied here to amino-modified nanoparticles, is distinctly much simple. We note that the labeled particles have very longwave absorption and emission which is desirable when working with biological samples. Such labels, like the squaraines,[43] can be photoexcited with low cost (diode) lasers which results in easily detectable fluorescence.

The method for detecting the presence of amino particles is simple in that a commercially available reagent (S-0378) is reacted at slightly elevated temperatures with the nanoparticles or surface to be tested. Even visual inspection already gives semi-quantitative information. The method is comparable to the one reported by Resch et al. for amino-modified surfaces[44] where a dye is used whose color changes from blue to red.

5.6 References

1 Wang L, Zhao W, Tan W (2008) **Bioconjugated silica nanoparticles: Development and applications**, Nano. Res. 1:99-115

2 Senarath-Yapa MD, Phimphivong S, Coym JW, Wirth MJ, Aspinwall CA, Saavedra SS (2007) **Preparation and Characterization of Poly(lipid)-Coated, Fluorophore-Doped Silica Nanoparticles for Biolabeling and Cellular Imaging,** Langmuir 23:12624-12633

3 Wang L, Wang K, Santra S, Zhao X, Hilliard LR, Smith JE, Wu Y, Tan W (2006) **Watching Silica Nanoparticles Glow in the Biological World,** Anal. Chem. 78:646-654.

4 Wang F, Tan WB, Zhang Y, Fan X, Wang M (2006) **Luminescent nanomaterials for biological labeling**, Nanotechnol. 17:R1-R13.

5 Mader HS, Li X, Saleh SM, Link M, Kele P, Wolfbeis OS (2008) **Fluorescent Silica Nanoparticles**, Ann. NY. Acad. Sci. 1130:218-223.

6 Santra S, Zhang P, Wang K, Tapec R, Tan W (2001) **Conjugation of Biomolecules with Luminophore-Doped Silica Nanoparticles for Photostable Biomarkers,** Anal. Chem. 73:4988-4993.

7 Ow H, Larson DR, Srivastava M, Baird BA, Webb W W, Wiesner U (2005) **Bright and Stable Core-Shell Fluorescent Silica Nanoparticles**, Nano. Lett. 5:113-117.

8 Lin HC, Lin HH, Kao CY, Yu AL, Peng WP, Chen CH (2010) **Quantitative Measurement of Nano-/Microparticle Endocytosis by Cell Mass Spectrometry**, Angew. Chem. Int. Edit. 49:3460-3464.

9 Borisov SM, Herrod DL, Klimant I (2009) **Fluorescent poly(styrene-block-vinylpyrrolidone) nanobeads for optical sensing of pH**, Sensor Actuat. B-Chem. 139:52-58.

10 Johnston HJ, Semmler-Behnke M, Brown DM, Kreyling W, Tran L, Stone V (2010) **Evaluating the uptake and intracellular fate of polystyrene nanoparticles by primary and hepatocyte cell lines in vitro**, Toxicol. Appl. Pharm. 242:66-78.

11 Kuerner JM, Wolfbeis OS, Klimant I (2002) **Homogeneous Luminescence Decay Time-Based Bioassay Using Energy Transfer from Nanospheres**, Anal. Chem. 74:2151-2156.

12 Kuerner JM, Klimant I, Krause C, Preu H, Kunz W, Wolfbeis OS (2001) **Inert Phosphorescent Nanospheres as Markers in Optical Assays**, Bioconj. Chem. 12:883-889.

13 Kuerner JM, Klimant I, Krause C, Pringsheim E, Wolfbeis OS (2001) **A New Type of Phosphorescent Nanospheres for Use in Advanced Time-Resolved Multiplexed Bioassays**, Anal. Biochem. 297:32-41.

[14] Mader HS, Kele P, Saleh SM, Wolfbeis OS (2010) **Upconverting Luminescent Nanoparticles for Use in Bioconjugation and Bioimaging**, Curr. Opin. Chem. Biol. 14: 582-596.

[15] Medintz IL, Clapp AR, Mattoussi H, Goldman ER, Fisher B, Mauro JM (2003) **Self-assembled nanoscale biosensors based on quantum dot FRET donors**, Nat. Mater. 2:630-638.

[16] Aubin-Tam ME, Hamad-Schifferli K (2008) Biomed. Mat. 3:034001.

[17] Wang L, Yang C, Tan W (2005) **Dual-Luminophore-Doped Silica Nanoparticles for Multiplexed Signaling**, Nano. Lett. 5:37-43.

[18] Zhou X, Zhou J (2004) **Improving the Signal Sensitivity and Photostability of DNA Hybridizations on Microarrays by Using Dye-Doped Core-Shell Silica Nanoparticles**, Anal. Chem. 76:5302-5312.

[19] Lu CW, Hung Y, Hsiao JK, Yao M, Chung TH, Lin YS, Wu SH, Hsu SC, Liu HM, Mou CY, Yang CS, Huang DM, Chen YC (2007) **Bifunctional Magnetic Silica Nanoparticles for Highly Efficient Human Stem Cell Labeling**, Nano. Lett. 7:149-154.

[20] Saleh SM, Müller R, Mader HS, Duerkop A, Wolfbeis OS (2010) **Novel multicolor fluorescently labeled silica nanoparticles for interface fluorescence resonance energy transfer to and from labeled avidin**, Anal. Bioanal. Chem. 398:1615-1623.

[21] Givan AL (2004) in: **Flow Cytometry: First Principles**, Wiley & Sons, New York.

[22] Perfetto SP, Chattopadhyay PK, Roederer M (2004) **Seventeen-colour flow cytometry: unravelling the immune system**, Nat. Rev. Immunol. 4:648-655.

[23] Prina-Mello A, Whelan AM, Atzberger A, McCarthy JE, Byrne F, Davies GL, Coey JMD, Volkov Y, Gun'ko YK (2010) **Comparative Flow Cytometric Analysis of Immunofunctionalized Nanowire and Nanoparticle Signatures**, Small 6:247-255.

[24] Santra S, Yang H, Dutta D, Stanley JT, Holloway PH, Tan W, Moudgil BM, Mericle RA (2004) **TAT conjugated FITC doped silica nanoparticles for bioimaging applications**, Chem. Comm. 2810-2811.

[25] Tallury P, Payton K, Santra S (2008) Special Focus: **Nanomaterials for Biomedical Diagnosis,** Nanomedicine 3:579-592.

[26] Shaertl S, Almes FJM, Calle EL, Siemers A, Kramer J (2000) **A Novel and Robust Homogeneous Fluorescence-Based Assay Using Nanoparticles for Pharmaceutical Screening and Diagnostics**, J. Biomol. Screen. 5:227-237.

[27] Dittrich PS, Manz A (2006) **Lab-on-a-chip: microfluidics in drug discovery**, Nat. Rev. Drug. Discov. 5:210-218

[28] Wang K, Tan W, He X (2005) **Biomedical Applications Based on Core-Shell Nanoparticles**, Eng. Med. Biol. Mag. Soc. 1:717-719.

[29] Rocco MA, Kim JY, Burns A, Kostecki J, Doody A, Wiesner U, DeLisa MP (2010) **Site-Specific Labeling of Surface Proteins on Living Cells Using Genetically Encoded Peptides that Bind Fluorescent Nanoparticle Probes**, Bioconj. Chem. 20:1482-1489.

[30] Wetzl BK, Yarmoluk SM, Craig DB, Wolfbeis OS (2004) **Chameleon labels for staining and quantifying of proteins,** Angew. Chem. Int. Ed. 43:5400–5402.

[31] Miller JN (2008) **in Long-Wavelength and Near-Infrared Fluorescence: State of the Art, Future Applications, and Standards; in Standardization and Quality Assurance in Fluorescence Measurements**, ed U. Resch-Genger, Springer, Berlin, vol. 5, pp 147.

[32] Fuji M, Ueno S, Takei T, Watanabe T, Chikazawa M (2000) **Surface structural analysis of fine silica powder modified with butyl alcohol**, Colloid. Polym. Sci. 278:30–36.

[33] Yi GS, Lu HC, Zhao SY, Yue G, Yang WJ, Chen DP, Guo LH (2004) **Synthesis, Characterization, and Biological Application of Size-Controlled Nanocrystalline $NaYF_4$:Yb,Er Infrared-to-Visible Up-Conversion Phosphors**, Nano. Lett. 4:2191-2196.

[34] Steiner MS, Meier RJ, Duerkop A, Wolfbeis OS (2010) **Chromogenic Sensing of Biogenic Amines Using a Chameleon Probe and the Red-Green Blue Readout of Digital Camera Images**, Anal. Chem. 82:8402-8405.

[35] Zollinger H (2003) in: **Color Chemistry, Synthesis, Properties, and Applications of Organic Dyes and Pigments**, 3rd (ed) Wiley-VCH, Zürich, pp 366.

[36] Fuji M, Ueno S, Takei T, Watanabe T, Chikazawa M (2000) **Surface structural analysis of fine silica powder modified with butyl alcohol**, Colloid. Polym. Sci. 278:30-36.

[37] Mader HS, Link M, Achatz DE, Uhlmann K, Li X, Wolfbeis OS (2010) **Surface-Modified Upconverting Microparticles and Nanoparticles for Use in Click Chemistries**, Chem. Eur. J. 16:5416-5424.

[38] Achatz DE, Reham A, Wolfbeis OS (2011) **Fluorescent Sensing, Biosensing, and Screening Using Upconverting Nanoparticles**, Topics. Curr. Chem. 300:29-50.

[39] Gorris HH, Ali R, Saleh SM, Wolfbeis OS (2011) **Tuning the Dual Emission of Photon-Upconverting Nanoparticles for Ratiometric Multiplexed Encoding**, Adv. Mater. in press.

[40] Patonay G, Salon J, Sowell J, Strekowski L (2004) **Noncovalent labeling of biomolecules with red and near-infrared dyes**, Molecules 9:40-49.

[41] Li X, Shi W, Chen S, Jia J, Ma H, Wolfbeis OS (2010) **A Near-Infrared Fluorescent Probe for Monitoring Tyrosinase Activity**, Chem. Comm. 2560-2562.

[42] Kele P, Li X, Link M, Nagy K, Herner A, Lörincz K, Beni S, Wolfbeis OS (2009) **Clickable Fluorophores for Biological Labeling - With or Without Copper**, Org. Biomol. Chem. 7:3486-3490.

[43] Oswald B, Patsenker L, Duschl J, Szmacinski H, Wolfbeis OS, Terpetschnig E (1999) **Synthesis, Spectral Properties and Detection Limits of Reactive Squaraine Dyes, a New Class of Diode Laser Compatible Fluorescent Protein Labels**, Bioconj. Chem. 10:925-931.

[44] Hoffmann K, Mix R, Resch-Genger U, Friedrich JF (2007) **Monitoring of Amino Functionalities on Plasma-Chemically Modified Polypropylene Supports with a Chromogenic and Fluorogenic Pyrylium Reporter**, Langmuir 23: 8411-8416.

6 Quenching of the Luminescence of Upconverting Luminescent Nanoparticles by Heavy Metal Ions

6.1 Abstract

This chapter reports on the finding that the luminescence of upconverting luminescent nanoparticles (UCLNPs) is quenched by heavy metal ions and halide ions in aqueous solution. The UCLNPs consist of hexagonal $NaYF_4$ nanocrystals doped with trivalent rare earth ions and were synthesized by both the oleic acid (solvothermal) method and the ethylenediaminetetraacetic acid (coprecipitation) method. Quenching was studied for the ions Cu(II), Hg(II), Pb(II), Cd(II), Co(II), Ag(I), Fe(III), Zn(II), bromide and iodide, and is found to be particularly strong for Hg(II). Stern-Volmer plots are virtually linear up to 10 – 25 mM concentrations of the quencher, but deviate from linearity at higher quencher concentrations where static quenching causes an additional effect. The UCLNPs display two main emission bands (blue, green, red or near-infrared), and the quenching efficiencies for these are found to be different. The effect seems to be generally associated with UCLNPs because it was observed for all particles doped with trivalent lanthanide ions including Yb(III), Er(III), Ho(III), and Tm(III). The results are discussed in terms of quenching mechanisms and with respect to potential applications such as optical sensing of heavy metal ions.

6.2 Introduction

Colloidal nanoparticles (NPs) are neither mono-dispersed molecules nor can they be considered as being a bulk material. Their properties often are highly different from those of the species they are made up from.[1] Virtually all solid species can be converted into NPs,[2,3] but those made from carbon,[4] (noble) metal ions,[5] certain semiconductors,[6] or the zinc/cadmium sulfide/selenide nanoparticles (also refered to as quantum dots or Q-dots).[7] The latter have attracted considerable attention in the past years as they display a (size-dependent) luminescence. Q-dots have been widely used as biolabels and in imaging.[7] Most notably, their luminescence is quenched by various inorganic ions,[8,9,10] by organic species such as amines,[11] biphenol A,[12] nitro compounds,[13] and by ruthenium-bipyridyl complexes in the presence of DNA,[14] to give a few examples. The efficiency of the quenching by heavy metal

ions[15,16] such as by Hg(II),[17] Cu(II),[18] Ag(I)[19] or Pb(II) ions[20] is surprisingly strong. This effect was applied to the determination of heavy metal ions[21,22,23,24] or explosives.[25] Surface-modified (such as cysteine-capped) Q-dots also were used as fluorescent probes for Cu(II) and Ni(II) ions.[26,27] Quenching by certain chromium(III) complexes is associated with the release of the messenger molecule NO from the respective Cr(III) complex.[21] The potential cell toxicity[28] of Q-dots, and the numerous possibilities they provide in context with biological systems[29] has been discussed recently.

Infrared-to-visible upconverting luminescent nanoparticles (UCLNPs) represent a rather new class of nanomaterials that have attracted attention owing to their unusual optical properties. They often are composed of $NaYF_4$ host crystals doped with trivalent lanthanide ions. UCLNPs are capable of converting low energy (near-infrared) radiation to higher-energy (visible) light by multi-photon absorption and subsequent emission of dopant-dependent luminescence.[30,31] The peak emission wavelengths of the UCLNPs are not size-dependent (as in the case of Q-dots), and multi-color emission can easily be accomplished by varying the kind of host crystal and the rare earth dopant (such as terbium or erbium).

UCLNPs possess attractive spectral properties.[32] They usually display two emission bands in the visible, and their large anti-Stokes shift (ranging from –100 to –500 nm) allows for an easy separation of the emission peaks from the (laser) excitation light source and from Raman scattering. They have the advantage of being photoexcitable in the NIR (around 980 nm), a wavelength where the auto-absorption and auto-luminescence of biological matter is quite weak if present at all. Even if auto-luminescence does occur, it will be at wavelengths of >980 nm, thereby reducing background of luminescence spectra in the visible to zero. In addition, they display fairly high quantum yields, narrow emission bands, high chemical stability, and do not bleach nor blink. Moreover, NIR light is safe to tissue which it can penetrate to a depth of up to several mm.[33,34]

UCLNPs have found applications in chemical sensing,[35] labeling of biomolecules,[36,37,38,39] and in enzymatic and affinity assays[40,41] and in intracellular sensing of temperature[42] because of their brightness and other attractive features, but also because the rigid crystal host lattice protects the emitting rare earth dopants from environmental perturbances. Despite many studies on the spectral properties of UCLNPs, it is rather surprising that the quenching of their luminescence by HMs has not been investigated so far. It is known, however, that UCLNPs undergo surface quenching effects associated with the size-dependent luminescence,[43] but this not related to external quenchers. We are reporting here for the first time that the

luminescence of UCLNPs nanocrystals is strongly quenched by heavy metal ions (HMs). We also discuss the mechanism of quenching and envision application of this new effect.

6.3 Experimental

6.3.1 Materials

Yttrium(III) chloride hexahydrate (99.99%), ytterbium(III) chloride hexahydrate (99.99%), erbium(III) chloride hexahydrate (99.99%), thulium(III) chloride hexahydrate (99.99%), holmium(III) chloride hexahydrate (99.99%), and oleic acid 90% were purchased from Sigma (www.sigmaaldrich.com) and ethylene diaminetetraacetic acid (EDTA) from Merck (www.merck-chemicals.de). Organic solvents were of analytical quality and used as received.

6.3.2 Instrumentation

Luminescence spectra of particles were recorded on a Cary Eclipse fluorometer (from Varian; www.varianinc.com). A 980-nm fiber optic diode laser (maximally 5 mW cw; from Roithner Lasertechnik; www.roithner-laser.com) was used as the light source for upconversion photoexcitation. Transmission electron microcopy images were acquired using a 120-kV Zeiss (www.smt.zeiss.com) instrument of type Leo 912AB equipped with a Proscan CCD (www.proscan.de) camera.

6.3.3 Synthesis of $NaYF_4$:Yb,X (X = Er, Ho, Tm) by the Solvothermal Method

In a typical protocol,[44] a total of 1 mmol of the respective lanthanide two chlorides was dispersed in 6 mL of oleic acid and 15 mL octadecene in a 50 mL bottle and heated to 150 °C with stirring to form a homogeneous solution. The ratio of lanthanide chlorides was adjusted as specified in table 6.1. The solutions were then left to cool to room temperature. After 30 min, 10 mL of a solution of 100 mg (2.5 mmol) of sodium hydroxide and 148 mg (4 mmol) of ammonium fluoride in methanol were added to the flask to quickly form a precipitate. The suspension was stirred for another 2 h to ensure that all fluoride has been consumed. Subsequently, the suspension was slowly heated to 90 °C (for around 10 min to evaporate methanol), then to 300 °C in a fume cupboard and maintained at this temperature for 1.5 h

under an atmosphere of argon. Nanocrystals were then precipitated from the cooled solution by adding 10 mL of ethanol and isolated and purified via three cycles of centrifugation (10 min at 4400 rpm) and washing (two times ethanol, one time acetone or toluene).

6.3.4 Synthesis of $NaYF_4$:Yb,X (X = Er, Ho, Tm) by the Coprecipitation Method

These were also synthesized according to a procedure described in the literature.[45] Briefly, solutions of 15.6 mL of 0.2 M of YCl_3, 4 mL of 0.2 M $YbCl_3$ and 0.4 mL of 0.2 M XCl_3 were mixed with 20 mL of a 0.2 M EDTA solution in order to form the respective EDTA complex. The ratio of the lanthanide chlorides was adjusted according to table 6.1. This solution was then quickly injected into 60 mL of a 50 mM solution of sodium fluoride, and the mixture stirred for 1 h at room temperature. The resulting precipitate was centrifuged, washed three times with water and once with ethanol. The precipitate was then dried in a furnace under vacuum. Annealing was carried out under an atmosphere of argon by heating the particles to 400 ºC at a rate of 20 ºC per min, maintaining this temperature for 5 h, and cooling to room temperature under the same atmosphere. The resulting (partial) conversion of the cubic into the hexagonal phase yields particles with much higher upconversion efficiency.

6.4 Results

6.4.1 Synthesis

The $NaYF_4$ nanoparticles were prepared by two methods. The first is the so-called oleic acid (solvothermal) method[44] and gave nanoparticles (NPs) referred to as UN-1 to UN-3. The second is the coprecipitation (EDTA) method[45] and gave particles UN-4 to UN-6. The composition and essential properties of the particles are listed in table 6.1. Varying concentrations of the dopants Yb^{3+}, Er^{3+}, Tm^{3+} and Ho^{3+} were adjusted. The UCLNPs display bright visible luminescence if excited with 980-nm laser light. All have two major emission bands whose peaks are also given in table 6.1.

Table 6.1 Composition of the UCLNPs studied in this work, ratio of dopants, wavelengths of main emission peaks (in nm), visible colors of emission, and average diameters (in nm).

Code	Composition	Fraction of dopants	Emission peaks (in nm)	Colors of emission	Diameter
UN-1	$NaYF_4$:Yb,Er [a)]	Yb(20%), Er(2%)	543, 657	green, red	~ 35 nm
UN-2	$NaYF_4$:Yb,Tm [a)]	Yb(20%), Tm(0.5%)	475, 802	blue, NIR	~ 35 nm
UN-3	$NaYF_4$:Yb,Ho [a)]	Yb(25%), Ho(0.5%)	541, 645	green, red	~ 35 nm
UN-4	$NaYF_4$:Yb,Er [b)]	Yb(20%), Er(2%)	543, 657	green, red	60 – 90 nm
UN-5	$NaYF_4$:Yb,Tm [b)]	Yb(20%), Tm(0.5%)	475, 802	blue, NIR	60 – 90 nm
UN-6	$NaYF_4$:Yb,Ho [b)]	Yb(25%), Ho(0.5%)	541, 645	green, red	60 – 90 nm

[a)] solvothermal ("oleic acid") method; [b)] coprecipitation ("EDTA") method

A TEM image of UN-1 nanocrystals is given in figure 6.1a and shows them to be hexagonal in shape, with a fairly uniform size of ~35 nm in diameter. They obviously self-assemble on the copper grid with a long range order. The NPs of type UN-1 were washed several times with toluene and ethanol to remove excess oleic acid on the surface and then were submitted to spectroscopy in order to remove the (shielding) oleate ligands from their surface. The stability of colloidal solutions of the UCLNPs was studied in aqueous solution (see figure 6.2). The slow decrease in the intensity of upconverted luminescence is indicative of good but not perfect temporal stability in aqueous solution (acetate buffer solution at pH 4).

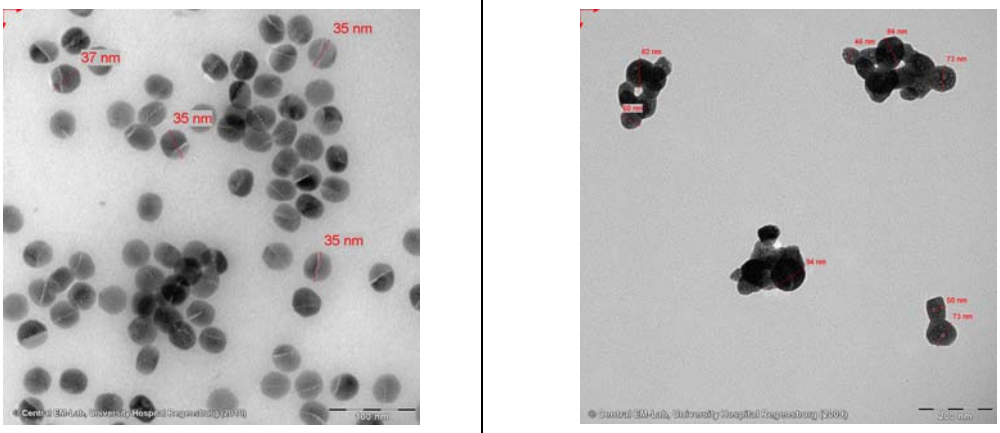

Figure 6.1 Transmission electron microscopy images of $NaYF_4$:Yb,Er nanoparticles. *Left:* Hexagonal upconverting luminescent nanoparticles of type UN-1 made by the solvothermal ("oleic acid") method, with a typical size of ~35 nm. Scale bar: 100 nm. *Right:* Type UN-4 nanoparticles made by the co-precipitation ("EDTA") method with a typical size of ~50 – 90 nm. Scale bar: 200 nm.

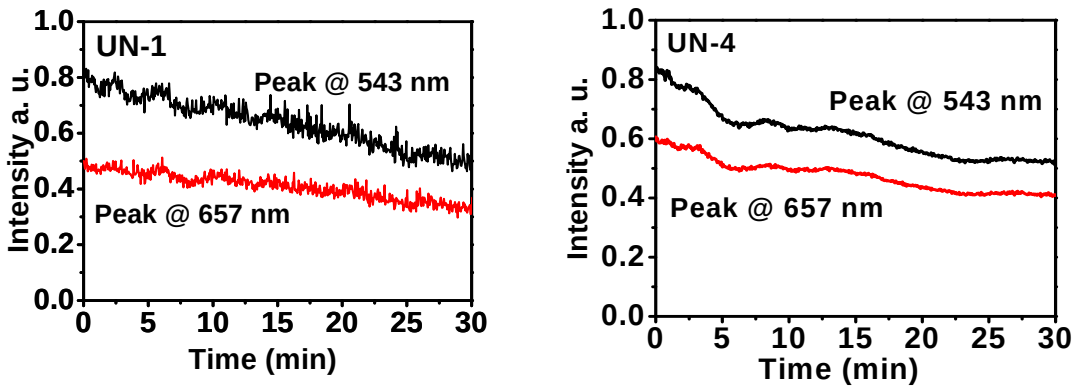

Figure 6.2 shows the luminescence intensity vs. time relation of UN-1 and UN-4 (concentration 0.2 mg/L) which demonstrates a good stability in acetate buffer solution at pH 4 upon diode laser excitation at 980 nm. Over 30 min showing very slow sedimentation.

The other UCLNPs of type UN-4 to UN-6 were synthesized via the co-precipitation method to give crystalline particles with diameters ranging from 60 to 90 nm (see figure 6.1b). These nanoparticles are less efficient upconverters but efficiency is distinctly enhanced if the particles are annealed at temperatures of ~400 °C for 5 h upon which they undergo a transformation from the mainly cubic phase to a hexagonal phase.[30] The NPs of type UN-3 to

UN-6 seem to have a higher tendency towards aggregation after the annealing process compared to the particles of type UN-1 and UN-4.

6.4.2 Quenching of the Luminescence of Nanoparticles of Type UN-1 by Heavy Metal Ions

The luminescence emission spectra of UN-1 under 980-nm laser excitation were recorded in acetate buffer solution of pH 4 in the presence of various concentrations of Hg(II) ion. The results are given in figure 6.3a and reveal efficient quenching even by millimolar concentrations of Cu(II), typically by around 20% in presence of 1.5 mmol L^{-1} of the ion. figure 6.3b shows that the respective plots are linear up to around 25 mM concentrations of quencher. Interestingly, the luminescences of the green band (peaking at 543 nm); and the red band (peaking at 657 nm) are quenched with different efficiency. Obviously, the respective main electronic transitions, which are of the $^4S_{3/2}) \rightarrow {}^4I_{15/2}$ and the $^4F_{9/2} \rightarrow {}^4I_{15/2}$ type, respectively, are quenched by Hg(II) ions with different efficiency. The quenching of the luminescence of the UN-1 particles by the ions Cu(II), Pb(II), Cd(II), Co(II), Ag(I), Fe(III) and Zn(II) was also examined and is shown in figure 6.4.

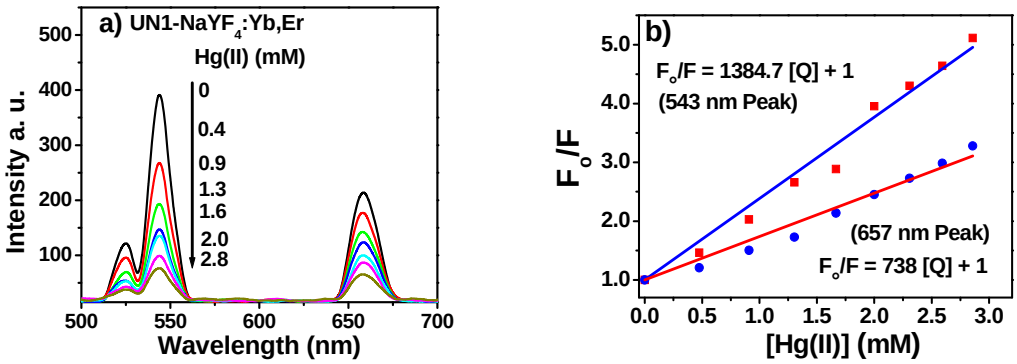

Figure 6.3 (a) Effect of the concentration of Hg(II) ions on the luminescence emission of particles of the type UN-1. The concentration of UN-1 is 0.2 mg mL^{-1}, and the concentrations of copper ions range from 0 to 10 mmol L^{-1}. (b) Respective Stern-Volmer plots for the two main emission bands.

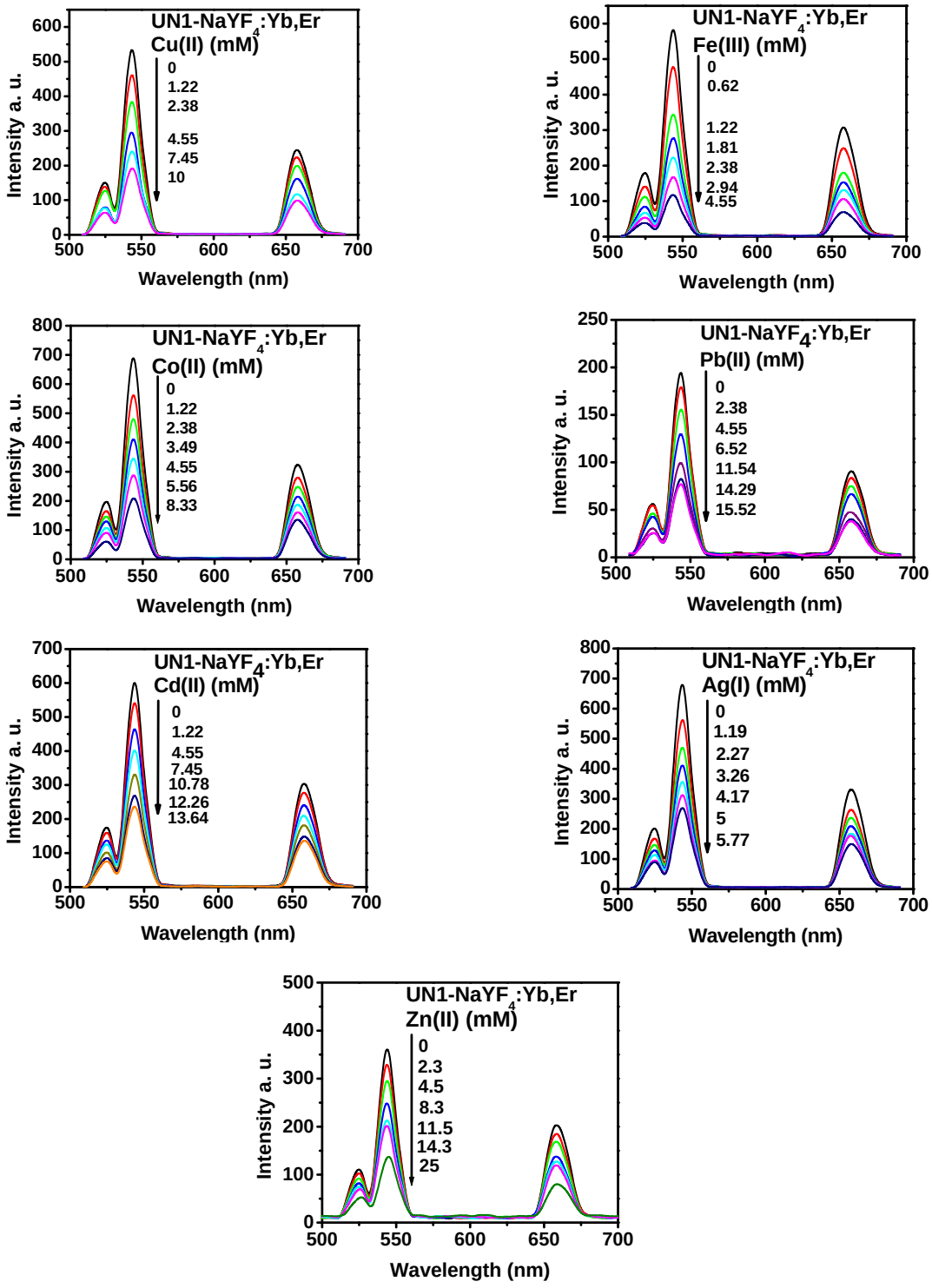

Figure 6.4 Quenching of the luminescence of NaY_4:Yb,Er nanoparticles (UN-1) by heavy metal ions in aqueous colloidal solution.

Dynamic quenching luminescence can be described by a Stern–Volmer relationship:

$$F_0/F = 1 + K_{SV}\,[Q]$$

where F_0 and F, respectively, are the luminescence intensities of the UCLNPs in absence and presence of HMs, [Q] is the concentration of the copper(II) ions, and K_{SV} is the Stern-Volmer constant. Data for the quenching of the luminescence of UN-1 and UN-4 by heavy metal ions are compiled in table 6.2.

Table 6.2 Stern-Volmer constants (K_{SV}, M^{-1}) of nanoparticles UN-1 and UN-4 for the quenching by heavy metal ions and anions.

	UN-1 (NaY_4:Yb,Er)		UN-4 (NaY_4:Yb,Er)	
Quencher (Q)	Ksv_1@543 nm	Ksv_2@657nm	Ksv_1@543 nm	Ksv_2@657 nm
Hg(II)	1385	738	278	356
Fe(III)	822	707	412	360
Co(II)	255	173	61	29
Ag(I)	224	192	158	129
Cu(II)	162	140	109	63
Pb(II)	90	81	43	36
Cd(II)	77	69	63	71
Zn(II)	61	56	45	50
I^-	110	142	56	64
Br^-	89	58	55	51

The mechanism of quenching at low concentration of metal ions is quite likely to involve dynamic quenching resulting from the collisions between HMs with the UCLNPs. The quenching constants are in the order of 60 to 180 M^{-1} and indicative of dynamic quenching. Static quenching also occurs but only at higher concentrations as will be shown below. The best way to differentiate between static and dynamic quenching is via measurement of decay times (which is strongly affected by static quenching, but not by dynamic quenching). However, the decay times of UCLNPs (which are in the order of 0.5 to 8 ms)[46,47] are quite complex due to the many electronic transitions that occur in parallel, so that decays are hardly

mono-exponential. Hence, they do not give a clear indication of whether static or dynamic quenching is operative.

In order to make quenching by HMs comparable, the quenching efficiencies were determined for all HMs in 2.3 mM concentration. Again, both emissions (with peaks at 543 and 657 nm, respectively) are strongly quenched. The data given in figure show the luminescence of UN-1 to be sensitive to Cu(II), Hg(II), Pb(II), Cd(II), Co(II), Ag(I), Fe(III) and Zn(II), while alkaline and earth alkaline ions in up to 20 mM concentration have virtually no effect. Respective Stern-Volmer plots (figure 6.5) are linear in up to 10 mM concentrations.

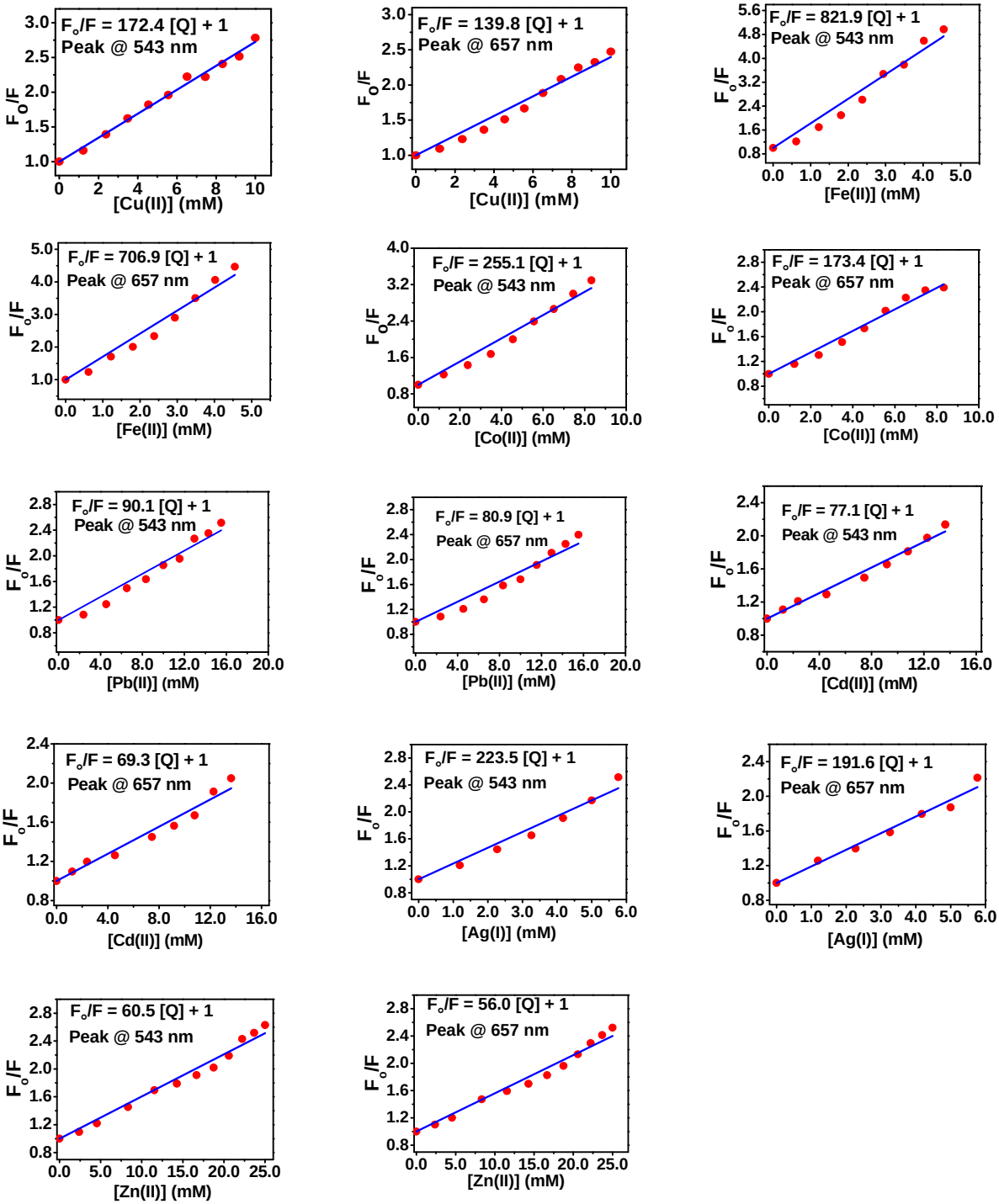

Figure 6.5 Stern-Volmer plots for the quenching of the luminescence of particles of type UN-1 by Cu(II), Fe(III), Co(II), Pb(II), Cd(II), Ag(I) and Zn(II) ions.

Figure 6.6 reveals that quenching by mercuric ions is particularly efficient, a finding that may pave the way to sense or image this ion. Quenching by >60% is observed in 2.3 mM concentration. Assuming that the intensity of the green emission band can be reliably detected if amounts to -2%, this will result in a detection limit of ~15 mM, equivalent to ~3 ppm, of mercury ion. One alternative way of read-out (possible only with dual emitters whose bands are quenched with different efficiency) is to determine the ratio of the intensities of the two bands. This also is a highly specific feature of UCLNPs.

Figure 6.6 Effect of HMs ions (all in 2.3 mM concentration) on the intensity of the red and green emission of nanoparticles of the type NaY_4:Yb,Er (UN-1) at pH 4. Quenching by ferric ion is particularly strong.

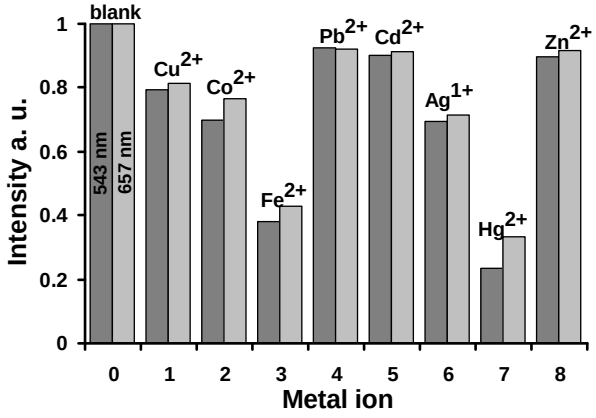

6.4.3 Quenching of the Luminescence of Nanoparticles of Type UN-4 by Heavy Metal Ions

The same procedure was applied to study the luminescence quenching of UN-4 (doped with Yb and Er; prepared by the coprecipitation method) by Hg(II) as shown in figure 6.7. Like in the case of the particles of the type UN-1 (which were prepared by the solvothermal method), the luminescence intensities of peaks at 543 and 657 nm are quenched, and Stern-Volmer plots showed good linear relationships in the range of 0 to 25 mmol L^{-1}, but the Stern-Volmer constants are somewhat smaller in general than those for particles of type UN-1 as can be seen from the data in table 6.2.

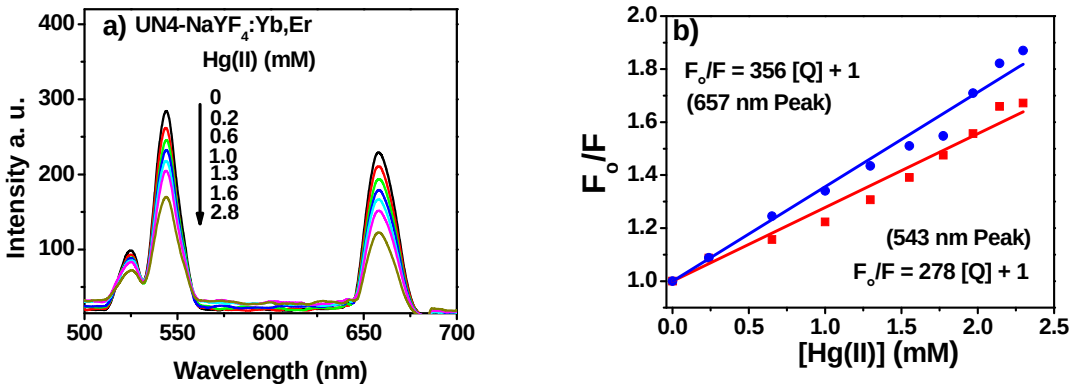

Figure 6.7 (a) Effect of various concentration of Hg(II) ions on luminescence of UN-4. The concentration of UN-4 is 0.2 mg/mL^{-1}, and the concentrations of copper ions range from 0 to 25 mmol L^{-1}. Right panel (b): Stern-Volmer plots for Hg(II) induced quenching of the UCLNPs.

Next, we have studied the quenching of UCLNPs of type UN-4 by Hg(II), Pb(II), Cd(II), Co(II), Ag(I), Fe(III) and Zn(II). Again, linear Stern–Volmer plots are obtained if the concentrations of the metal ions are below 10 – 20 mM. The respective K_{SV} values (table 6.2) show that quenching is less efficient than in case of UN-1.

6.4.4 Static Quenching of the Luminescence of UCLNPs at Higher Concentration of Heavy Metal Ions

The quenching of the luminescence of UCLNPs by heavy metal ions (HMs) deviates from linearity at concentration of higher than 5 to 10 mM depending on the ion. Plots of F_0/F versus the concentration of Cu(II) and Fe(III) are shown in Figure 6.8. Such a plot is typical[1,48] for situations where both dynamic quenching and static quenching occur. Dynamic quenching involves the collision and subsequent formation of a transient complex between an excited-state fluorophore (here the UCLNPs) and a ground-state quencher (here the HM ion) during the excited-state lifetime of the UCLNPs. The excited-state complex dissociates upon nonradiative deactivation, leaving both the UCLNPs and quencher in the ground state. The Stern-Volmer relation is linear if either static quenching or dynamic quenching are the only mechanisms for deactivation. This is the case here for quenchers present in concentrations of up to typically 5 to 10 mM depending on the kind of ion, and quenching constants are typical for dynamic quenching. Static quenching, in contrast, implies the formation of a ground-state (and non-fluorescent) complex between the UCLNPs and the HMs. This complex is

temporally stable and thus quite different from the uncomplexed UCLNPs and the excited state complex formed during dynamic quenching.[48]

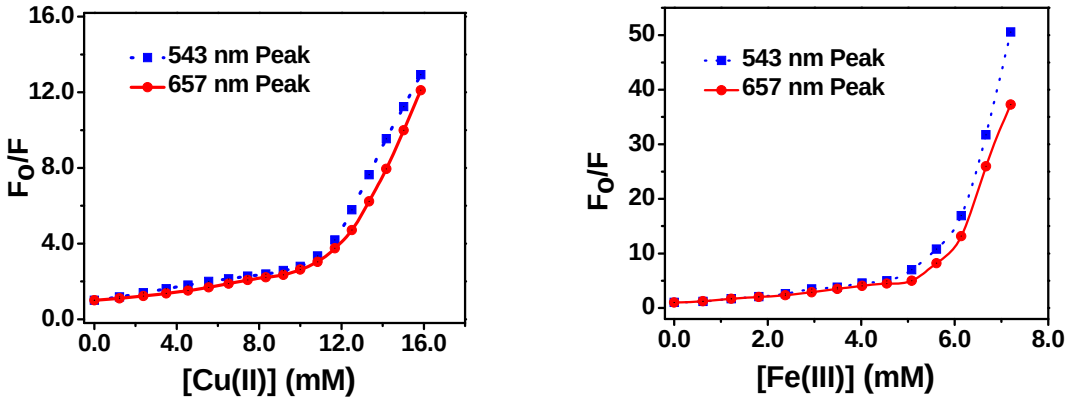

Figure 6.8 Deviation from linearity in Stern-Volmer plots of the quenching of the luminescence of nanoparticles of the type UN-1 by Cu(II) and Fe(III) ions at higher quencher concentrations.

6.4.5 Quenching of the Luminescence of UN-1 and UN-4 Particles by Halide Ions

Bromide and iodide (unlike fluoride and chloride) are notorious quenchers of luminescence. We therefore also have studied their effect and find the luminescence of both peaks (at 543 nm and 657 nm) of the two kinds of UCLNPs to be strongly quenched (figure 6.9). Plots of F_0/F versus the concentration of HMs ions fit conventional linear Stern–Volmer equation as shown in figure 6.10, and K_{SV} values are given in table 6.2. Like in case of cations, the quenching constants are different for the green and red emission bands.

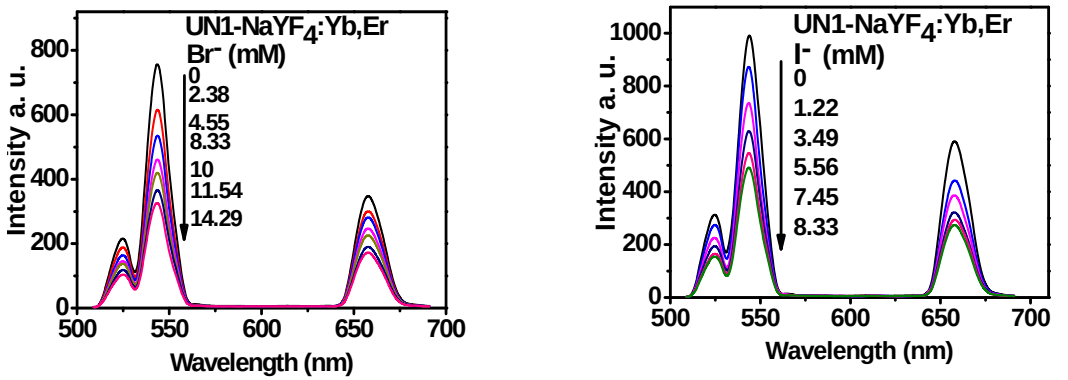

Figure 6.9 Quenching of the luminescence emission spectra of UCLNPs of type UN-1 by bromide and iodide in acetate buffer of pH 4 under 980-nm diode laser excitation.

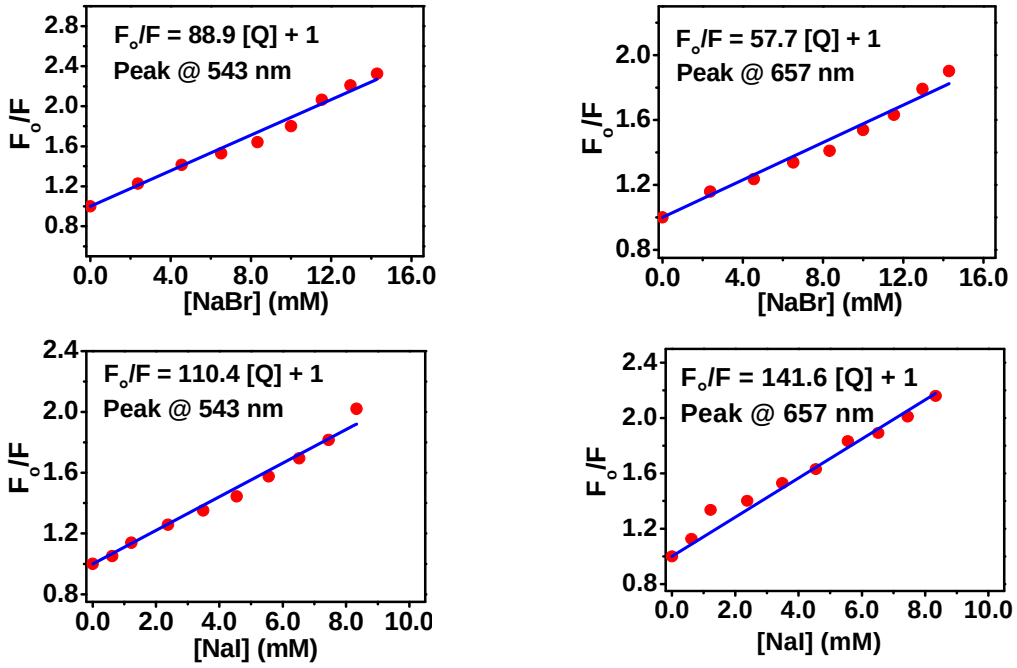

Figure 6.10 Stern-Volmer plots of the quenching of the luminescence of UCLNPs of type UN-1 by bromide and iodide in acetate buffer of pH 4. Quenching constants again are different for the two main emission bands (i.e., the kind of electronic transition from the excited state).

6.4.6 Variation of Dopants

The effect of quenching of luminescence is not limited to particles of the type UN-1 and UN-4. In fact, all the other UCLNPs studied show the effect. For example, the luminescence of the UCLNPs doped with Yb,Tm (UN-2) or Yb, Ho (UN-3) are quenched by Cu(II) ions in concentrations between 0 and 15 mM (see figure 6.11). The particles of type UN-2 (doped with Yb and Tm) display a blue peak at 475 nm (assigned to the $^1G_4 \rightarrow {}^3H_6$ transition), and a near-infrared peak at 802 nm (the $^3H_4 \rightarrow {}^3H_6$ transition). Particles of type UN-3 (doped with Yb and Ho) display a green peak at 541 nm (the $^5F_4/{}^5S_2 \rightarrow {}^5I_8$ transition) and a red peak at 645 nm (the $^5F_5 \rightarrow {}^5I_8$ transition). Again, quenching constants are different for the respective (blue, green, red, or near-infrared) emissions as can be seen from the data given in table 6.3. Similar results were obtained with other ions. Plots of F_0/F versus [Q] showed good linear relationships for the quenching by Cu(II), Fe(III) and Pb(II) ions as shown in Figures 6.12 (particles of type UN-2) and 14 (particles of type UN-3) in the Suppl. Information. However, this is the case only at quencher concentrations of up to 10 to 20 mM.

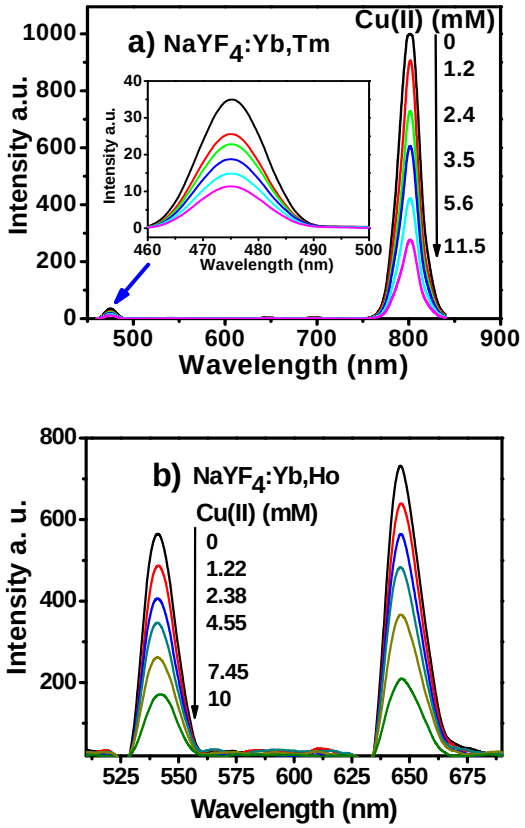

Figure 6.11 Effect of Cu(II) ions concentration on the luminescence of UCLNPs of type UN-2 and UN-3. The concentration of UCLNPs is 0.2 mg mL^{-1}. (a) Particles of type UN-2. (b) UCLNPs of type UN-3.

Table 6.3 Stern-Volmer constants (K_{SV}, 1/M) for the quenching of the two main emission bands of UCLNPs of type of NaY_4:Yb,Tm and NaY_4:Yb,Ho.

Particle type: NaY_4:Yb,Tm				
Quencher	UN-2 (solvothermal)		UN-5 (coprecipitation)	
	Ksv_1@ 475 nm	Ksv_2@ 802 nm	Ksv_1@ 475 nm	Ksv_2@ 802 nm
Cu(II)	142	160	116	68.5
Fe(III)	1417	898	410	502
Pb(II)	167	189	144	181
Particle type: NaY_4:Yb,Ho				
Quencher	UN-3 (solvothermal)		UN-6 (coprecipitation)	
	Ksv_1@ 541 nm	Ksv_2@ 645 nm	Ksv_1@ 541 nm	Ksv_2@ 645 nm
Cu(II)	210	208	165	154
Fe(III)	1225	1610	645	632
Pb(II)	145	121	60.9	44.1

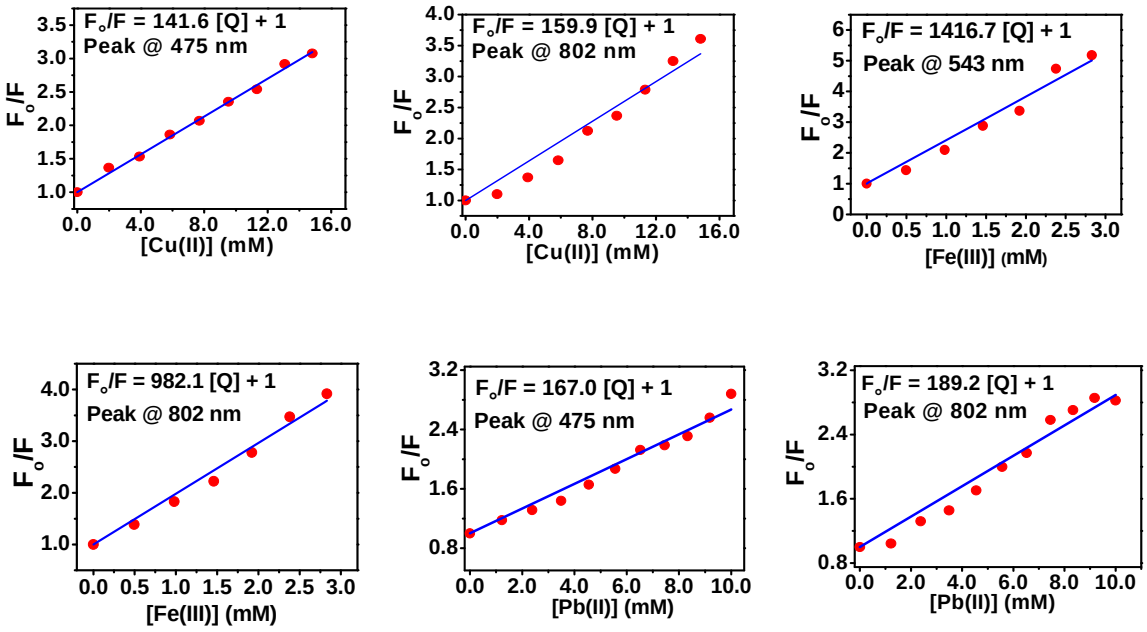

Figure 6.12 Stern-Volmer plots for the quenching of the luminescence of nanoparticles of type UN-2 by heavy metal ions in acetate buffer solution of pH 4.

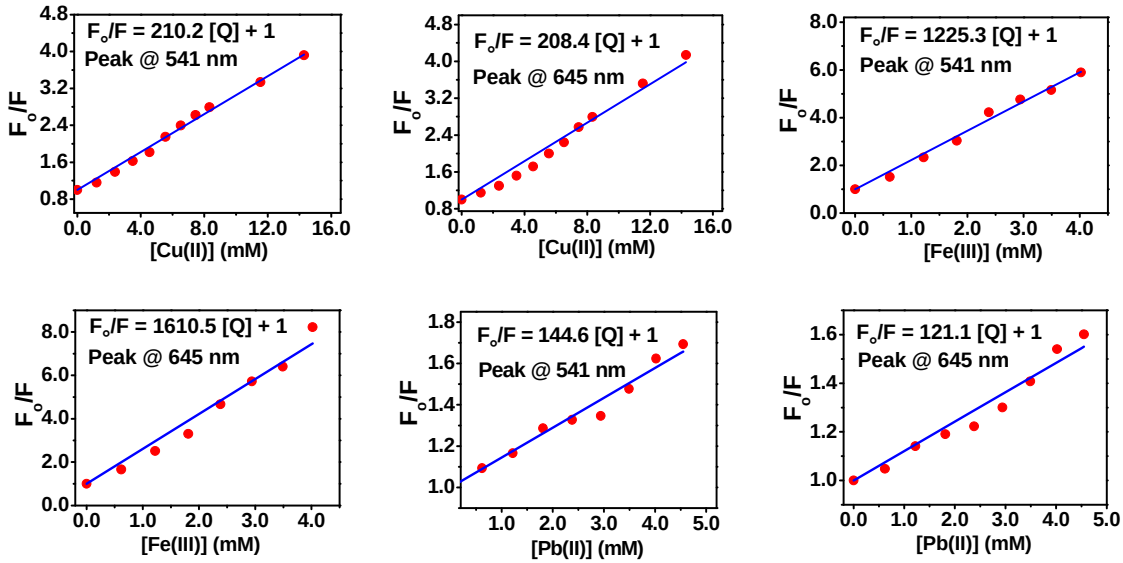

Figure 6.13 Stern-Volmer plots for HMs concentration dependence of the luminescence of particles of type UN-3 in acetate buffer of pH 4 and at diode laser excitation at 980 nm.

6.4.7 Effect of pH Value

The effect of the pH value on quenching was studied for the of the 543-nm and 657-nm peaks of the UN-1 particles in the presence of a constant concentration (4.55 mM) of Cu(II). The plot in figure 6.14A gives the effect of pH value on the ratio F/F_0 (where F_0 is the intensity of luminescence in absence of quenching, and F is the intensity at a given pH value. The plot reveals that luminescence intensity decreases with increasing pH values in the range from 4 to 6. Quenching is rather weak at pH values above, probably because the metal ions are precipitated as their hydroxides at such high pH values. The effect of pH on the quenching constant is given in figure 6.14B which also reveals that pH values of 4 or higher should be chosen if strong quenching is desired.

Figure 6.14 Effect of pH on (A) the relative luminescence intensity of UN-1 and (B) the quenching constant of UN-1 in presence of copper(II) ion (4.55 mM).

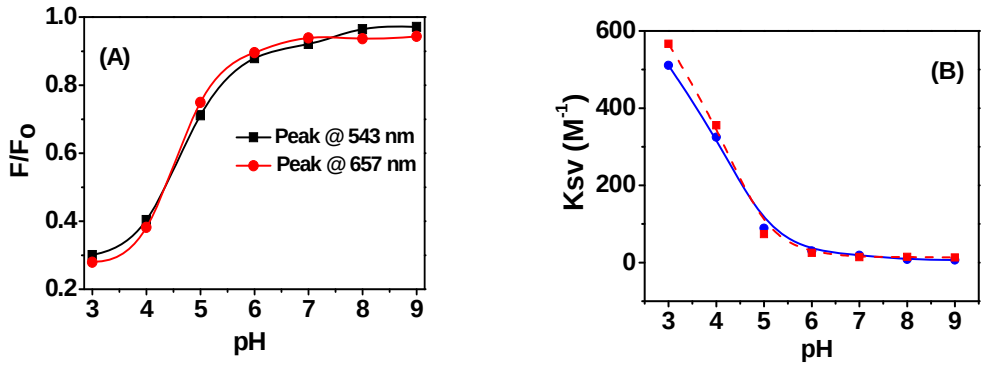

6.5 Discusion

We demonstrate here that the luminescence of the $NaYF_4$ nanoparticles doped with the rare earth metal ions Yb, Er, Ho/Tm is strongly quenched in the presence of HMs or halides in aqueous solution. The decrease in the quantum yield of the emission is a result of both dynamic and static quenching processes and not limited to a single kind of UCLNPs. The differences in the efficiencies of the quenching of the two main luminescence bands are explained by differences on the interaction between quencher and respective excited state species. The K_{SV} values for the UCLNPs prepared by the solvothermal method are higher than those of the coprecipitation method. This may be due to the formation of EDTA complexes by the EDTA ligand on the surface of the UCLNPs. This is supported by FTIR data (see figure

6.15). FTIR measurements wear carried out for two samples of UN-4, before and after annealing at 400 °C. The spectra show that the spectra do not significantly change as a result of the annealing process. The peaks at 1647 and 1413 cm^{-1} are assigned to the carboxy groups of EDTA. The broad band centered at 3375 cm^{-1} is attributed to the stretching vibrations of hydroxy groups, water molecules in the interlayer, and physically adsorbed water.

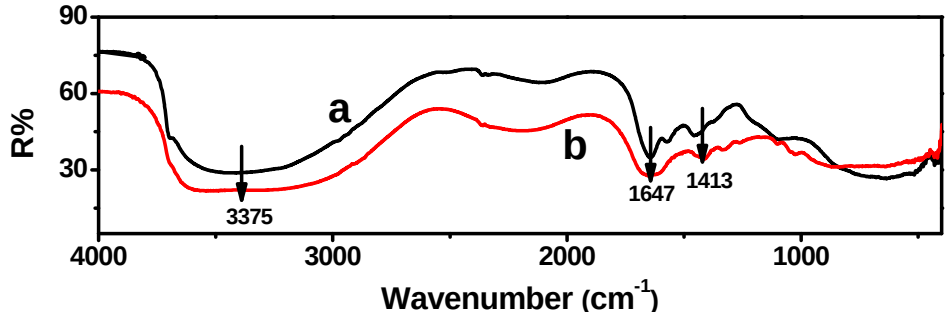

Figure 6.15 FTIR-Spectra of UN-4 (a) as prepared NPs and (b) after NPs annealed at temperature of ~400 °C.

In addition, the ^{1}H NMR spectrum (300 MHz, CDCl3) of UN-4 has a strong peak at 1.5 ppm which is typical for the CH_2 group of EDTA. Both findings are good proof for the presence of EDTA on the surface of the NPs of type UN-4. Mechanistically seen, the presence of EDTA will cause the formation of respective metal ion complexes, and this – in turn – will decrease the effieciency of dynamic quanching and – possibly – cause stronger static quenching.

Compared to the well-studied quenching of the luminescence of quantum dots (QDs) (table 6.4) , we note that Stern-Volmer constants are distinctly smaller for UCLNPs, possibly because the data we have available are for surface modified QDs. Table 6.4 summarizes the data available for QDs. They reveal that quenching constants are higher by factors from 1,000 to 10,000. This can be explained by the fact that the surface-to-volume ratio of the QDs with their diameters between 3 and 10 nm is much larger than that of the UCLNPs studied here (with diameters of ~35 nm and 60 – 90 nm, respectively). As a result, the probability of a collision between an emitting center of the UCLNPs, and even the probability of coming close to it, is distinctly smaller. However, other effects are also likely to be operative, but are more difficult to elucidate than quenching processes that occur in molecular solutions due to the

complexicity of the photophysics of colloidal UCLNPs.

The efficient quenching of the luminescence of such nanoparticles by HMs and halide ions has several implications. The effect may serve to sense and even image heavy metal ions, for example inside cells (and in a non-destructive manner), or in microstructures and volumes where other methods cannot be applied easily. The feature of photoexcitation in the near-infrared red (980 nm) is particularly attractive because this is in the optical window of most biomatter so that penetration depths of up to 5 cm become possible if hemoglobin is not present in respective tissue. The effect also may be used for rapid and cost effective general screening for metal ions.

Table 6.4 Stern-Volmer constants (K_{sv}, M^{-1}) for the quenching of different types of quantum dots by heavy metal ions and related quenchers.

Quantum dot (material)	*Size*	*quencher*	K_{sv}	*Ref.*
L-cysteine-capped CdS	5-10 nm	Cu(II)	$2.3 \cdot 10^6$	15
		Hg(II)	$6.3 \cdot 10^6$	
		Co(II)	$0.9 \cdot 10^6$	
		Ni(II)	$0.2 \cdot 10^6$	
Glutathione-capped ZnCdSe	3 nm	Pb(II)	$1.3 – 25 \cdot 10^6$	20
Thiol-capped CdTe	3.3 nm	Pb(II)	$1.3 \cdot 10^4$	24
	2.6 nm	Pb(II)	$9.2 \cdot 10^4$	
L-cysteine capped ZnS	8-10 nm	Cu(II)	$2.2 \cdot 10^3$	26
Glutathione-capped CdTe	3.4 nm	$Ru(bpy)_3^{2+}$	$2.5 \cdot 10^3$	14

Quenching is not selective and limited to heavy metals and two halides. It was shown, however,[8] that the selectivity and efficiency of the quenching of CdS Q-dots can be markedly enhanced by proper modification of the surface. Polyphosphate-capped Q-dots are sensitive to nearly all mono- and divalent cations and show no selectivity for ions. Thioglycerol-capped Q-dots are sensitive to only copper and iron ions but cysteine-capped dots are sensitive to zinc ions but insensitive to other physiologically important cations, such as copper, calcium, and magnesium ions. Mercaptopropionic causes strong quenching by copper ion,[23] We expect that similar improvements in selectivity can be achieved by modifying the surface of the UCLNPs reported here.

6.6 Reference

1 Carlson ED (2009) **Encyclopedia of Nanotechnology**, Nova Science Publ. Inc., NY.

2 Müller A, Cheetham AK (2007) **Nanomaterials Chemistry**, Wiley-VCH, Weinheim

3 Schmid, G. Nanoparticles, Wiley, New York, 2010.

4 Yang S, Cao L, Luo PG, Lu F, Wang X, Wang H, Meziani MJ, Liu MJ, Qi G, Sun Y (2009) **Carbon Dots for Optical Imaging in Vivo**, J. Am. Chem. Soc. 131:11308-11309.

5 Chow PE (2010) **Gold nanoparticles: properties, characterization and fabrication**, Nova Science Publ. Inc.

6 Chen Z, O'Brien S (2008) **Structure Direction of II−VI Semiconductor Quantum Dot Binary Nanoparticle Superlattices by Tuning Radius Ratio**, ACS Nano 2:1219–1229

7 Knoss RW (2008) **Quantum Dots: Research, Technology and Applications**, Nova Sci. Publ., Commack, NY.

8 Chen YF, Rosenzweig Z (2002) **Luminescent CdS quantum dots as selective ion probes**, Anal. Chem. 74:5132-5138.

9 Nikoobakht B, Burda C, Braun M, Hun M, El-Sayed M A (2002) **The quenching of CdSe quantum dots photoluminescence by gold nanoparticles in solution**, Photochem. Photobiol. 75:591-597.

10 Heafey E, Laferriere M, Scaiano JC (2007) **Comparative study of the quenching of core and core-shell CdSe quantum dots by binding and non-binding nitroxides**, Photoch. Photobio. Sci. 6:580-584.

11 Landes CF, Braun M, El-Sayed MA (2001) **On the nanoparticle to molecular size transition: Fluorescence quenching studies,** J. Phys. Chem. B 105:10554-10558.

12 Kuang R, Kuang X, Pan S, Zheng X, Duan J, Duan Y (2010) **Synthesis of cysteamine-coated CdTe quantum dots for the detection of bisphenol A**. Microchim. Acta 169:109-115.

13 Shi GH, Shang ZB, Wang Y, Jin WJ, Zhang TC (2008) **Fluorescence quenching of CdSe quantum dots by nitroaromatic explosives and their relative compounds**, Spectrochim. Acta A 70:247-252.

14 Gao D, Sheng Z, Han H (2010) **A novel method for the analysis of calf thymus DNA based on CdTe quantum dots-Ru(bpy)$_3^{2+}$ photoinduced electron transfer system,** Microchim. Acta 168:341-345.

15 Chen J, Zheng A, Gao Y, He C, Wu G, Chen Y, Kai X, Zhu C (2008) **Functionalized CdS quantum dots-based luminescence probe for detection of heavy and transition metal ions in aqueous solution**, Spectrochim, Acta, Part A 69:1044-1052.

16 Wang J, Liang J, Sheng Z, Han H (2009) **A novel strategy for selective detection of Ag^+ based on the red-shift of emission wavelength of quantum dots**, Microchim. Acta 167:281-287.

17 Long YF, Jiang DL, Zhu X, Wang JX, Zhou FM (2009) **Trace Hg^{2+} Analysis via Quenching of the Fluorescence of a CdS-Encapsulated DNA Nanocomposite**, Anal. Chem. 81:2652-2657.

18 Xie HY, Liang HG, Zhang ZL, Liu Y, He Z K, Pang DW (2004) **Luminescent CdSe-ZnS quantum dots as selective Cu^{2+} probe**, Spectrochim. Acta A 60:2527-2530.

19 Zhang B-H, Qi L, Wu F-Y(2010) **Functionalized manganese-doped zinc sulfide core/shell quantum dots as selective fluorescent chemodosimeters for silver ion** Microchim. Acta 170:147-153.

20 Ali EM, Zheng YG, Yu HH, Ying JY (2007) **Ultrasensitive Pb^{2+} detection by glutathione-capped quantum dots**, Anal. Chem. 79:9452-9458.

21 Neuman D, Ostrowski AD, Mikhailovsky AA, Absalonson RO, Strouse GF, Ford PC (2008) **Quantum dot fluorescence quenching pathways with Cr(III) complexes. Photosensitized NO production from trans-Cr(cyclam)$(ONO)_2^+$**, J. Am. Chem. Soc.130:168-175.

22 Ruedas-Rama MJ, Hall EAH (2009) **Multiplexed energy transfer mechanisms in a dual-function quantum dot for zinc and manganese,** *Analyst 134*:159-169.

23 Bo C, Ping Z (2005) **A new determining method of copper(II) ions at ng ml^{-1} levels based on quenching of the water-soluble nanocrystals fluorescence** Anal. Bioanal. Chem.381:986-992.

[24] Wu HM, Liang J G, Han HY (2008) **A novel method for the determination of Pb^{2+} based on the quenching of the fluorescence of CdTe quantum dots**, *Microchim. Acta 161*, 81-86.

[25] Freeman R, Willner I (2009) **NAD^+/NADH-Sensitive Quantum Dots: Applications To Probe NAD^+-Dependent Enzymes and To Sense the RDX Explosive**, Nano Letters 9:322-326.

[26] Koneswaran M, Narayanaswamy R (2009) **L-Cysteine-capped ZnS quantum dots based fluorescence sensor for Cu^{2+} ion**, Sens. Actuat. B 139:104-109.

[27] Zhang FF, Li L, Ding YP, Wang YP (2010) **Application of Functionalized ZnSe Nanoparticles to Determinate Heavy Metal Ions**, J. Fluoresc. 20:837-842.

[28] Krug HF, Wick P (2011) **Nanotoxicology: An Interdisciplinary Challenge**. Angew. Chem. 123:1294-1314.

[29] Stark WJ (2011) **Nanoparticles in Biological Systems**, Angew. Chem. *123*: 1276-1293.

[30] Auzel F (2004) **Upconversion and anti-Stokes processes with f and d ions in solids**, Chem. Rev. 104:139-173.

[31] Wang F, Liu X (2009) **Recent advances in the chemistry of lanthanide-doped upconversion nanocrystals**, *Chem. Soc. Rev. 38*:976-989.

[32] Lin Z (2001) **Upconversion Nanocrystals: Synthesis, Properties, Assembly and Applications**. Sci. Adv. Mater. 3:26-40

[33] Jalil RA, Zhang Y (2008) **Biocompatibility of silica coated $NaYF_4$ upconversion fluorescent nanocrystals**. Biomaterials 29:4122-4128.

[34] Wang M, Mi C C, Zhang YX, Liu JL, Li F, Mao CB, Xu SK (2009) **NIR-Responsive Silica-coated $NaYbF_4$:Er/Tm/Ho Upconversion Fluorescent Nanoparticles with Tunable Emission Colors and Their Applications in Immunolabeling and Fluorescent Imaging of Cancer Cells,** J. Phys. Chem. C 113:19021-19027.

[35] Achatz DE, Reham A, Wolfbeis OS (2010) **Luminescent Chemical Sensing, Biosensing, and Screening Using Upconverting Nanoparticles**, Topic Curr. Chem. 300:29-50.

[36] Wang F, Liu XG (2008) **Upconversion multicolor fine-tuning: Visible to near-infrared emission from lanthanide-doped $NaYF_4$ nanoparticles**, J. Am. Chem. Soc.130:5642-5643.

[37] Sivakumar S, Diamente PR, van Veggel FC (2006) **Silica-coated Ln(3+)-doped LaF_3 nanoparticles as robust down- and upconverting biolabels**, Chem. Eur. J. **2006**, 12:5878-5884.

[38] Kong DY, Quan ZW, Yang J, Yang PP, Li CX, Lin J (2009) **Avidin conjugation to up-conversion phosphor $NaYF_4$:Yb^{3+}, Er^{3+} by the oxidation of the oligosaccharide chains**. J. Nanopart. Res.11:821-829.

[39] Mader HS, Kele P, Saleh SM, Wolfbeis OS (2010) **Upconverting luminescent nanoparticles for use in bioconjugation and bioimaging**, *Curr. Opin. Chem. Biol. 14*:582-596.

[40] Rantanen T, Jarvenpaa ML, Vuojola J, Kuningas K, Soukka T (2008) **Fluorescence-quenching-based enzyme-activity assay by using photon upconversion,** Angew. Chem. Int. Edit. 47:3811-3813.

[41] Morgan CG, Dad S, Mitchell AC (2008) **Present status of, and future prospects for, upconverting phosphors in proximity-based bioassay**, J. Alloys Compd. 451:526-529.

[42] Vetrone F, Naccache R, Zamarron A, de la Fuente A.J, Sanz-Rodrıguez F, Maestro LM, Rodriguez EM Jaque, D Sole J G, Capobianco J A (2010) **Temperature Sensing Using Fluorescent Nanothermometers** ACS Nano 4:3254-3258.

[43] Wang F, Wang JA, Liu XG (2010) **Direct Evidence of a Surface Quenching Effect on Size-Dependent Luminescence of Upconversion Nanoparticles**, Angew. Chem. Int. Edit. 49:7456-7460.

[44] Li ZQ, Zhang Y (2008) **An efficient and user-friendly method for the synthesis of hexagonal-phase $NaYF_4$: Yb, Er/Tm nanocrystals with controllable shape and upconversion fluorescence**, *Nanotechnol. 19*.

[45] Yi GS, Lu HC, Zhao SY, Yue G, Yang WJ, Chen DP, Guo LH (2004) **Synthesis, characterization, and biological application of size-controlled nanocrystalline $NaYF_4$:Yb,Er infrared-to-visible up-conversion phosphors**, Nano Lett. 4:2191-2196.

[46] Suyver JF, Grimm J, van Veen, MK, Biner D, Krämer KW, Güdel HU (2006) **Upconversion spectroscopy and properties of $NaYF_4$ doped with Er^{3+}, Tm^{3+} and/or Yb^{3+}**, J. Luminesc. 117:1–12.

[47] Singh SK, Kumar K, Rai SB (2009) **Er^{3+}/Yb^{3+} codoped Gd_2O_3 nano-phosphor for optical thermometry**, Sens. Actuators, part A 149:16-21.

[48] Lakowicz JR (2006) **Principles of Luminescence Spectroscopy**, 3rd ed., Plenum Press, New York, pp. 282-283.

7 Summary

7.1 In English

This thesis describes the potential of various kinds of luminescent nanoparticles with respect to chemical sensing and biosensing. First, fluorescent silica nanoparticles (SiNPs) were prepared by covalent attachment of fluorophores to the amino-modified surface of SiNPs with a typical diameter of 15 nm. The SiNPs were used in novel kinds of Förster resonance energy transfer (FRET)-based affinity assays at the interface between nanoparticle and sample solution. Various labels were employed to obtain a complete set of colored SiNPs, with excitation maxima ranging from 337 to 659 nm and emission maxima ranging from 436 nm to the near infrared (710 nm). The nanoparticles were characterized in terms of size and composition using transmission electron microscopy, thermogravimetry, elemental analysis, and dynamic light scattering. The surface of the fluorescent SiNPs was biotinylated, and binding of labeled avidin to the surface was studied via FRET in two model cases.

Secondly, the upconverting luminescent nanoparticles (UCLNPs) consist of hexagonal $NaYF_4$ nanocrystals doped with trivalent rare earth ions were synthesized by both the oleic acid (solvothermal) method and the ethylenediaminetetraacetic acid (coprecipitation) method. The nanoparticles were codoped using Yb^{3+} as the sensitizer ion, Er^{3+}, Tm^{3+}, or Ho^{3+} respectively as the emitting activator ions. An affinity system was demonstrated based on the interaction of two types of nanoparticles. The first type consists of UCLNPs of the type $NaYF_4$:Yb,Er absorbing light in the infrared and showing green luminescence at 521 and 543 nm and red luminescence at 657 nm. The second type consists of gold nanoparticles (Au-NPs) with a size of about 50 nm, which absorb the green luminescence of the UCLNPs, but do not influence their red luminescence. A model system for a self referenced affinity system were established by labeling the UCLNPs with avidin and the AuNPs with biotin. In the presence of avidin-modified UCLNPs, the biotinylated Au-NPs can be detected in the range from 12 to 250 $\mu g \cdot mL^{-1}$ by rationing the intensity of the red (analyte-independent) emission band to that of the green (analyte-dependent) emission band. All nanoparticles were characterized in terms of size and composition using transmission electron microscopy, thermo-gravimetry, and FTIR spectroscopy.

Thirdly, different types of nanoparticles (made from silica, polystyrene and UCLNPs) carrying longwave absorbing and emitting fluorescent labels were prepared by conjugating reactive dyes to the surface of amino-modified particles. The dyes have a reactive chloro group capable of reacting with amino groups and thereby undergoing a change in color, typically from green to blue (the so-called chameleon effect). The latter show the effect of upconversion in that near-infrared laser light is converted into visible luminescence. They also show the unusual property of displaying dual emission, depending on whether their luminescence is photoexcited with visible light or near-infrared light. The amino groups on the surface of nanoparticles were detected via the chameleon effect of the applied amino-reactive dyes.

Fourth, the quenching effect of heavy metal ions and halide ions on the luminescence of UCLNPs in aqueous solution was studied. The effect was investigated for the ions Cu(II), Hg(II), Pb(II), Cd(II), Co(II), Ag(I), Fe(III), Zn(II), bromide and iodide, and was found to be particularly strong for Hg(II). Stern-Volmer plots were virtually linear up to 10 – 25 mM concentrations of the quencher, but deviate from linearity at higher quencher concentrations where static quenching caused an additional effect. The UCLNPs display two main emission bands (blue, green, red or near-infrared), and the quenching efficiencies for these found to be different. The effect seems to be generally associated with UCLNPs because it was observed for all particles doped with trivalent lanthanide ions including Yb(III), Er(III), Ho(III), and Tm(III).

7.2 In German

Diese Doktorarbeit beschreibt das Potential verschiedener Arten lumineszenter Nanopartikel in Hinblick auf ihren Einsatz als Bestandteil chemischer Sensoren und Biosensoren. Zuerst wurden fluoreszente Silica Nanopartikel (SiNPs) mit einem typischen Durchmesser von 15 nm durch kovalente Bindung von Fluorophoren an die amino-modifizierte Oberfläche der SiNPs hergestellt. Die SiNPs wurden für neuartige Förster Resonanz Energie Transfer (FRET) basierte Affinitätsassays an der Grenzfläche zwischen Nanopartikel und Probelösung eingesetzt. Diverse Fluoreszenzmarker wurden verwendet um einen kompletten Satz von farbigen SiNPs zu erhalten, deren Anregungsmaxima zwischen 337 nm und 659 nm und Emissionsmaxima zwischen 436 nm und dem Nah-Infrarot (710 nm) liegen. Die Nanopartikel

wurden bezüglich ihrer Größe und Zusammensetzung mit Hilfe von Transmissionselektronenmikroskopie, Thermogravimetrie, Elementaranalyse und Dynamischer Lichtstreuung charakterisiert. Die Oberfläche der fluoreszenten SiNPs wurde biotinyliert und die Bindung von markiertem Avidin an die Partikeloberfläche wurde mittels FRET anhand zweier Musterfälle untersucht.

Zweitens wurden upconvertierende lumineszente Nanopartikel (UCLNPs), bestehend aus hexagonalen $NaYF_4$ Nanokristallen, die mit trivalenten Selten-Erd-Ionen dotiert wurden, sowohl mittels der Ölsäure- (Solvothermalen) Methode als auch der Ethylendiamintetraacetat- (Co-Präzipitations) Methode synthetisiert. Die Partikel wurden mit Yb^{3+} als Sensitizer Ion und Er^{3+}, Tm^{3+} beziehungsweise Ho^{3+} als emittierendes Aktivator Ion co-dotiert. Ein Affinitätssystem wurde vorgestellt, dass auf der Wechselwirkung zweier verschiedenartiger Nanopartikel beruht. Beim ersten Nanopartikeltyp handelte es sich um UCLNPs der Art $NaYF_4$:Yb,Er, die Licht im Infraroten absorbieren und grüne Lumineszenz bei 521 nm und 543 nm, sowie rote Lumineszenz bei 657 nm zeigen. Als zweiter Typ wurden Goldnanopartikel (Au-NPs) mit einer Größe von ungefähr 50 nm verwendet, die die grüne Lumineszenz der UCLNPs absorbieren, deren rote Lumineszenz aber nicht beeinflussen. Ein Modellsystem für ein selbstreferenziertes Affinitätsassay wurde erstellt, indem die UCLNPs mit Avidin und die Au-NPs mit Biotin markiert wurden. In Gegenwart der Avidin-modifizierten UCLNPs konnten die biotinylierten Au-NPs in einem Konzentrationsbereich von 12 bis 250 $\mu g \cdot mL^{-1}$ bestimmt werden, indem das Verhältnis der Intensität des roten (Analyt-unabhängen) Emissionspeaks zu der des grünen (Analyt-abhängigen) Emissionspeaks der UCLNPs gebildet wurde. Alle Nanopartikel wurden bezüglich ihrer Größe und Zusammensetzung mittels Transmissionsemissionsmikroskopie, Thermogravimetrie und FTIR Spektroskopie untersucht.

Drittens wurden unterschiedliche Arten von Partikeln (bestehend aus Silica, Polystyrol und UCLNPs), welche langwellig absorbierende und emittierende fluoreszente Marker tragen, hergestellt, indem reaktive Farbstoffe an die Oberfläche der amino-modifizierten Partikel konjugiert wurden. Die Farbstoffe verfügten über eine reaktive Chloro-Gruppe, die in der Lage ist mit Aminogruppen zu reagieren. Dabei unterlaufen die Farbstoffe eine Farbänderung, üblicherweise von grün nach blau (der sogenannte Chamäleon Effekt). Die Partikel basierend auf $NaYF_4$ zeigen den Upconversionseffekt, bei dem Nahinfrarot-laserlicht in sichtbare Lumineszenz umgewandelt wird. Diese Partikel weisen außerdem die ungewöhnliche

Eigenschaft der dualen Emission auf. Diese ist abhängig von der eingesetzten Anregungslichtquelle (Nahinfrarotlaser oder sichtbares Licht). Die Aminogruppen auf der Nanopartikeloberfläche wurden über den Chamäleoneffekt der eingesetzten amino-reaktiven Farbstoffe nachgewiesen.

Viertens wurde der Löscheffekt von Schwermetallionen und Halogenionen auf die Lumineszenz der UCNLPS in wässriger Lösung untersucht. Der Effekt wurde für die Ionen Cu(II), Hg(II), Pb(II), Cd(II), Co(II), Ag(I), Fe(III), Zn(II), Bromid und Iodid erforscht, wobei Hg(II) Ionen hierbei ein besonders starkes Löschverhalten zeigten. Die Stern-Volmer-Diagramme waren bis zu einer Konzentration von 10 – 25 mM des jeweiligen Quenchers nahezu linear. Bei höheren Konzentrationen weichen die Kurven von der Linearität ab, da hier statisches Quenchen einen zusätzlichen Einfluss ausübt. Die UCLNPs zeigen jeweils zwei Hauptemissionsbanden (blau und nah-infrarot, bzw. grün und rot), für die jeweils unterschiedliche Quencheffizienzen gefunden wurden. Dieser Effekt scheint für generell für UCLNPs zu gelten, da er für alle Partikel auftritt, die mit trivalenten Lanthanidionen wie Yb(III), Er(III), Ho(III), und Tm(III) dotiert sind.

8 Curriculum Vitae

El_Sayed Mahmoud Mohamed Saleh

born on June 23, 1976 in Suez, Egypt

Education

09/1982 – 06/1988	**Primary School, El-Mahmodia School, Suez, Egypt**
09/1988 – 06/1991	**Prep School, El-Sbah School, Suez, Egypt**
09/1991 – 06/1994	**Secondary School, El-Salam School, Suez, Egypt**
09/1994 – 05/1998	**Bachelor of Science in Chemistry, Chemistry Department , Faculty of Sciences, Suez Canal University, Ismailia, Egypt.**
07/1999 – 08/2000	**Post Graduate Courses, Inorganic Chemistry, Chemistry Department , Faculty of Sciences, Suez Canal University, Ismailia, Egypt.**
08/2000 – 08/2004	**Master of Science, Inorganic Chemistry, Chemistry Department , Faculty of Sciences, Suez Canal University, Ismailia, Egypt.**
07/2007 - present	**PhD Thesis at the Institute of Analytical Chemistry, Chemo- and Biosensors, Prof. Otto S. Wolfbeis: "New Photo Luminescent Inorganic Materials High-tec Application in Chemical Sensing and Labeling"**

Work Experience

01/1999 – 10/2004	**Demonstrator, Chemistry Department, Faculty of Petroleum and Mining Engineering, Suez Canal University, Suez, Egypt.**
10/2004 - present	**Associate Lecturer, Chemistry Department, Faculty of Petroleum and Mining Engineering, Suez Canal University, Suez, Egypt.**

Language Skills

Arabic (native), English (good), German (basic).

9 List of Publications

Mader HS, Li X, Saleh SM, Link M, Kele P, Wolfbeis OS (2008) **Fluorescent Silica Nanoparticles**, Ann. NY. Acad. Sci. 1130:218-223.

Saleh SM, Müller R, Mader HS, Dürkop A, Wolfbeis OS (2010) **Novel multicolor fluorescently labeled silica nanoparticles for interface fluorescence resonance energy transfer to and from labeled avidin**, Anal. Bioanal. Chem. 398:1615-1623.

Ali R, Saleh SM, Meier RJ, Azab HA, Elgawad I, Wolfbeis OS (**2010**) **Upconverting Nanoparticle Based Optical Sensor for Carbon Dioxide,** Sens. Actuat. B 150:126–131.

Mader HS, Kele P, Saleh SM, Wolfbeis OS (2010) **Upconverting luminescent nanoparticles for use in bioconjugation and bioimaging**, Curr. Opin. Chem. Biol. 14:582-596.

Gorris HH, Ali R, Saleh SM, Wolfbeis OS (2011) **Tuning the Dual Emission of Photon-Upconverting Nanoparticles for Ratiometric Multiplexed Encoding**, Adv. Mater. 23:1652–1655.

Ali R, Lang T, Saleh SM, Meier RJ, Wolfbeis OS (2011) **Optical Sensing Scheme for Carbon Dioxide Using a Solvatochromic Probe,** Anal. Chem. 83:2846–2851

Saleh SM, Ali R, Hirsch T, Wolfbeis OS (2011) **Optical Detection of Biotin-Avidin Affinity Binding by Exploiting a Self-Referenced System Composed of Upconverting Nanoparticles and Gold Nanoparticles,** J. Nanoparticle Res.(in press); DOI:10.1007/s11051-011-0424-x.

Saleh SM, Ali R, Wolfbeis OS (2011) **Preparation of nanoparticles labeled with longwave absorbing and emitting chameleon labels, and a method for detecting amino groups on surfaces,** Microchim. Acta (accepted); DOI: 10.1007/s00604-011-0627-y.

Gorris HH,* Saleh SM,* Grögel D, Mustroph H, Wolfbeis OS (2011) **Long-Wavelength Absorbing and Fluorescent Chameleon Labels for Proteins, Peptides and Amines, Bioconjugate Chem**. (accepted) **(***authors contributed equally**)**

Saleh SM, Ali R, Wolfbeis OS (2011) **Quenching of the Luminescence of Upconverting Luminescent Nanoparticles by Heavy Metal Ions,** Chem. Eur. J., (to be submitted)

Eidesstattliche Erklärung

Ich erkläre hiermit an Eides statt, dass ich die vorliegende Arbeit ohne unzulässige Hilfe Dritter und ohne Benutzung anderer als der angegebenen Hilfsmittel angefertigt habe; die aus anderen Quellen direkt oder indirekt übernommenen Daten und Konzepte sind unter Angabe des Literaturzitats gekennzeichnet. Weitere Personen waren an der inhaltlich materiellen Herstellung der vorliegenden Arbeit nicht beteiligt. Insbesondere habe ich hierfür nicht die entgeltliche Hilfe eines Promotionsberaters oder anderer Personen in Anspruch genommen. Niemand hat von mir weder unmittelbar noch mittelbar geldwerte Leistungen für Arbeiten erhalten, die im Zusammenhang mit dem Inhalt der vorgelegten Dissertation stehen. Diese Arbeit wurde bisher weder im In- noch im Ausland in gleicher oder ähnlicher Form einer anderen Prüfungsbehörde vorgelegt.

Regensburg, den --. June 2011,

El-Sayed Mahmoud Mohamed Saleh